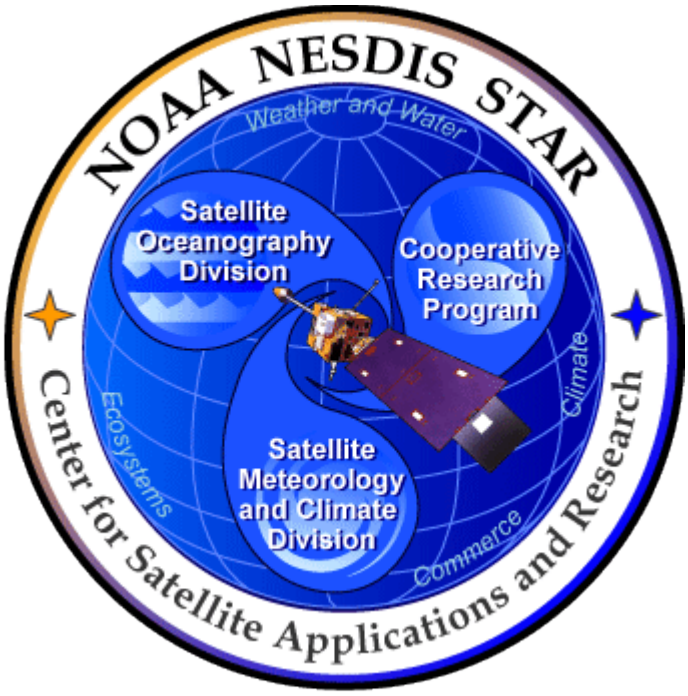

NOAA NESDIS
CENTER for SATELLITE APPLICATIONS and RESEARCH

Enterprise Document For Low Cloud and Fog

Corey Calvert, UW/CIMSS
Mike Pavolonis, NOAA/NESDIS/STAR

Version 5.0
March 2, 2021

TABLE OF CONTENTS

LIST OF FIGURES

LIST OF TABLES

LIST OF ACRONYMS

ABI – Advanced Baseline Imager
AC – Above Cloud
AGL – Above Ground Level
ASOS – Automated Surface Observing System
AIADD – Algorithm Interface and Ancillary Data Description
ARM – Atmospheric Radiation Measurement
ATBD – Algorithm Theoretical Basis Document
AVHRR – Advanced Very High Resolution Radiometer
BT – Brightness Temperature
CONUS – Continental United States
CSI – Critical Success Index
DOD – Department of Defense
EOS – Earth Observing System
ESA – European Space Agency
F&PS – Functional & Performance Specification
FAA – Federal Aviation Administration
GFS – Global Forecast System
FLS – Fog/Low Status
FPT – Focal Plane Temperature
GOES – Geostationary Operational Environmental Satellite
IFR – Instrument Flight Rules
LHP – Loop Heat Pipe
LIFR – Low Instrument Flight Rules
LRC – Local Radiative Center
LUT – Look-up Table
MVFR – Moderate Visual Flight Rules
NASA – National Aeronautics and Space Agency
NCEI – National Centers for Environmental Information
NESDIS – National Environmental Satellite, Data, and Information Service
NOAA – National Oceanic and Atmospheric Administration
NWP – Numerical Weather Prediction
NWS – National Weather Service
PQI – Product Quality Information
QF – Quality Flag
RAP – Rapid Refresh
RH – Relative Humidity
RTM – Radiative Transfer Model
SEVIRI – Spinning Enhanced Visible and Infrared Imager
SODAR – Sonic Detection And Ranging
SSEC – Space Science and Engineering Center
STAR – Center for Satellite Applications and Research
TOA – Top of Atmosphere
VFR – Visual Flight Rules

ABSTRACT

This document provides a high level description of the physical basis of the enterprise fog/low stratus (FLS) detection algorithm. The enterprise FLS detection product is designed to quantitatively identify clouds that produce at least Marginal Visual Flight Rules (MVFR) conditions, defined as having a cloud ceiling between 1000-3000 ft (305-914 m) above ground level (AGL) or surface visibility between 3-5 mi (4.8-8.1 km). Additionally, the enterprise FLS algorithm also quantitatively identifies clouds that produce Instrument Flight Rules (IFR) conditions, defined as having a cloud ceiling between 500-1000 ft (152-305 m) or surface visibility between 1-3 mi (1.6-4.8 km), or Low Instrument Flight Rules (LIFR), defined as having a cloud ceiling below 500 ft (152 m) AGL or surface visibility less than 1mi (1.6 km). At night, the algorithm utilizes the 3.9 and 11 μm channels to detect FLS. Fog/low stratus detection during the day is determined using the 0.65, 3.9, and 11 μm channels. The FLS detection algorithm utilizes textural and spectral information, as well as modeled relative humidity data and the difference between the cloud radiative temperature and surface temperature. The FLS detection scheme is probabilistic in nature using a naïve Bayes model to combine information from all the data. At night, the cloud geometric thickness (FLS depth) is estimated using a 3.9 μm based empirical relationship. During the day, FLS depth is calculated using the cloud Liquid Water Path (LWP) product and an assumption regarding the vertical distribution of cloud water.

There are a few important caveats that users need to be aware of. Passive satellite measurements do not provide direct information on cloud base or ceiling, so the properties of the cloud layer actually sensed by the radiometer must be used to indirectly infer information on cloud base. Since the properties of the cloud base are not directly measured, variations in cloud base due to local boundary layer effects (e.g. local moisture sources/sinks and local turbulent mixing processes) generally will not be captured. Secondly, limited spatial resolution and errors in forecast model temperature data may make accurate fog/low cloud detection difficult in mountainous regions due to underlying terrain that may not be accurately accounted for. As such, not every surface observation underneath a detected low cloud will necessarily indicate a ceiling below 3000 ft AGL or surface visibility less than 5 miles, however, when pixels with Visual Flight Rules (VFR) conditions are included the probability is usually relatively low, which is desirable.

The enterprise fog/low cloud detection algorithm is required to achieve a detection accuracy of 0.70 and thickness accuracy of within 500 m. Validation efforts indicate the algorithm meets these specifications.

1 INTRODUCTION

1.1 Purpose of This Document

The fog/low cloud detection algorithm theoretical basis document (ATBD) provides a high level description of the physical basis for detecting low cloud and fog which produces at least Marginal Visual Flight Rules (MVFR), Instrument Flight Rules (IFR) or Low Instrument Flight Rules (LIFR) conditions, with images taken by NOAA's geostationary GOES-NOP imagers and the Advanced Baseline Imager (ABI). MVFR conditions occur when the cloud base is between 1000-3000 ft (305-914 m) above ground level (AGL) or the surface visibility is between 3-5 mi (4.8-8.1 km), IFR conditions occur when the cloud base is between 500-1000 ft (152-305 m) or the surface visibility is between 1-3 mi (1.6-4.8 km), and LIFR conditions occur when the cloud base is less than 500 ft (152 m) or the surface visibility is less than 1 mi (1.6 km). Rather than a yes/no binary mask, the fog/low stratus algorithm (herein called the FLS algorithm) provides a quantitative probability that MVFR/IFR/LIFR conditions are present as well as an estimate of the fog/low cloud thickness for a given satellite pixel.

1.2 Who Should Use This Document

The intended users of this document are those interested in understanding the physical basis of the FLS algorithm. This document also provides information useful to anyone maintaining or modifying the original algorithm.

1.3 Inside Each Section

This document is broken down into the following main sections.

- **System Overview**: Provides relevant details of current geostationary satellite imagers and a brief description of the products generated by the algorithm.
- **Algorithm Description**: Provides all the detailed description of the algorithm including its physical basis, its input and its output.
- **Test Data Sets and Outputs:** Provides a detailed description of the data sets used to develop and test the enterprise FLS algorithm and describes the algorithm output.
- **Practical Considerations:** Provides a description of algorithm programming and quality control considerations.

- **Assumptions and Limitations**: Provides an overview of the current limitations of the approach and gives the plan for overcoming these limitations with further algorithm development.

1.4 Related Documents

- GOES-NOP/R Functional & Performance Specification Document (F&PS)
- GOES-NOP/R Fog/Low Cloud Detection Validation Plan Document
- Algorithm Interface and Ancillary Data Description (AIADD) Document

1.5 Revision History

- 9/30/2009 - Version 0.1 of this document for the GOES-R FLS algorithm was created by Corey Calvert (UW-CIMSS). Version 0.1 represents the first draft of this document.

- 7/31/2010 – Version 1.0 of this document for the GOES-R FLS algorithm was created by Corey Calvert (UW-CIMSS) and Michael Pavolonis (NOAA/NESDIS). In this revision, Version 0.1 was revised to meet 80% delivery standards.

- 9/15/2010 – Version 1.0 of this document for the GOES-R FLS algorithm was revised by Corey Calvert (UW-CIMSS) and Michael J Pavolonis (NOAA/NESDIS/STAR). In this revision, Version 1.0 was revised based on reviewer comments.

- 7/1/2011 – Version 2.0 of this document for the GOES-R FLS algorithm was created by Corey Calvert (UW-CIMSS) and Michael Pavolonis (NOAA/NESDIS/STAR). In this revision, Version 1.0 was revised to meet 100% delivery standards.

- 9/1/2015 – Version 3.0 of this document for the GOES-NOP FLS algorithm was created by Corey Calvert (UW-CIMSS) and Michael Pavolonis (NOAA/NESDIS/STAR) by editing and updating the previous version created for the GOES-R FLS algorithm.

- 7/18/2018 – Version 4.0 of this document for the enterprise FLS algorithm was created by Corey Calvert (UW-CIMSS) and Michael Pavolonis (NOAA/NESDIS/STAR) by editing and updating the previous version created for the GOES-NOP/GOES-R FLS algorithm.

- 3/2/2021 – Version 5.0 of this document for the enterprise FLS algorithm was created by Corey Calvert (UW-CIMSS) and Michael Pavolonis

(NOAA/NESDIS/STAR) by editing and updating Version 4.0 created for the GOES-NOP/GOES-R FLS algorithm to include content for GOES-17.

2 OBSERVING SYSTEM OVERVIEW

This section describes the products generated by the FLS algorithm and the requirements it places on the sensor.

2.1 Products Generated

The FLS algorithm is responsible for detecting fog/low stratus clouds (those that produce MVFR/IFR/LIFR Conditions) and estimating its geometric thickness (FLS depth).

2.1.1 Product Requirements

The F&PS requirements for fog/low cloud are listed in Table 1 and Table 2.

Table 1: F&PS requirements for GOES-NOP fog/low cloud products.

Name	Fog/Low Stratus Clouds
User & Priority	Enterprise GS
Geographic Coverage	FD (full disk)
Temporal Coverage Qualifiers	Day and Night
Product Extent Qualifier	Quantitative out to at least 70 degrees LZA and qualitative beyond
Cloud Cover Conditions Qualifier	All cloud cover conditions
Product Statistics Qualifier	Over low cloud and FLS cases with at least 42% occurrence in the region
Vertical Resolution	0.5 km (Depth)
Horizontal Resolution	4 km
Mapping Accuracy	1 km

Measurement Range	0 – 100 %
Measurement Accuracy	70% Correct Detection
Refresh Rate/Coverage Time Option (Mode 3)	15 min
Refresh Rate Option (Mode 4)	5 min
Data Latency	159 sec
Long-Term Stability	TBD
Product Measurement Precision	Undefined

Table 2 - F&PS requirements for ABI fog/low cloud products.

Name	Fog/Low Stratus Clouds
User & Priority	Enterprise GS
Geographic Coverage	FD (full disk)
Temporal Coverage Qualifiers	Day and Night
Product Extent Qualifier	Quantitative out to at least 70 degrees LZA and qualitative beyond
Cloud Cover Conditions Qualifier	All cloud cover conditions
Product Statistics Qualifier	Over low cloud and FLS cases with at least 42% occurrence in the region
Vertical Resolution	0.5 km (Depth)
Horizontal Resolution	2 km
Mapping Accuracy	1 km
Measurement Range	0 – 100 %
Measurement Accuracy	70% Correct Detection

Refresh Rate/Coverage Time Option (Mode 3)	Full Disk - 15 min CONUS - 5 min
Refresh Rate Option (Mode 4)	Full Disk - 15 min CONUS - 5 min
Data Latency (Mode 3)	Full Disk - 806 sec CONUS - 266 sec
Long-Term Stability	TBD
Product Measurement Precision	Undefined

2.2 Instrument Characteristics

The FLS algorithm will be applied to each earth-located satellite pixel with valid L1b data. Table 3 and Table 4 summarize the channels used by the FLS algorithm. Even though the FLS algorithm directly utilizes only a few channels, it indirectly utilizes many more channels through its dependence of up-stream cloud mask, cloud phase, and daytime optical properties algorithms.

Table 3: Channel numbers and wavelengths for the GOES-NOP imagers.

Channel Number	*Wavelength (μm)*	*Used in FLS Detection*
1	0.65	✓
2	3.9	✓
3	6.7	
4	10.7	✓
6	13.3	

Table 4: Channel numbers and wavelengths for the ABI

Channel Number	*Wavelength (μm)*	*Used in ACT*
1	0.47	
2	0.64	✓
3	0.86	
4	1.38	
5	1.61	
6	2.26	
7	3.9	✓
8	6.15	
9	7.0	
10	7.4	
11	8.5	
12	9.7	

13	10.35	
14	11.2	✓
15	12.3	
16	13.3	

The FLS algorithm relies on spectral tests and is therefore sensitive to any imagery artifacts or instrument noise. Due to the use of other cloud algorithms, any instrument-related artifacts, which impact the cloud mask, cloud phase or cloud optical properties may impact the FLS algorithm. The channel specifications are given in the F&PS section 3.4.2.1.4.0. We are assuming the performance outlined in the F&PS during our development efforts.

3 ALGORITHM DESCRIPTION

This section offers a complete description of the enterprise FLS algorithm.

3.1 Algorithm Overview

The enterprise fog/low stratus algorithm is designed to quantitatively identify clouds that produce at least Marginal Visual Flight Rules (MVFR) conditions, defined as having a cloud ceiling between 1000-3000 ft (305-914 m) above ground level (AGL) or surface visibility between 3-5 mi (4.8-8.1 km), Instrument Flight Rules (IFR) conditions, defined as having a cloud ceiling between 500-1000 ft (152-305 m) AGL or surface visibility between 1-3 mi (1.6-4.8 km), or Low Instrument Flight Rules (LIFR) conditions, defined as having a cloud ceiling below 500 ft (152 m) AGL or surface visibility less than 1 mi (1.6 km). The enterprise FLS products return the probability MVFR/IFR/LIFR conditions are present. At night, the algorithm utilizes the 3.9 and 11 μm channels to detect FLS. FLS detection during the day is determined using the 0.65, 3.9, and 11 μm channels. The FLS detection algorithm utilizes textural and spectral information, as well as modeled relative humidity (RH) and the difference between the cloud radiative temperature and surface temperature. The FLS detection scheme is probabilistic in nature using a naïve Bayes model to combine information from all the data. At night, the FLS geometric thickness (FLS depth) is estimated using a 3.9 μm based empirical relationship. During the day, FLS depth is calculated using the cloud Liquid Water Path (LWP) product and an assumption regarding the vertical distribution of cloud water.

The enterprise FLS detection algorithm derives the following products listed in the F&PS

- Probability that MVFR conditions are present
- Probability that IFR conditions are present
- Probability that LIFR conditions are present
- FLS depth (the geometric thickness of the stratus layer)

All of these products are derived at the pixel level.

In addition, the FLS detection algorithm derives the following products that are not included in the F&PS.

- Quality Flags (defined in section 3.5.1.1)
- Product Quality Information (defined in section 3.5.1.2)
- Metadata (defined in section 3.5.1.3)

3.2 Processing Outline

As discussed earlier, the FLS algorithm is dependent on several cloud products. Thus, prior to calling the FLS algorithm, the cloud mask, cloud phase, and daytime cloud optical properties must be generated. While the FLS algorithm does not directly utilize output

from the cloud height algorithm, the daytime optical properties algorithm does depend on the cloud height output. As such, the algorithm processing precedence required to generate the FLS products is as follows: cloud mask → cloud phase/type → cloud height → daytime microphysical properties → FLS detection and depth. The FLS detection algorithm requires at least 3 scan lines of satellite data due to the spatial analysis that is utilized in the algorithm. The processing outline of the FLS detection algorithm is summarized in Figure 1.

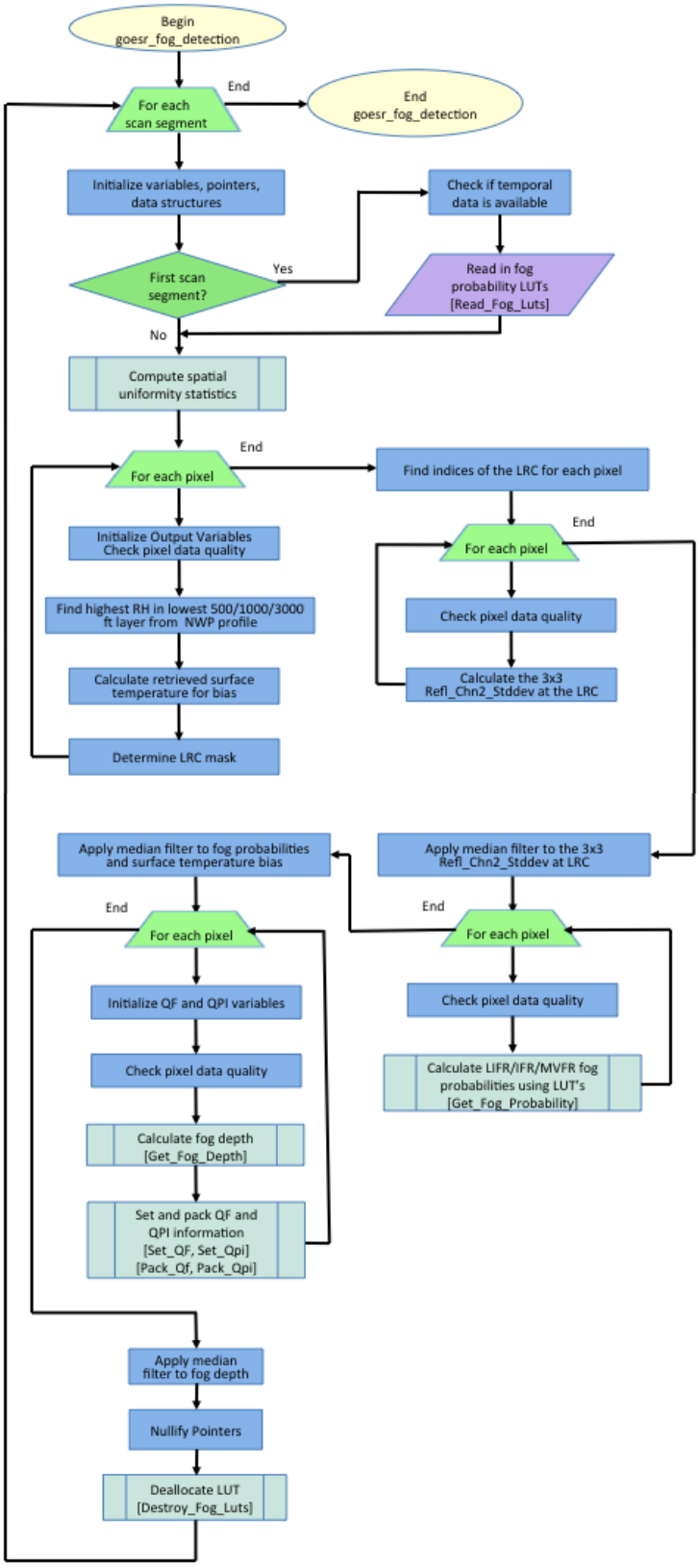
Begin
goesr_fog_detection
For each
scan segment
End
End
goesr_fog_detection
Initialize variables, pointers,
data structures
Check if temporal
data is available
First scan
segment?
Yes
Read in fog
probability LUTs
[Read_Fog_Luts]
No
Compute spatial
uniformity statistics
For each pixel
End
Find indices of the LRC for each pixel
Initialize Output Variables
Check pixel data quality
For each pixel
End
Find highest RH in lowest 500/1000/3000
ft layer from NWP profile
Check pixel data quality
Calculate retrieved surface
temperature for bias
Calculate the 3x3
Refl_Chn2_Stddev at the LRC
Determine LRC mask
Apply median filter to fog probabilities
and surface temperature bias
Apply median filter to the 3x3
Refl_Chn2_Stddev at LRC
End
For each pixel
End
For each pixel
Initialize QF and QPI variables
Check pixel data quality
Check pixel data quality
Calculate fog depth
[Get_Fog_Depth]
Calculate LIFR/IFR/MVFR fog
probabilities using LUT's
[Get_Fog_Probability]
Set and pack QF and
QPI information
[Set_QF, Set_Qpi]
[Pack_Qf, Pack_Qpi]
Apply median
filter to fog depth
Nullify Pointers
Deallocate LUT
[Destroy_Fog_Luts]

Figure 1 - High-level flowchart of the enterprise FLS algorithm illustrating the main processing sections.

The FLS algorithm is run in a framework that reads in all model and ancillary data, performs all clear sky radiance calculations, performs all necessary input/output and runs all other algorithms needed by the FLS algorithm. When the framework was run using 2 km resolution GOES-16 full disk and CONUS images the entire run time from start to finish was 12 min 7 sec for full disk and 1 min 53 sec for CONUS. The following list breaks down how long each part of the framework took to run:

Full Disk (pixel dimensions: 5424x5424):

Overall runtime: 12:07 (minutes: seconds)
Reading of ancillary data, clear sky calculations, input/output, etc.: 8:10
Upstream Algorithms (cloud mask, cloud phase, etc.): 2:08
FLS algorithm: 1:49

CONUS (pixel dimensions: 2500x1500):

Overall runtime: 1:53 (minutes: seconds)
Reading of ancillary data, clear sky calculations, input/output, etc.: 1:17
Upstream Algorithms (cloud mask, cloud phase, etc.): 0:16
FLS algorithm: 0:20

Note: These times are machine-specific, but they do give the user a rough idea of an example computational timeline.

3.3 Algorithm Input

This section describes the input needed to process the FLS algorithm. While the products are derived for each pixel, the use of spatial information requires knowledge of the surrounding pixels. Therefore, a minimum of 3 scan lines is required by the spatial analysis routines.

3.3.1 Primary Sensor Data

The lists below contain the primary and derived sensor data used by the FLS algorithm. By primary sensor data, we mean information that is derived solely from the imager observations and geolocation information.

- Calibrated reflectances for the 0.65 μm and 3.9 μm channels
- Calibrated radiances for the 11 μm channel
- Calibrated brightness temperature for the 11 μm channel
- Imager-specific L1b quality information from calibration for 0.65 μm, 3.9 μm and 11 μm channels

- Space mask (is the pixel geolocated on the surface of the Earth?)
- Solar zenith angle

3.3.2 Derived Data

The FLS algorithm needs the following upstream-derived products:

- Cloud mask output (product developed by cloud team)
- Cloud phase output (product developed by cloud team)
- Cloud Liquid Water Path (LWP) (product developed by the cloud team)

3.3.3 Ancillary Data

The following lists and briefly describes the ancillary data required to run the FLS algorithm. By ancillary data, we mean data that requires information not included in the satellite imager observations or geolocation data.

- **Relative Humidity**
  Fog/low stratus, like all water clouds are composed of water droplets formed as the moisture in the air condenses. Condensation occurs as the RH approaches 100% and the air becomes saturated. In order to identify areas with high humidity, RH information from a Numerical Weather Prediction (NWP) model is required. Accurate information on the spatial gradients of the RH is very important so NWP models with the highest spatial resolution are preferred. The enterprise FLS algorithm was developed using the Rapid Refresh (RAP) and Global Forecast System (GFS) NWP models. The RAP is not a global model so three meso-scale Rapid Refresh (RAP) domains were used to cover Alaska at a spatial resolution of 11.25 km, the continental United States (CONUS) at a resolution of 13 km and North America at a resolution of 32 km. Where the RAP was not available the GFS was used at a resolution of 0.5 deg (see Figure 6). For any given satellite point, data from the highest spatial resolution NWP model available is used. The GOES-NOP FLS algorithm was developed using 12-hour GFS forecasts initialized four times per day (0Z, 6Z, 12Z and 18Z) and 2- and 3-hour RAP forecasts initialized every hour. Although any model forecast in the 0-24 hr range is acceptable, it is highly recommended to use same model forecasts (or ones with higher spatial/temporal resolution) the algorithm was developed with. Details concerning the NWP data can be found in the AIADD Document.

- **Surface temperature**
  Relative to other cloud types, fog/low stratus has a very similar temperature as the surface. In order to identify clouds that have a similar temperature as the surface, surface temperature information from a NWP model is required. Once again, although any forecast in the 0 to 24 hour range is acceptable, it is highly recommended to use same GFS (12-hr) and RAP (2- and 3- hr) model forecasts (or

ones with higher spatial/temporal resolution) the algorithm was developed with. Details concerning the NWP data can be found in the AIADD Document.

3.3.4 Radiative Transfer Models

The following lists and briefly describes the data that must be calculated by a radiative transfer model and derived prior to running the FLS detection algorithm. See the AIADD Document for a more detailed description.

- **Clear sky transmittance profile for the 11 μm channel**
  The FLS detection algorithm requires a profile (from the surface to the Tropopause) of clear sky transmittance, where the transmittance at a given level in the profile is the upwelling clear sky transmittance integrated from that level to the top of the troposphere.

- **Clear sky radiance profile for the 11 μm channel**
  The FLS detection algorithm requires a profile (from the surface to the Tropopause) of clear sky radiance, where the radiance at a given level in the profile is the upwelling clear sky radiance integrated from that level to the top of the troposphere.

3.4 Theoretical Description

FLS detection is the process of determining the probability that pixels contain clouds with bases and/or corresponding surface visibilities that meet MVFR, IFR and LIFR requirements. The thickness of the fog/low stratus cloud is the vertical distance between the cloud base and the cloud top. The channel combination used to detect FLS depends on the solar zenith angle. At night, the FLS detection algorithm directly utilizes the 3.9 μm (GOES-NOP channel 2, ABI channel 7) and 11 μm (GOES-NOP channel 4, ABI channel 14) channels. During the day, the FLS detection algorithm directly utilizes the 0.65 (GOES-NOP channel 1, ABI channel 2), 3.9 μm (GOES-NOP channel 2, ABI channel 7), and 11 μm (GOES-NOP channel 4, ABI channel 14) channels. The central wavelength of each channel will be used throughout this document in lieu of GOES-NOP or ABI channel numbers.

3.4.1 Physics of the Problem

Fog/low stratus has the following physical properties (among others) (e.g. Pruppacher and Klett, 1997; Rogers and Yau, 1989).

- Composed mainly of liquid water
- Low cloud base
- Fog/low stratus layers are highly spatially uniform in both temperature and reflectance since vertical velocities are typically weak

- FLS has a similar temperature as the surface
- Fog/low stratus is generally composed of small droplets due to the high concentration of cloud condensation nuclei in the boundary layer and reduced collision/coalescence processes
- Low water content (primarily due to low vertical velocities).

The above physical properties allow FLS to be differentiated from other cloud types (when it is the highest cloud layer) using a combination of visible, near-infrared, and infrared observations from passive satellite sensors like the GOES-NOP imager or ABI. For instance, a common method for detecting fog/low cloud at night involves using the difference between the 11- and 3.9-μm brightness temperatures on a variety of instruments (Eyre et al. 1984; Turner et al. 1986; Ellrod 1995; Lee et al. 1997; Bendix 2002). Ellrod (2003) also used the difference between the 11 μm temperature and surface temperature at night to estimate the probability that cloud base heights were below 1000 ft, the threshold for IFR. Daytime FLS detection is more challenging due to solar contamination of the 3.9 μm channel. Cermak and Bendix (2008) address this problem by using spatial metrics and the microphysical properties of clouds to estimate cloud thickness and height to detect fog/low cloud during the day for both MODIS and SEVIRI. The final enterprise algorithm will be a quantitative, probabilistic naïve Bayesian algorithm (see section 3.4.2.2.1) based on common FLS detection methods.

3.4.2 Mathematical Description

These subsections describe in detail how the FLS detection algorithm is implemented. First, the metrics used to determine if FLS is potentially present are described.

It is important to note that the methodology used to detect FLS is solar zenith-angle dependent. At solar zenith angles < 90°, the daytime methodology is used. The nighttime methodology is used when the solar zenith angle > 90°. It should also be noted that FLS detection between solar zenith angles of 70°-90° (terminator) can be very difficult so temporal data (up to 1 hour old) is used to smoothly transition through the terminator region until the daytime methodology can again produce valid results.

3.4.2.1 FLS Property Metrics

A series of radiometric and textural metrics are used to determine which, if any, of the physical properties of FLS are present. These metrics are described in the following sections.

3.4.2.1.1 *The 3.9 μm Pseudo-emissivity*

The 3.9 – 11 μm brightness temperature difference (BTD(3.9-11 μm)) has been traditionally used to identify potential areas of fog/low cloud (e.g. Ellrod 1995). In lieu of the BTD(3.9-11 μm), we utilize the 3.9 μm pseudo-emissivity (ems(3.9 μm)) shown in Equation 1. The 3.9 μm pseudo-emissivity is simply the ratio of the observed 3.9 μm

radiance (numerator) and the 3.9 μm blackbody radiance calculated using the 11 μm brightness temperature (denominator). In Equation 1, BT is "brightness temperature" and B is the Planck Function. The 3.9 μm pseudo-emissivity is preferred over the BTD(3.9-11 μm) because it is less sensitive to the scene temperature. The ems(3.9 μm) was used previously by Pavolonis and Heidinger (2004) to infer cloud phase at night. Figure 2 shows the maximum amount of skill (see section 4.2.2.1 for details of skill score calculation) both the ems(3.9 μm) and BTD(3.9-11 μm) have when detecting fog/low clouds alone. SEVIRI data were used in this analysis. As Figure 2 shows, the ems(3.9 μm) parameter results in a greater possible skill score (blue line) when an optimal threshold of 0.7 is used compared to the optimal threshold of -7.0 for the BTD(3.9-11 μm). For the ems(3.9 μm) parameter, a maximum skill score of 0.69 can be obtained compared to 0.59 when using the BTD(3.9-11 μm), further backing up the reasoning behind using the ems(3.9 μm) parameter over the BTD(3.9-11 μm) for fog/low cloud detection.

$$ems(3.9\mu m) = \frac{R_{obs}(3.9\mu m)}{B(3.9\mu m, BT(11\mu m))} \qquad \text{Eq. 1}$$

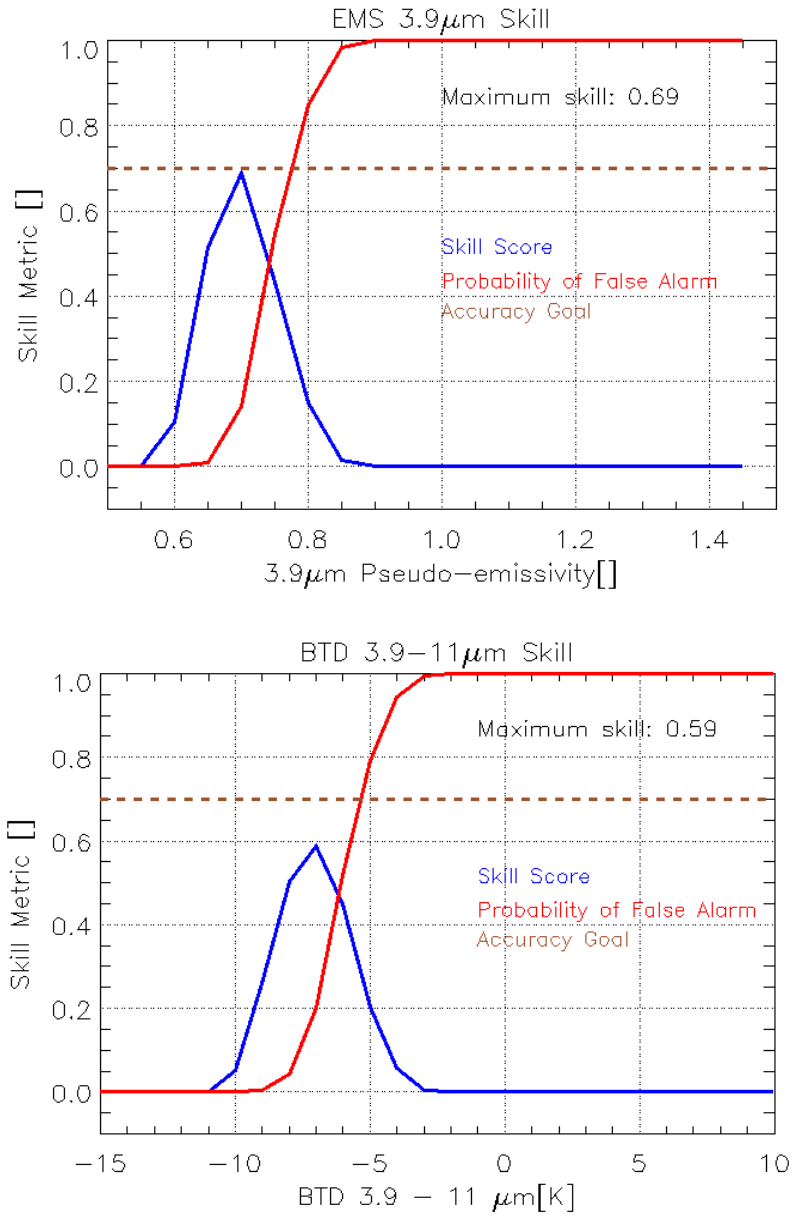

Figure 2 - The calculated skill score (blue line) obtained using the ems(3.9 μm) parameter (top) or BTD(3.9-11 μm) (bottom) when attempting to detect fog/low cloud alone. SEVIRI data were used in this analysis. The peak of the blue line represents the optimal threshold (x-axis) for each parameter, which resulted in the highest skill score. The red line represents the false alarm rate obtained using any given threshold. The dotted line represents the accuracy goal of the enterprise fog/low cloud detection algorithm.

The same skill analysis was performed using the ems(3.9 μm) and BTD(3.9-11 μm) measurements from GOES-12. The results are shown in Figure 3. Unlike with SEVIRI data, the skill results using GOES-12 data were very similar. This is because the 3.9 μm channel on SEVIRI has a significantly broader spectral width than current GOES satellites

(including the GOES-NOP and ABI) that overlaps the CO_2 absorption band near 4 μm leading to the difference in skill between the ems(3.9 μm) and BTD(3.9-11 μm). On current GOES imagers the spectral width of the 3.9 μm channel is smaller and does not overlap into the CO_2 absorption band so there is less of a difference. Although the max skill scores were very similar, and to be consistent with the SEVIRI analysis, the ems(3.9 μm) was chosen over the BTD (3.9-11 μm) because it has less sensitivities to the spectral response functions.

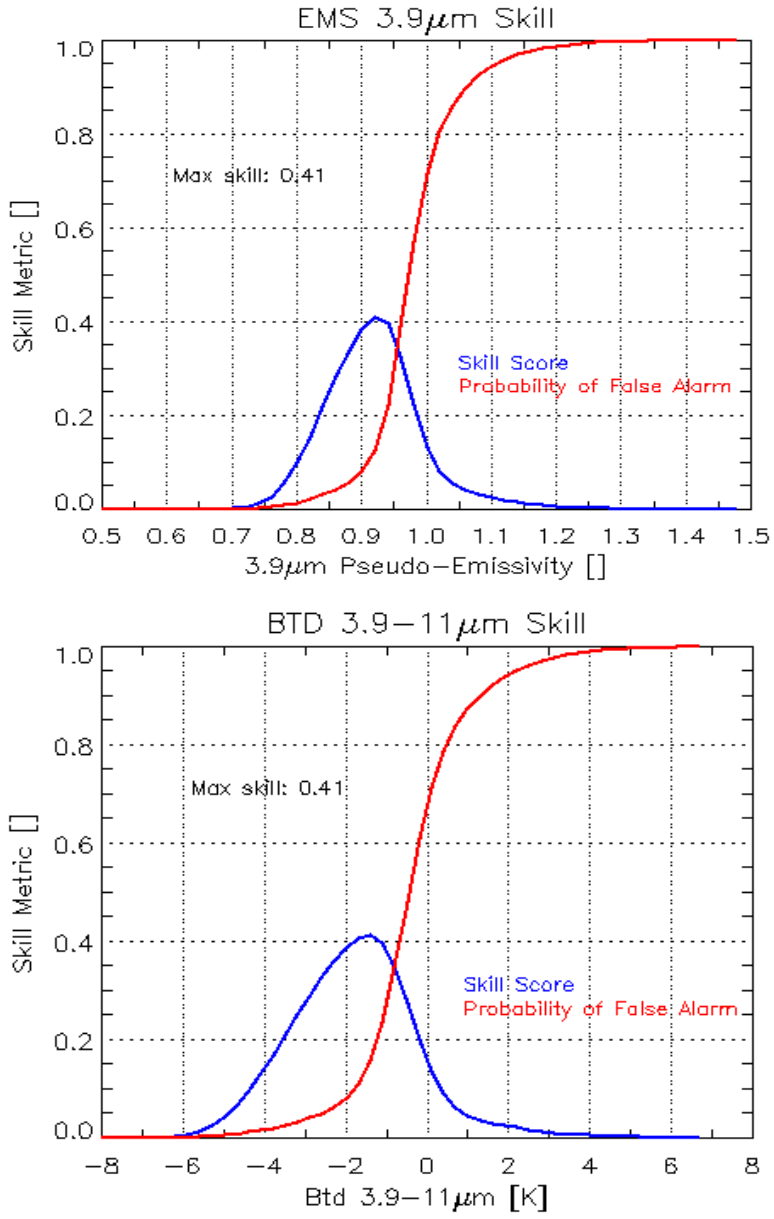

Figure 3 - The calculated skill score (blue line) obtained using the ems(3.9 μm) parameter (top) or BTD(3.9-11 μm) (bottom) when attempting to detect fog/low cloud alone. GOES-12 data were used in this analysis. The peak of the blue line represents

the optimal threshold (x-axis) for each parameter, which resulted in the highest skill score. The red line represents the false alarm rate obtained using any given threshold.

3.4.2.1.2 *Radiometric Surface Temperature Bias*

In window channels, infrared radiances can be used to retrieve the surface temperature (T_{sfc}) if the surface emissivity (ε_{sfc}), total gaseous atmospheric transmittance (t_{atm}), and the top of atmosphere upwelling clear sky atmospheric radiance (R_{atm}) are all known. The radiometric surface temperature bias can then be calculated as the difference between the modeled surface temperature (skin temperature) and the retrieved surface temperature. Equations 2 and 3 show the steps required to calculate the 11 μm surface temperature.

$$R_{sfc}(11\mu m) = \frac{R_{obs}(11\mu m) - R_{atm}(11\mu m)}{t_{atm}(11\mu m)} \qquad \text{Eq. 2}$$

$$T_{sfc}(11\mu m) = \frac{B^{-1}(11\mu m, R_{sfc}(11\mu m))}{\varepsilon_{sfc}(11\mu m)} \qquad \text{Eq. 3}$$

where $B^{-1}(\ )$ is the inverse Plank function. The radiometric surface temperature bias is then calculated using Equation 4 by taking the difference between the radiometric surface temperature and the surface temperature from an NWP model.

$$T_{bias} = T_{sfc}(11\mu m) - T_{sfc}(NWP) \qquad \text{Eq. 4}$$

In an ideal scenario, where the surface emissivity (ε_{sfc}), total gaseous atmospheric transmittance (t_{atm}), and the top of atmosphere upwelling clear sky atmospheric radiance (R_{atm}) are all known exactly and the modeled surface temperature was also correct, the radiometric surface temperature bias where clouds are not present should be very close to 0 K. However, errors in the modeled surface temperature and the variables needed to calculate the radiometric surface temperature result in biases in the radiometric surface temperature difference calculation. Heidinger and Pavolonis (2009) used Advanced Very High Resolution Radiometer (AVHRR) data to determine the bias between the retrieved 11 μm surface temperature and modeled surface temperature where clouds were not present. That study found that the biases were the greatest over land around the local solar noon (when the Sun is directly overhead), while over water the biases stayed small. This is most likely due to solar heating of the land that may not be fully accounted for in the modeled surface temperature. The same analysis performed by Heidinger and Pavolonis (2009) was replicated using GOES-12 data for a 24-hour period on July 1, 2009 and is shown in Figure 4. The biases over land again were found to be greatest (~ 6±6 K) around the local solar noon while the bias at night and over water remained relatively small (~ -2±2 K). Although currently not being taken into account, these biases may be helpful to diurnally correct the radiometric surface temperature bias for use in the fog/low cloud algorithm.

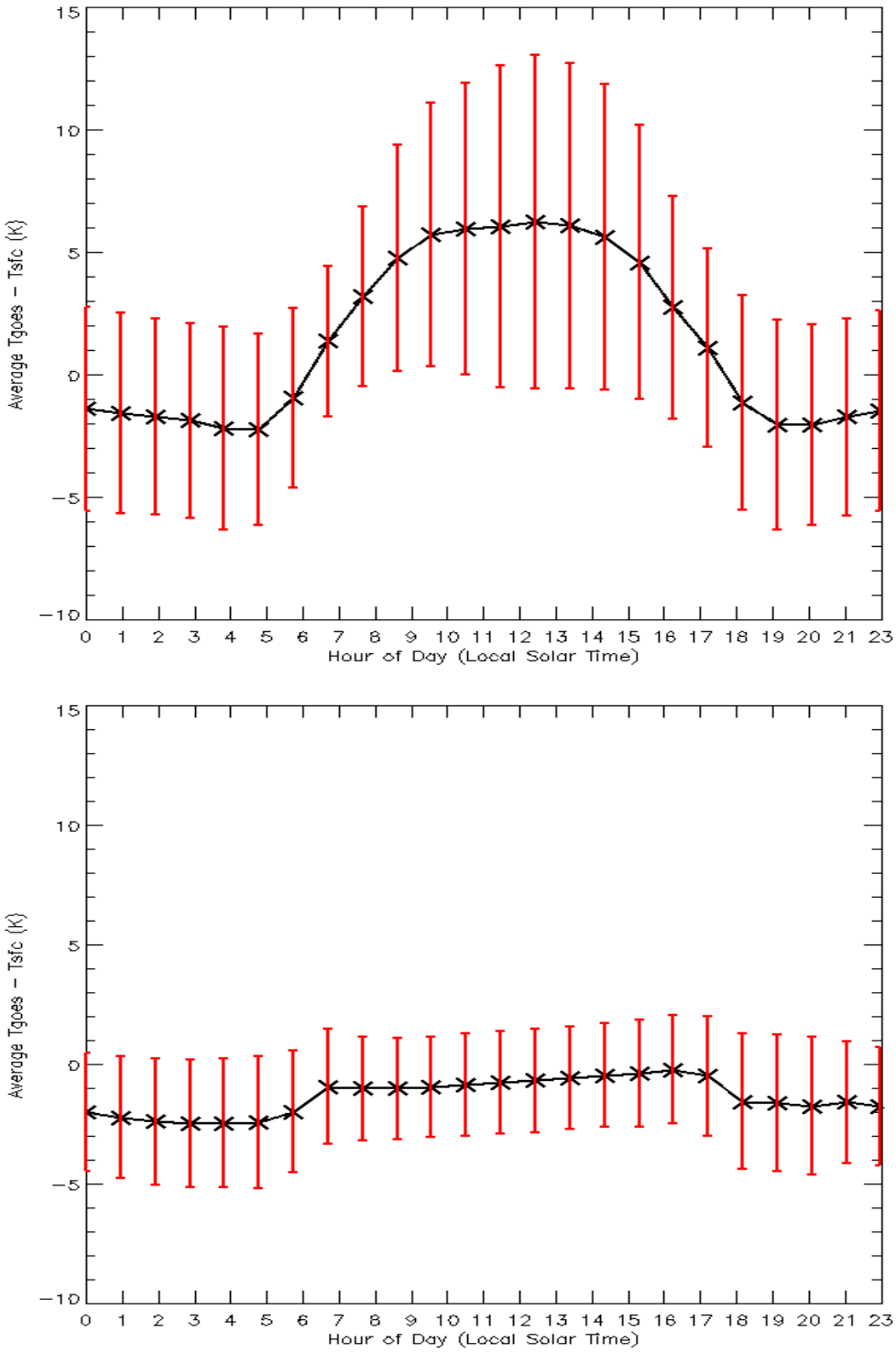

Figure 4 – 24-hour analysis of the clear sky, full disk radiometric surface temperature bias (GOES-12 11 μm retrieved temperature – modeled surface temperature) over land (top) and water (bottom) at each pixel's local solar time. The black lines and

symbols represent the average temperature difference while the red error bars represent the standard deviation.

The radiometric surface temperature bias is useful for distinguishing FLS from liquid water clouds with high bases that do not meet the fog/low cloud criteria. Fog and low stratus clouds are close to the surface and therefore should have a radiometric surface temperature that is similar to the actual surface temperature. Higher-based and non-stratus clouds tend to be colder than the surface and usually have a radiometric surface temperature that is significantly colder than the surface temperature. Ellrod (2000) used a similar metric to help identify clouds that cause Instrument Flight Rule (IFR) conditions. Figure 5 shows an example RGB image and the corresponding radiometric surface temperature bias for a GOES-13 scene over the continental United States (CONUS).

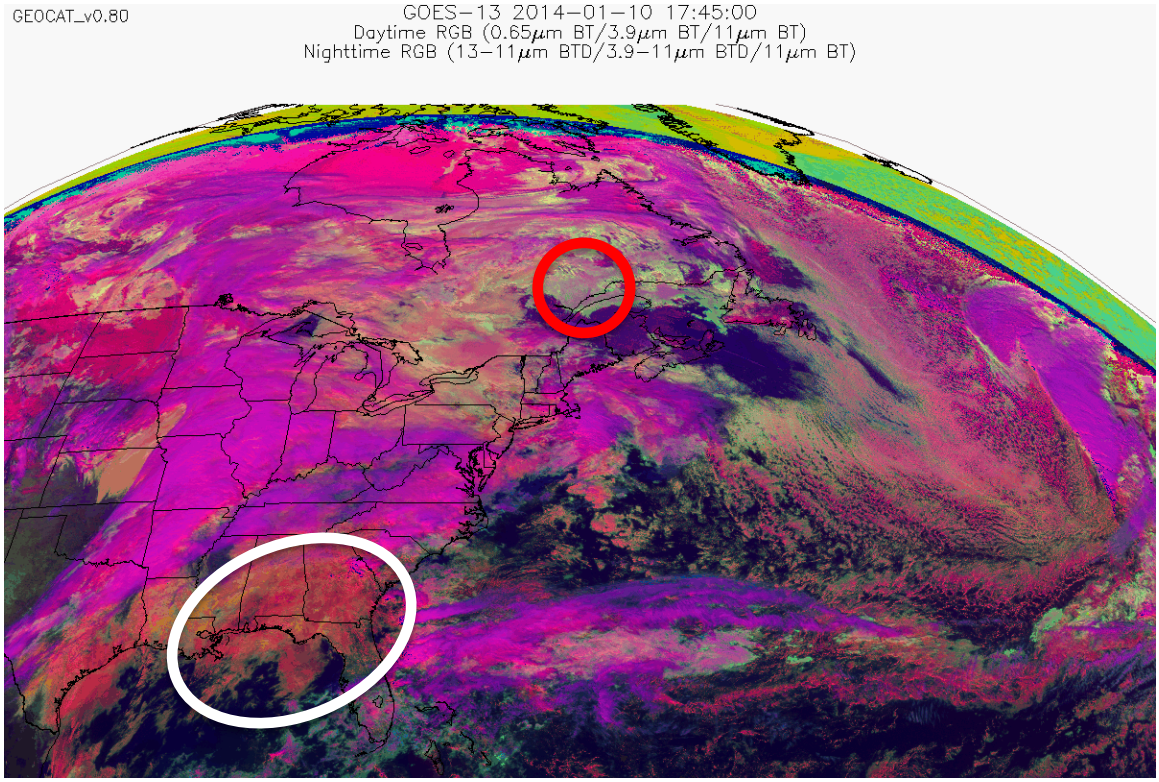

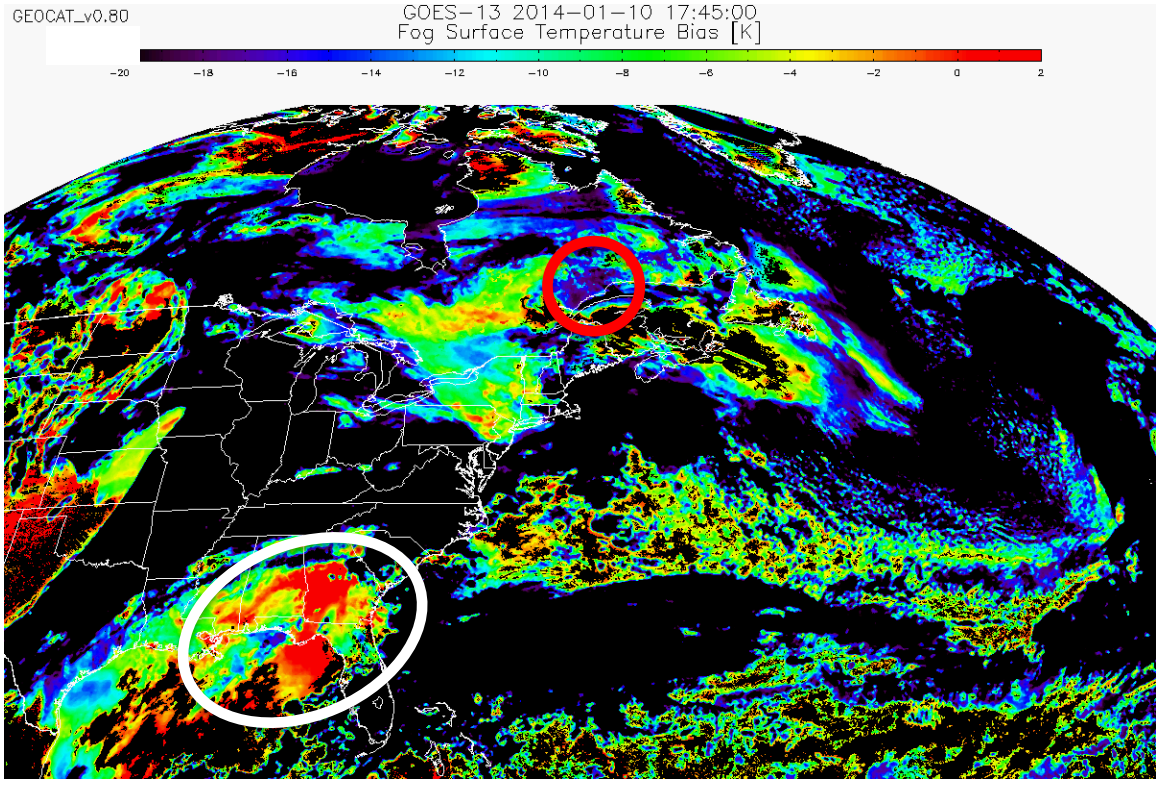

Figure 5 – GOES-13 false color image (top) using the 0.65, 3.9 and 11 μm channels (top) and corresponding radiometric surface temperature bias (bottom) calculated over CONUS from January 10, 2014 at 17:45 UTC. White-circled area shows stratus clouds with relatively low surface temperature bias meaning they are likely close to the surface. Red-circled area indicates stratus clouds with relatively large bias meaning they are not likely to be close to the surface.

In Figure 5, the areas colored in yellow to red indicate where there is clear sky or very low clouds. The blue to black areas show where higher, colder clouds are likely present.

3.4.2.1.3 *Relative Humidity*

Fog and low stratus cloud form in environments where the air is saturated and the water vapor condenses onto condensation nuclei to form water droplets. For the enterprise FLS algorithm RH data is read in from NWP models such as the GFS and RAP. Although fog is defined as a cloud with a base that touches the surface, low stratus decks that meet MVFR/IFR/LIFR criteria often have ceilings above the surface where the RH will be higher than at ground level. For this reason the modeled surface RH and RH profiles are used for the enterprise FLS algorithm. Using the RH profiles the highest RH within a 3000/1000/500 ft layer AGL are stored to help identify areas that meet MVFR/IFR/LIFR criteria respectively. An example of the maximum modeled RH in a 1000 ft layer AGL is shown in Figure 6.

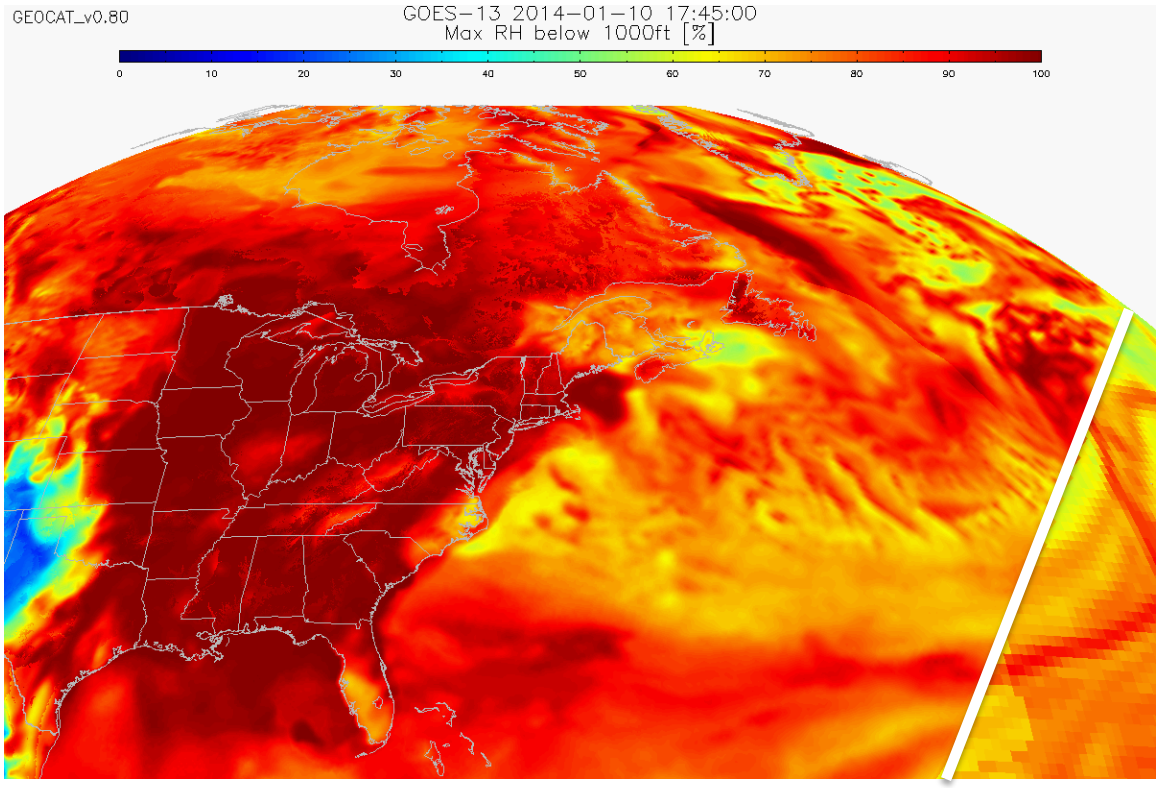

Figure 6 – Maximum modeled relative humidity within a 1000 ft layer AGL from the RAP over CONUS for January 10, 2014 at 17:45 UTC. The white line denotes the boundary of the RAP domain to the west and the GFS to the east.

3.4.2.1.4 *Spatial Uniformity*

Fog and low cloud usually form in relatively stable environments with little vertical motion. For this reason fog/low cloud tend to be spatially uniform in both temperature and reflectivity. The spatial uniformity metric is used in the FLS detection algorithm for the 0.65 μm reflectance. The spatial uniformity is determined by calculating the standard deviation of a 3x3 pixel array centered on any given pixel. The standard deviation of the 9 pixels is stored as the spatial uniformity value for the central pixel. This calculation is performed for each valid pixel in a given scene.

3.4.2.1.5 *Identifying a Pixel's Local Radiative Center*

As previously mentioned, during the daytime, FLS is generally spatially uniform in reflectance. Therefore, one of the parameters used to detect FLS during the day is the 0.65 μm reflectance spatial uniformity metric. However, using this spatial uniformity at cloud edges becomes troublesome. This is due to relatively low reflectance (unless snow/ice is present) from clear sky pixels adjacent to relatively high reflectance from cloud pixels at the cloud edge being included in the spatial uniformity calculation, causing the spatial

uniformity metric to be relatively high near cloud edges compared to one that is calculated inside a cloud but away from the edges. To address this problem, the gradient filter procedure, which is described in detail in the AIADD Document, is used to determine the Local Radiative Center (LRC) of each valid pixel. A pixel is valid if it has a valid Earth latitude and longitude and has valid spectral data (based on the L1b calibration flags). The 0.65 μm reflectance is used to compute the LRC. The gradient filter inputs (which are described in detail in the AIADD Document) for this application are listed in Table 5.

Gradient Variable	Minimum Valid Value of Gradient Variable	Maximum Valid Value of Gradient Variable	Gradient Stop Value	Apply Gradient Filter To
0.65 μm reflectance	0.0	110.0	110.0	All pixels with a valid Earth lat/lon and valid spectral data for the 0.65 μm channel

Table 5: Inputs used in calculation of Local Radiative Center (LRC). The gradient filter function used in the calculation is described in the AIADD document.

The gradient filter allows one to consult the spectral information at an interior pixel within the same cloud in order to avoid using the spectral information offered by pixels with a very weak cloud radiative signal or sub-pixel cloudiness associated with cloud edges. Overall, this use of spatial information allows for a more spatially and physically consistent product. This concept is also explained in Pavolonis (2011). Once the spatial uniformity at the LRC is performed on all pixels, a median filter is used to reduce noise in the scene. The median filter simply replaces the value at each pixel with the median value of a 3 x 3 pixel array centered on that pixel. The generic median filter procedure is described in the AIADD Document.

3.4.2.1.6 *Cloud Mask and Phase*

The enterprise FLS detection algorithm requires cloud mask and cloud phase products. During the day, the cloud mask is used to eliminate all pixels flagged by the cloud mask as being cloud free. The cloud phase is used during the day and at night to determine which pixels contain clouds composed of liquid water, clouds composed of ice or multilayered clouds. The cloud mask output is not used at night, as it was not specifically designed to detect low clouds at night. The FLS algorithm currently does not specifically look to identify ice FLS due to its rare occurrence (temperature below -30°F with a sufficient amount of water vapor), although previous analysis of ice fog events in the Yukon Territory of Canada indicate that ice fog events can be detected by the enterprise FLS algorithm because these cloud layers are often classified as mixed phase by the cloud phase algorithm. Figure 7 shows an example GOES-13 false color image and the corresponding cloud phase/type product.

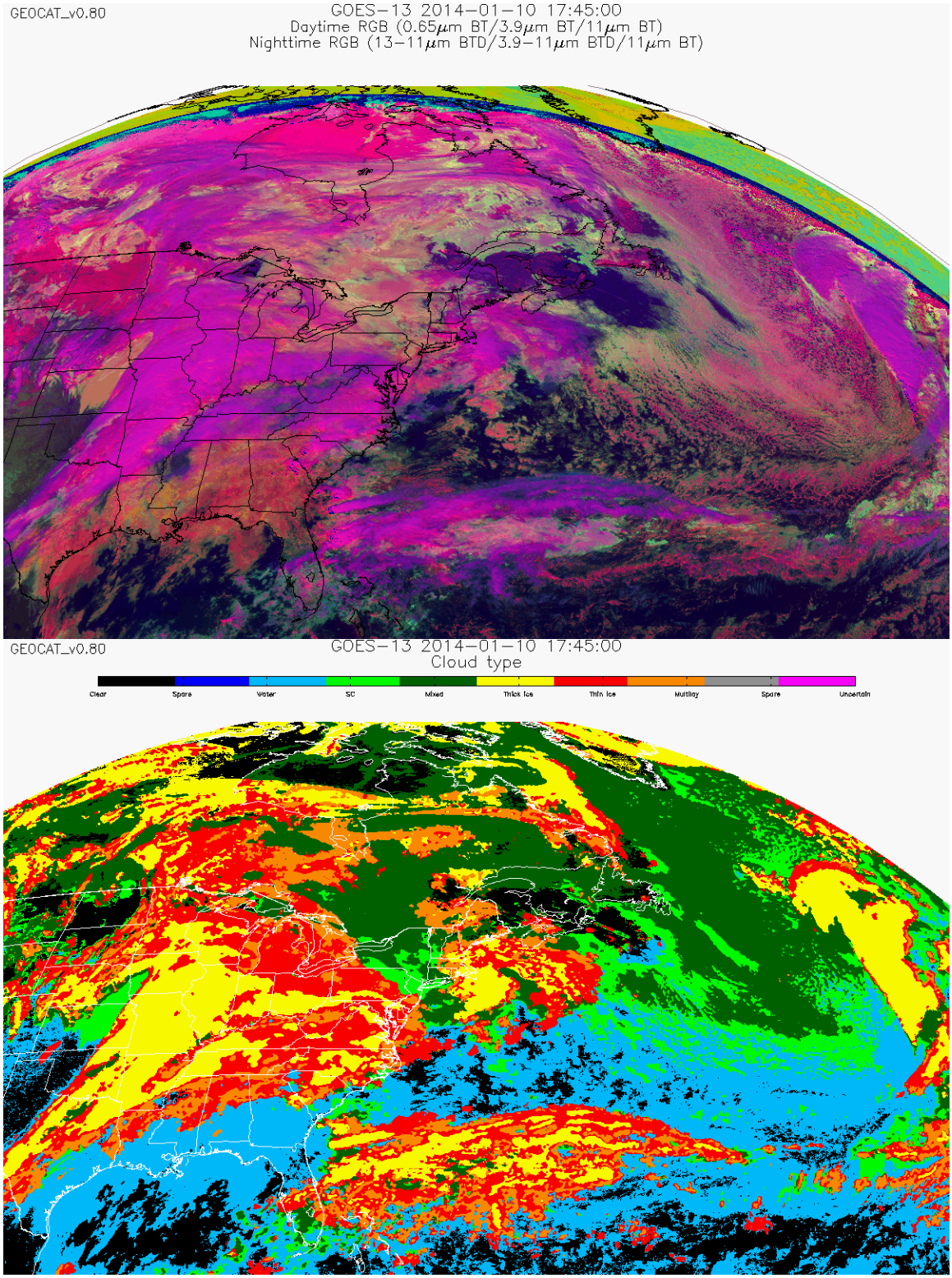

Figure 7 - GOES-13 false color image (top) using the 0.65, 3.9 and 11 μm channels with accompanying cloud type product (bottom) from the GOES-NOP cloud type algorithm. The cloud type category 'SC' refers to super cooled-type clouds. Therefore, light green areas indicate where clouds composed of super cooled water

droplets are present and light blue areas indicate where clouds composed of liquid water droplets are present.

3.4.2.2 Assessing FLS Probability

The enterprise FLS algorithm uses a "naïve Bayes" probabilistic approach to detect fog and low stratus clouds. Therefore, after the cloud mask and type check is performed the next step is to use the Bayesian model to estimate the probability that each pixel contains fog/low cloud. This is done using pre-determined look-up tables (LUT's). The naïve Bayes model and associated LUT's are described in detail in the following sections.

3.4.2.2.1 *Naïve Bayes Probabilistic Model*

The enterprise FLS algorithm utilizes a "naïve" Bayes probabilistic model and classifier (Zhang 2006; Domingos and Pazzani 1997). Wilks (2006) and Kossin and Sitkowski (2008) provide detailed descriptions of Bayes' theorem along with examples of how it can be used for meteorological applications. The discussion herein summarizes the description of the naïve Bayesian probabilistic model from Kossin and Sitkowski (2008).

The Bayes' model returns a conditional probability that an "event" will occur given a set of measureable features and can be described by the following equation.

$$P(C_{yes} \mid F) = \frac{P(C_{yes})P(F \mid C_{yes})}{P(F)} \qquad \text{Eq. 5}$$

The term $P(C_{yes})$ is the probability that the event will occur given no measured features. For a meteorological application this can be represented by a climatological probability that the event occurs. $P(F \mid C_{yes})$ represents the conditional probability that the set of features are observed given the event occurs and $P(F)$ is the probability that the set of features are observed independent of event occurrence. The conditional probabilities $P(F \mid C_{yes})$, and its counterpart $P(F \mid C_{no})$, are obtained by training the model using known data. A problem that arises with this method is that even with a relatively small number of features the calculations can become very computationally expensive, growing exponentially with respect to the number of features used. A way around this issue is to make a reasonable assumption that all the features are independent of one another. This assumption produces the "naïve" aspect of the Bayes' classifier (Kossin and Sitkowski 2008). With this assumption the term $P(F \mid C_{yes})$ can be represented by $\prod_{i=1}^{N} P(F_i \mid C_{yes})$ where F_i is a single feature of the set F and Equation 5 can be written as

$$P(C_{yes} \mid F) = \frac{P(C_{yes}) \prod_{i=1}^{N} P(F_i \mid C_{yes})}{P(F)} \quad \text{Eq. 6}$$

Due to the relationship $P(C_{yes} \mid F) + P(C_{no} \mid F) = 1$ the denominator in Equation 6 can be rewritten as

$$P(F) = P(C_{yes}) \prod_{i=1}^{N} P(F_i \mid C_{yes}) + P(C_{no}) \prod_{i=1}^{N} P(F_i \mid C_{no}) \quad \text{Eq. 7}$$

Equations 6 and 7 now represent a more computationally friendly model initially described by Equation 5.

For the enterprise FLS algorithm the "event" in the naïve Bayesian model is that FLS is present at a given pixel and the measureable features are RH, radiometric surface temperature bias, 3.9 μm pseudo-emissivity (night only), 3.9 μm reflectance (day only) and 0.65 μm reflectance spatial uniformity (day only). The MVFR/IFR/LIFR climatological 'yes' probabilities for FLS ($P(C_{yes})$) were calculated using 12 weeks of satellite data (one week for each month to cover all seasons) with collocated surface observations and are summarized in Table 6 and Table 7.

Table 6 – Climatological probabilities that MVFR/IFR/LIFR FLS is present based on GOES-13-collocated surface observations of cloud ceiling and surface visibility calculated using 12 weeks of data from 2013.

FLS Category Distinction	Climatological Probability of FLS
MVFR	0.23
IFR	0.09
LIFR	0.04

Table 7 - Climatological probabilities that MVFR/IFR/LIFR FLS is present based on GOES-16-collocated surface observations of cloud ceiling and surface visibility calculated using 12 weeks of data from 2017-2018.

FLS Category Distinction	Climatological Probability of FLS
MVFR	0.21
IFR	0.10

LIFR	0.06

To get to climatological 'no' probabilities for FLS ($P(C_{no})$) you simply subtract the climatological 'yes' probabilities from 1.0. The following sections describe in detail the LUT's that were created, or "trained", to get the conditional probabilities using these features for the naïve Bayesian model. Final results of the FLS probability output are shown in section 3.4.2.2.4.

3.4.2.2.2 *Nighttime Probability*

There are two LUT's used to determine the nighttime probability that FLS is present. The first nighttime LUT is dependent on the following two parameters:

1. 3.9 μm pseudo-emissivity (ems(3.9μm))
2. Radiometric surface temperature bias (T_{bias})

The 3.9 μm pseudo-emissivity, which was discussed in Section 3.4.2.1.1, is a key parameter in the nighttime FLS probability LUT. Low water clouds with small particles have a smaller cloud emissivity at 3.9 μm than 11 μm. In addition, FLS tends to be located in vertical layers that have a very small lapse rate, which limits the impacts of cloud transmission on the observed radiance. Thus, the 11 μm brightness temperature will be larger than the 3.9 μm brightness simply because the 11 μm cloud emissivity is greater than the 3.9 μm cloud emissivity and the impact of cloud transmission is minimal due to the small lapse rate. As such, the ems(3.9μm) is most often << 1.0 when FLS is present, and clouds that have a ems(3.9μm) << 1.0 will have a higher FLS probability. Figure 8 shows an example false color image and the corresponding ems(3.9μm) for a GOES-13 scene over CONUS. Values of ems(3.9μm) < 0.9 often correspond to areas of FLS.

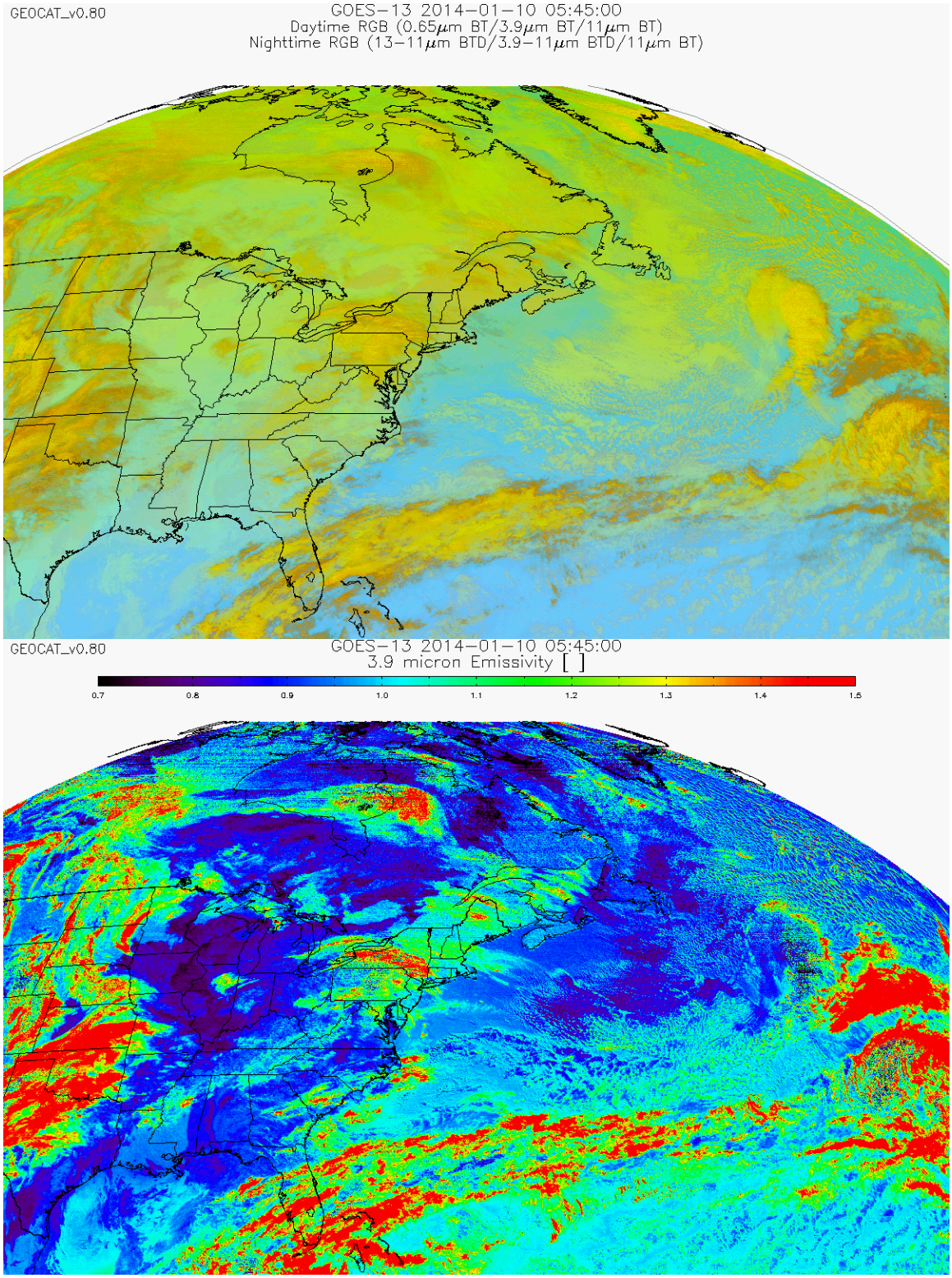

Figure 8 – GOES-13 false color image (top) using the 13-11 BTD, 3.9-11 BTD and 11 μm channels and 3.9 μm pseudo-emissivity (bottom) over CONUS on January 28, 2007 at 7:45 UTC. The darker blue to purple areas indicate relatively low 3.9 μm

pseudo-emissivities meaning they are clouds composed of small liquid water particles and might be FLS depending on their cloud ceilings.

The radiometric surface temperature bias (see Section 3.4.2.1.2) is also a predictor in the FLS probability LUT. As described earlier, FLS and low stratus clouds generally form in an isothermal or near-isothermal atmosphere with little vertical motion and vertical extent. Since fog/low stratus clouds are close to the ground the temperature of the cloud should be similar to the surface temperature. Due to the atmospheric lapse rate, clouds located above the boundary layer generally cool with respect to height; therefore cloud decks higher above the surface should be colder and thus have a larger radiometric surface temperature bias.

The second nighttime LUT is dependent on relative humidity (see Figure 6). The maximum RH within the lowest 3000/1000/500 ft layer AGL is determined from the NWP surface RH and RH profiles and is used for the RH metric. As the modeled RH increases the probability that FLS is present also increases. In Figure 9, this relationship is illustrated as the probability that FLS is present in a given pixel increases rapidly as the RH increases above about 70%.

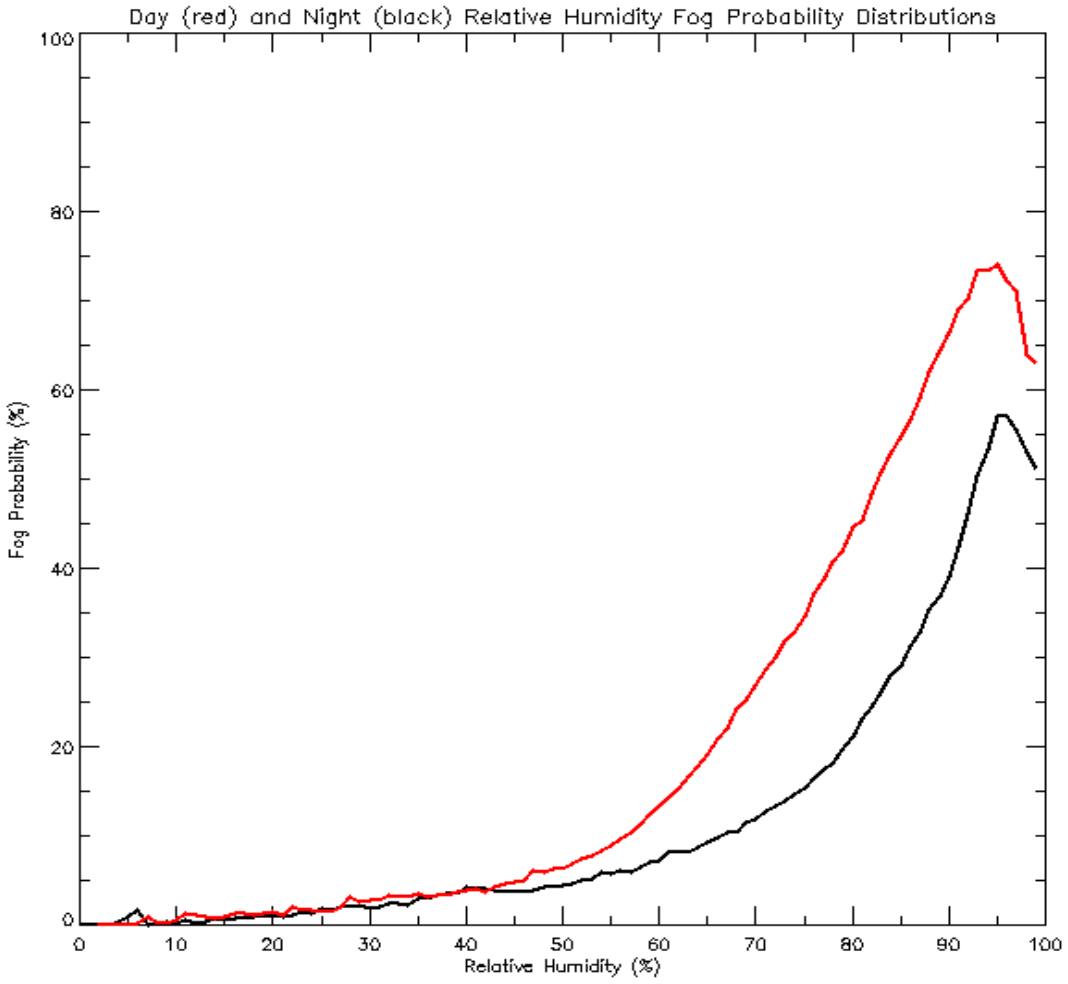

Figure 9 – Probability that fog/low stratus is present during day/night (red/black) given the modeled relative humidity. Surface observations of cloud ceiling and surface visibility were used to determine whether fog/low stratus was present.

The two LUT's described above must be created, or "trained", separately for MVFR, IFR and LIFR conditions and for each NWP model. Therefore three sets of LUT's are needed for both the GFS and RAP.

3.4.2.2.2.1 Nighttime FLS Probability LUT's

Using the parameters described above in section 3.4.2.2.2, two sets of LUT's were created to estimate the probability that fog/low stratus clouds are present given a pixel's spectral information and modeled RH. Each set is used to determine the probability that MVFR, IFR and LIFR conditions are present. Twelve weeks of GFS, RAP and GOES-13 data (one week for each month of 2013) along with collocated surface observations (see section 4.1.3 for information about source and accuracy) were used to create the GOES-NOP LUT's. Twelve weeks of GFS, RAP and GOES-16 data (one week for each month of 2017-2018) along with collocated surface observations were used to create the ABI LUT's. Surface observations of cloud ceiling and surface visibility were used to identify pixels that met MVFR, IFR and LIFR criteria. These LUT's represent the conditional probabilities that a pixel's spectral information and modeled RH are measured given that FLS is and is not present. These conditional probabilities are used by the naïve Bayesian model to calculate the final probability that FLS is present at a given pixel. Once again, it is important to note that in order for the naïve Bayesian model to work properly the probability that a pixel's spectral information and modeled RH are measured given that FLS is present ($P(F \mid C_{yes})$) and also the probability given that FLS is not present ($P(F \mid C_{no})$) are needed.

The first LUT is two-dimensional with respect to ems(3.9μm) and surface temperature bias. The surface temperature bias is separated into 22 bins ranging from -20 K to 0 K with a bin size of 1 K. The first bin contains all values that are less than -20 K and the last bin is for all values greater than 0 K. The 3.9 μm pseudo-emissivity is separated into 15 bins ranging from 0.80 to 1.06 with a bin size of 0.02. Again, the first bin contains all values less than 0.80 and the last bin contains all values greater than 1.06. This results in a 2x15x22 bin array LUT where the first 15x22 array stores the 'conditional yes' probabilities and the second 15x22 array stores the 'conditional no' probabilities. All pixels with a collocated surface observation for the sample period were separated into their respective bin depending on their pseudo-emissivity and surface temperature bias. A count of surface observations that indicated FLS or no FLS was recorded for each bin and used to calculate the conditional probabilities (2 sets of probabilities - 'conditional yes' and 'conditional no') that specific values of a pixel's 3.9 μm pseudo-emissivity and surface temperature bias information were measured when fog/low stratus was or was not found to be present. The impacts of the conditional probabilities alone are difficult to fully-understand by simply illustrating them. The actual values of the conditional probabilities are not really apparent until the Bayesian model combines them all together. For this reason, instead of showing

the conditional probability LUT's, the ratio of the IFR conditional yes/no probabilities for given a pixel's measured 3.9 μm pseudo-emissivity and surface temperature bias information (see Figure 10) is illustrated to show which values are generally associated with a higher probability of FLS. Again, the ratio that is shown is **not** a conditional probability (probability that the features' measured values are seen when FLS is present or is not present) used in the naïve Bayesian model, but rather a ratio of the yes/no conditional probabilities given the measured features.

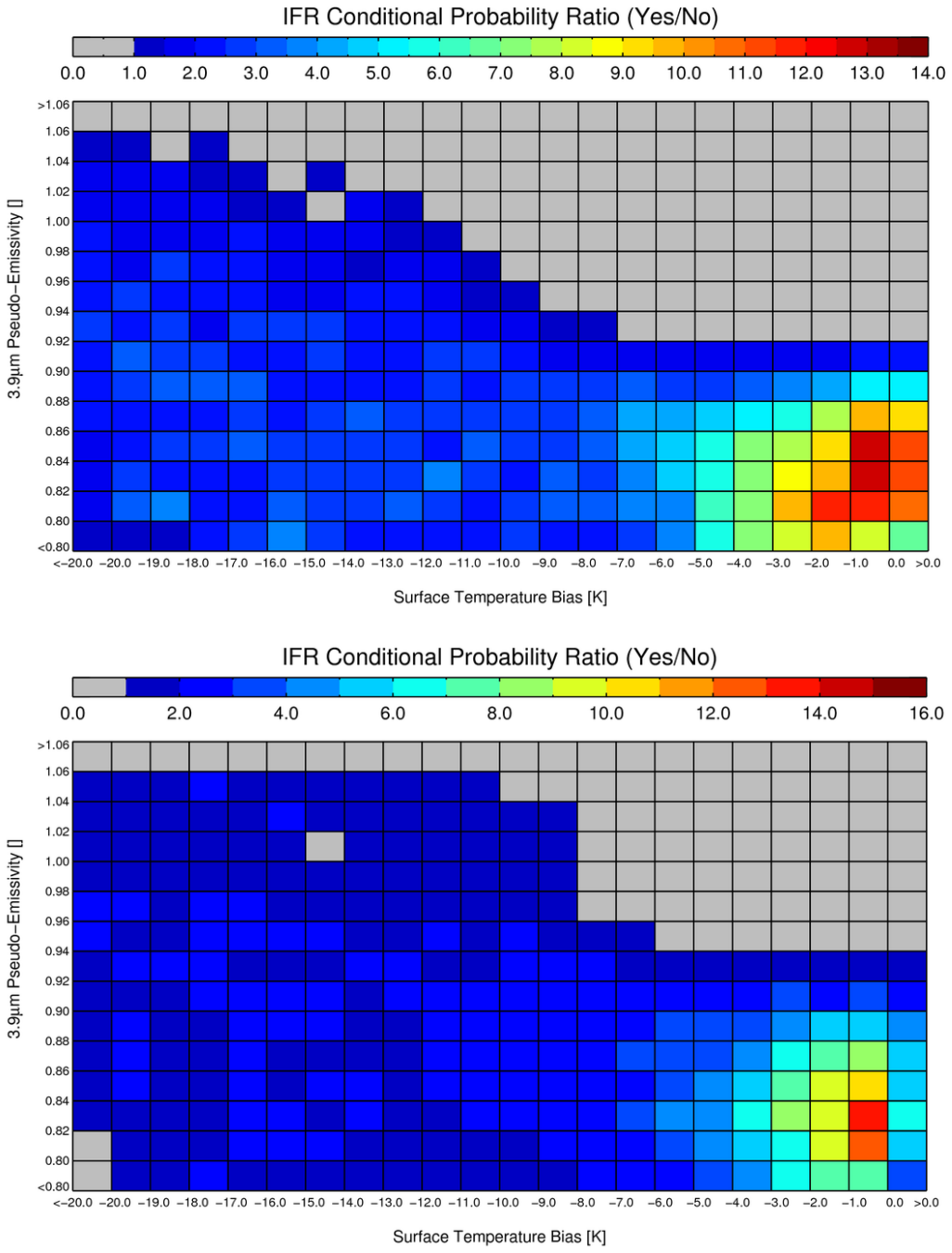

Figure 10 – Ratio of the nighttime IFR yes/no conditional probabilities depending on the 3.9 µm pseudo-emissivity and radiometric surface temperature bias for GOES-NOP (top) and ABI (bottom). Surface observations of cloud ceiling and surface visibility were used to determine whether fog/low stratus, in this case IFR conditions, were present.

The second LUT is one dimensional with respect to RH. The maximum RH in the lowest 3000/1000/500 ft layer AGL from the NWP surface RH and RH profiles is separated into 100 bins ranging from 0-100 % with a bin size of 1 %. Once again a count of surface observations that indicated FLS or no FLS was recorded for each bin and used to calculate the conditional probabilities that specific values of a pixel's RH was modeled when fog/low cloud was or was not determined to be present. Once again, instead of the conditional probabilities, the ratio of the IFR yes/no conditional probabilities is illustrated in Figure 11 to show which values of RH are generally associated with a higher probability of FLS.

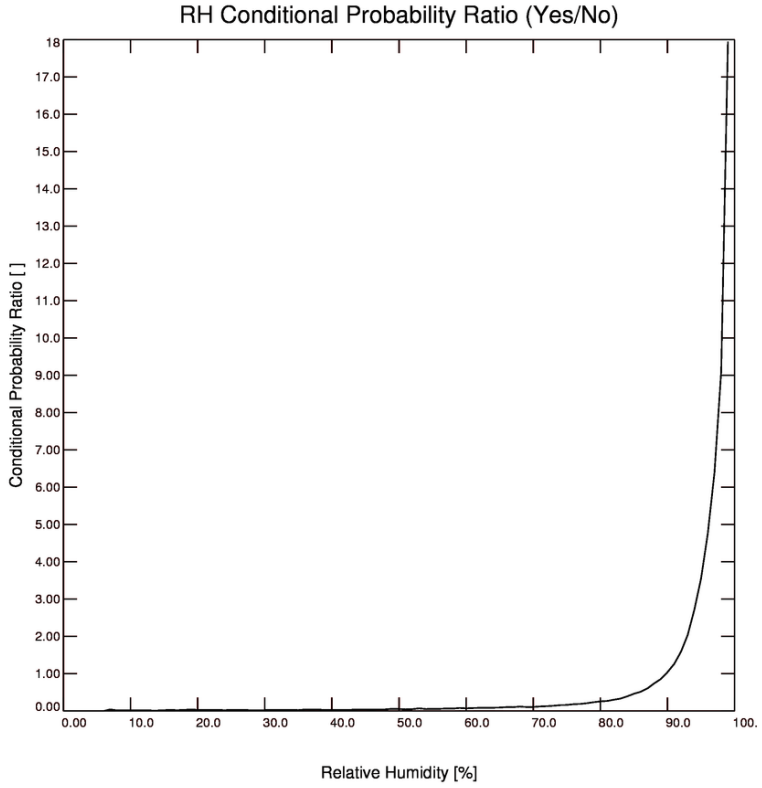

Figure 11 – Ratio of the IFR conditional yes/no probabilities from the modeled relative humidity. Surface observations of cloud ceiling and surface visibility were used to determine whether fog/low stratus, in this case IFR conditions, were present.

3.4.2.2.3 *Daytime Probability*

Like nighttime, two LUT's are used during the day. The first daytime LUT used to estimate the probability that fog/low cloud is present is dependent on the following three parameters:

1. 3.9 μm reflectance
2. 0.65 μm reflectance spatial uniformity at the LRC
3. Radiometric surface temperature bias

As previously discussed, fog/low stratus clouds tend to be spatially uniform in 0.65 µm reflectance. This is because FLS and low stratus clouds form in relatively stable environments with little vertical motion. This is in contrast to cumulus clouds that form in unstable environments with large spatial variations in vertical motion creating the puffy, bubbly texture seen in the visible satellite channels. The 3x3 (pixel array) 0.65 µm reflectance spatial uniformity calculation at the LRC, paired with the radiometric surface temperature bias, can be used to identify pixels that are located in a low cloud that is spatially uniform in reflectance, and therefore have a higher probability of being a stratus cloud meeting MVFR/IFR/LIFR criteria. The 0.65 µm reflectance spatial uniformity metric is available for solar zenith angles less than 85° and, along with the radiometric surfaced temperature bias, is smoothed using a median filter to remove noise before use. The median filter simply replaces the value at each pixel with the median value of a 3 x 3 pixel array centered on that pixel. The generic median filter procedure is described in the AIADD Document. Figure 12 shows an example false color image, the 3.9 µm reflectance and smoothed 0.65 µm reflectance spatial uniformity at the cloud LRC for a GOES-13 scene over CONUS. FLS clouds usually consist of smaller water droplets (except for ice fog) compared to higher liquid water cloud layers. Smaller water droplets have a higher reflectivity at 3.9 µm than larger droplets (see Figure 12). Therefore, the 3.9 µm reflectance is used to help identify clouds that are composed of smaller droplets.

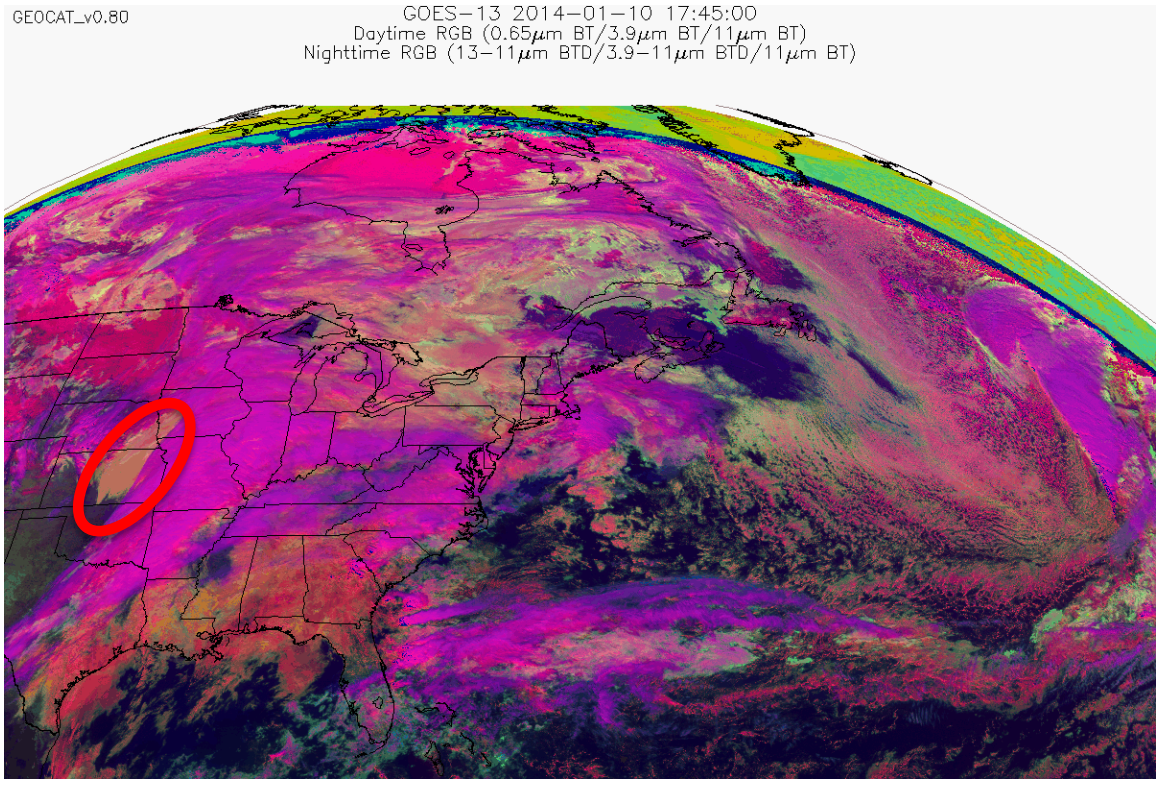

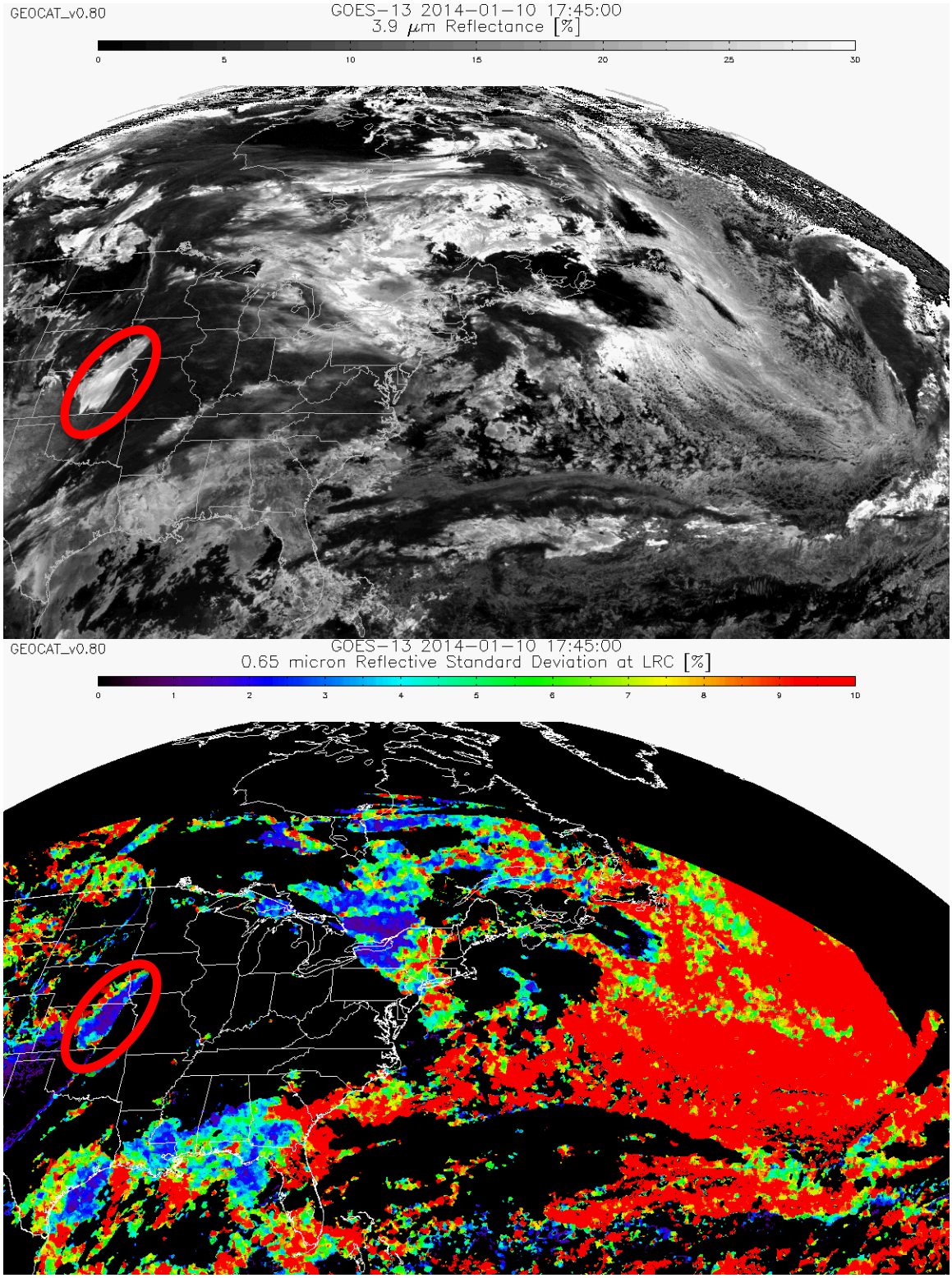

Figure 12 – False color image (top), 3.9 μm reflectance (middle) and the 3x3 pixel 0.65 μm reflectance spatial uniformity at the LRC (bottom) calculated for a GOES-13 scene over CONUS on January 10, 2014 at 17:45 UTC. Circled area represents cloud

with relatively high 3.9 μm reflectance and relatively low 0.65 spatial uniformity meaning it should have a high probability of being FLS.

The second daytime LUT is the same as the nighttime LUT based solely on the maximum RH within the lowest 3000/1000/500 ft layer AGL.

The two LUT's described above must be created, or "trained", separately for MVFR, IFR and LIFR conditions and for each NWP model. Therefore three sets of LUT's are needed for both the GFS and RAP.

3.4.2.2.3.1 Daytime Fog/Low Cloud Probability LUT

Using the parameters described above, two sets of two LUT's were created to estimate the probability that MVFR/IFR/LIFR FLS is present during the day. Twelve weeks of modeled RAP, GFS and GOES-13 data (one week for each month of 2013) along with collocated surface observations were used to create the GOES-NOP LUT's. Twelve weeks of modeled RAP, GFS and GOES-16 data (one week for each month of 2017-2018) along with collocated surface observations were used to create the ABI LUT's. Again, surface observations of cloud ceiling were used to identify pixels that contained fog/low cloud meeting MVFR/IFR/LIFR conditions.

The 3.9 μm reflectance is separated into 4 bins (0-10, 10-15, 15-20, >20) with varying size in order to capture the most detail or the clouds of interest. The surface temperature bias is separated into 22 bins ranging from -20 K to 0 K with a bin size of 1 K. The first bin contains all values that are less than -20 K and the last bin is for all values greater than 0 K. The 0.65 μm reflectance spatial uniformity is separated into 11 bins ranging from 0.0 to 20.0 with a bin size of 2.0. The last bin contains all values greater than 20.0. This results in a 2x4x11x22 bin array LUT where the first 4x11x22 array stores the 'conditional yes' probabilities and the second 4x11x22 array stores the 'conditional no' probabilities. All pixels with a collocated surface observation for the sample period were separated into their respective bin depending on their 3.9 μm reflectance, 0.65 μm reflectance spatial uniformity and surface temperature bias. A count of surface observations that indicated FLS or no FLS was recorded for each bin and used to calculate the conditional probability that specific values of a pixel's spectral, spatial and surface temperature bias information were measured when fog/low stratus was or was not found to be present. As previously noted, the impacts of the conditional probabilities alone are difficult to fully-understand by simply illustrating them as the true values of the conditional probabilities are not really apparent until the Bayesian model combines them all together. For this reason, instead of showing the conditional probability LUT's, the ratio of the IFR conditional yes/no probabilities for given a pixel's measured 3.9 μm reflectance, 0.65 μm reflectance spatial uniformity and surface temperature bias information (see Figure 13) is illustrated to show which values are generally associated with a higher probability of FLS. Again, the ratio that is shown is **not** a conditional probability (probability that the features' measured values

are seen when FLS is present or is not present) used in the naïve Bayesian model, but rather a ratio of the yes/no conditional probabilities given the measured features.

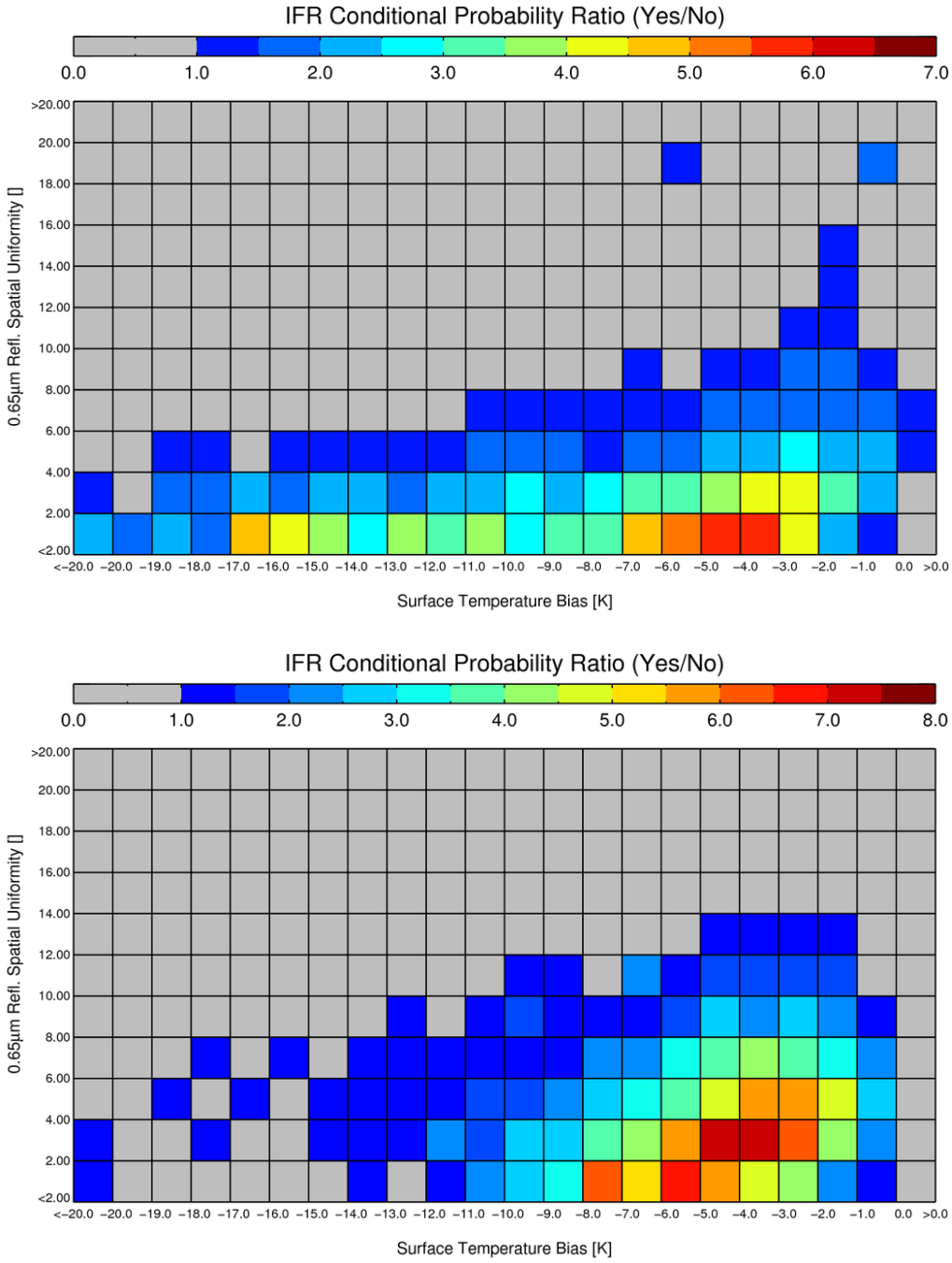

Figure 13 – Ratio of the daytime IFR yes/no conditional probabilities for pixels with 3.9 µm reflectance values between 15-20 % dependent upon the 0.65 µm reflectance spatial uniformity and radiometric surface temperature bias for GOES-NOP (top) and ABI (bottom). Surface observations of cloud ceiling and surface visibility were used to determine whether fog/low stratus, in this case IFR conditions, were present.

The second daytime LUT is the same as the nighttime LUT based solely on the maximum RH within the lowest 3000/1000/500 ft layer AGL (Figure 11).

3.4.2.2.4 *Naïve Bayesian FLS Probabilities*

Once the LUT's are trained the naïve Bayesian MVFR, IFR and LIFR probabilities can be calculated using the naïve Bayesian model and LUT's described above. A median filter is used to smooth out any noise in the probabilities. The median filter simply replaces the value at each pixel with the median value of a 3 x 3 pixel array centered on that pixel. The generic median filter procedure is described in the AIADD Document. An example of the IFR FLS probability output from the enterprise FLS algorithm for a GOES-13 daytime scene is shown in Figure 14.

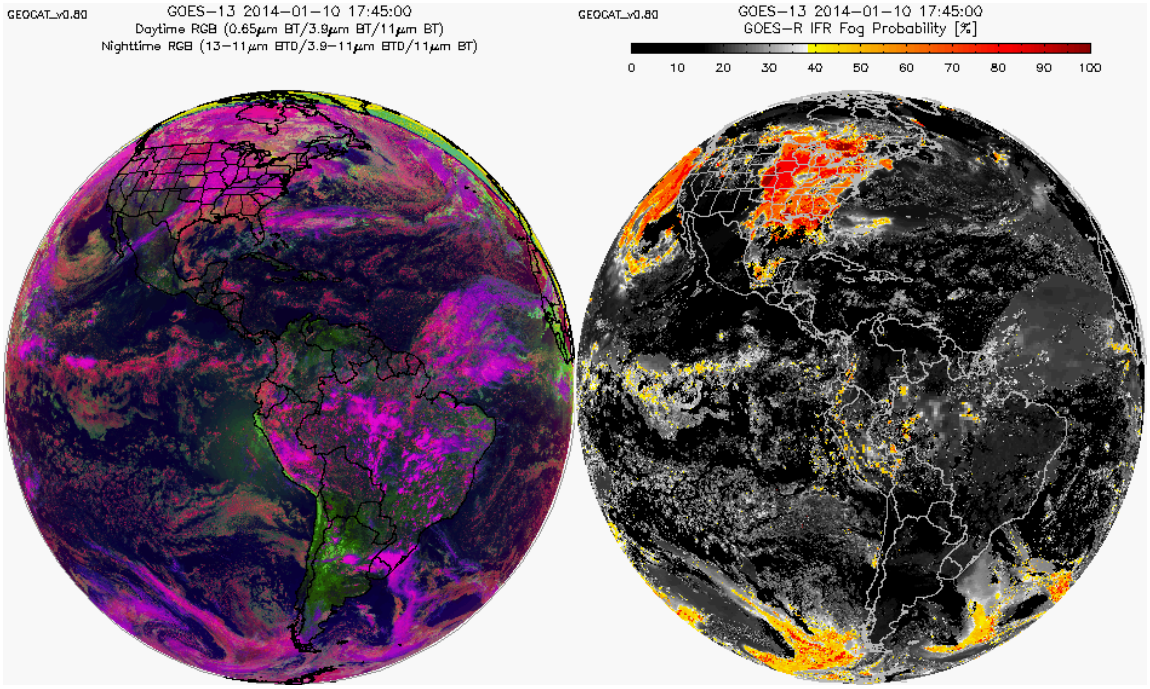

Figure 14 - GOES-13 false color image (left) using the 0.65, 3.9 and 11 μm channels with accompanying daytime IFR FLS probabilities (right) over CONUS on January 10, 2014 at 17:45 UTC.

Figure 15 shows the same scene as Figure 14 above, zoomed in over the eastern CONUS. Surface observations in the false color image are color-coded to correspond to the following flight rule categories they report: VFR (green), MVFR (blue), IFR (yellow), LIFR (magenta). The MVFR/IFR/LIFR probabilities also contain surface observations with the same basic color code, however, for each probability product the magenta colored observation points represent those stations reporting the category of interest, or below. For

example, the magenta-colored surface observations on the IFR probability image represent surface stations reporting IFR or LIFR conditions.

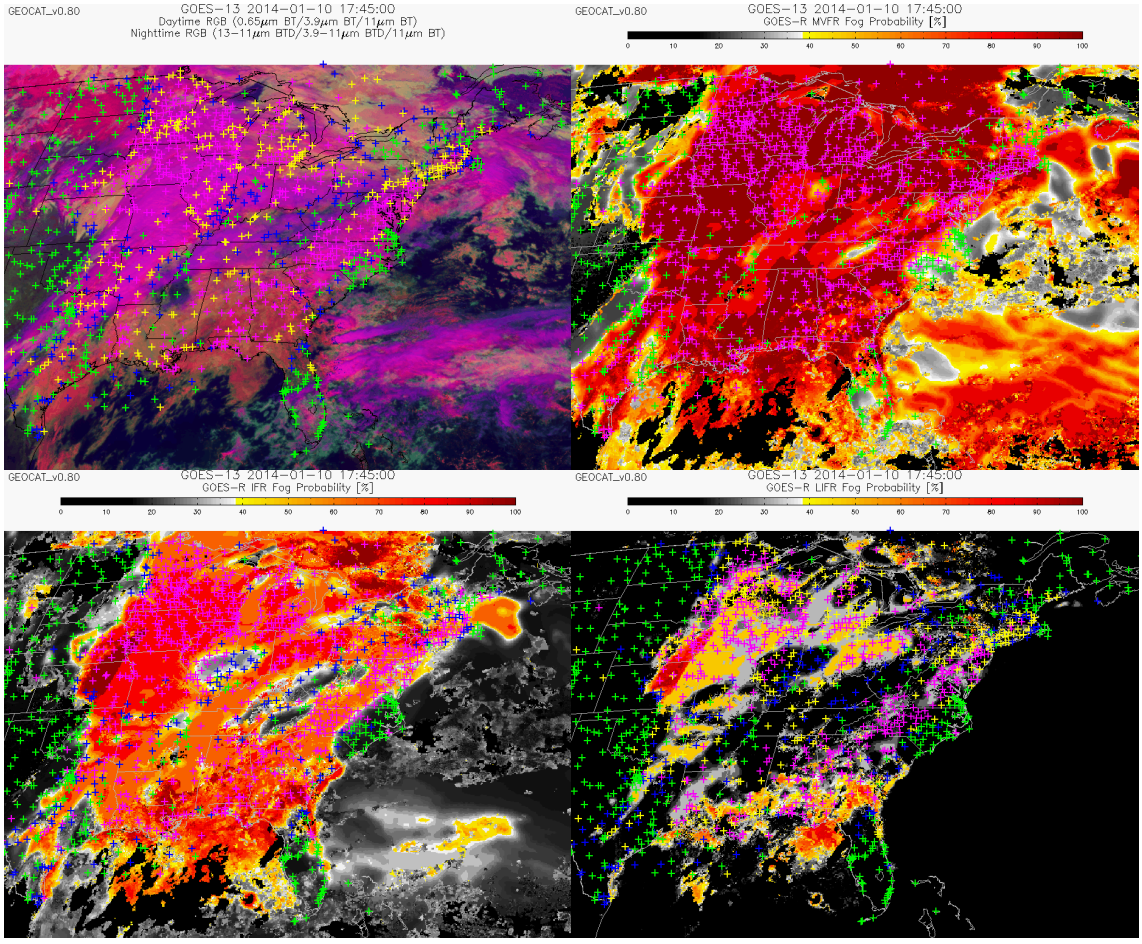

Figure 15 - GOES-13 false color image (top left) using the 0.65, 3.9 and 11 μm channels with accompanying daytime MVFR FLS probabilities (top right), IFR FLS probabilities (bottom left) and LIFR FLS probabilities (bottom right) over CONUS on January 10, 2014 at 17:45 UTC. In the false color image, 'crosses' are colored-coded to the following aviation flight rule categories representing surface observations: VFR (green), MVFR (blue), IFR (yellow), LIFR (magenta). For the 3 probability images the surface observations colored magenta represent stations that report the category being detected, or lower.

An example of the IFR FLS probability output from the enterprise FLS algorithm for a GOES-13 nighttime scene is shown in Figure 16.

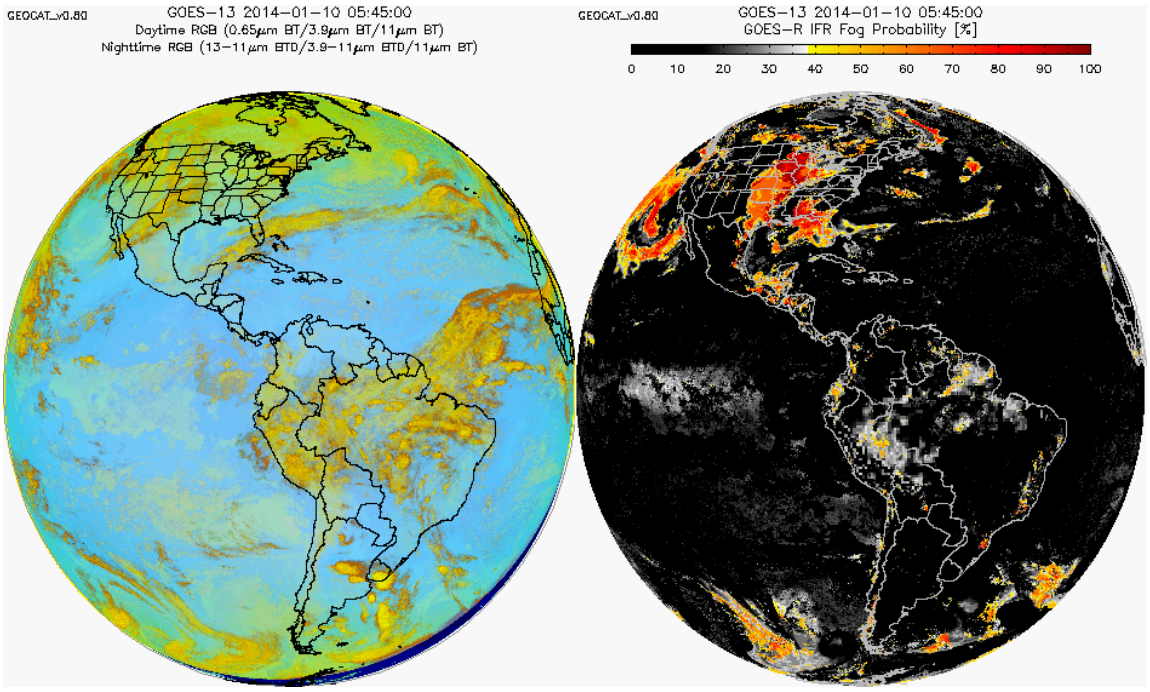

Figure 16 - GOES-13 false color image (left) using the 13-11 μm BTD, 3.9-11 μm BTD and 11 μm channels with the nighttime GOES-NOP IFR FLS probabilities (right) over CONUS on January 10, 2014 at 05:45 UTC.

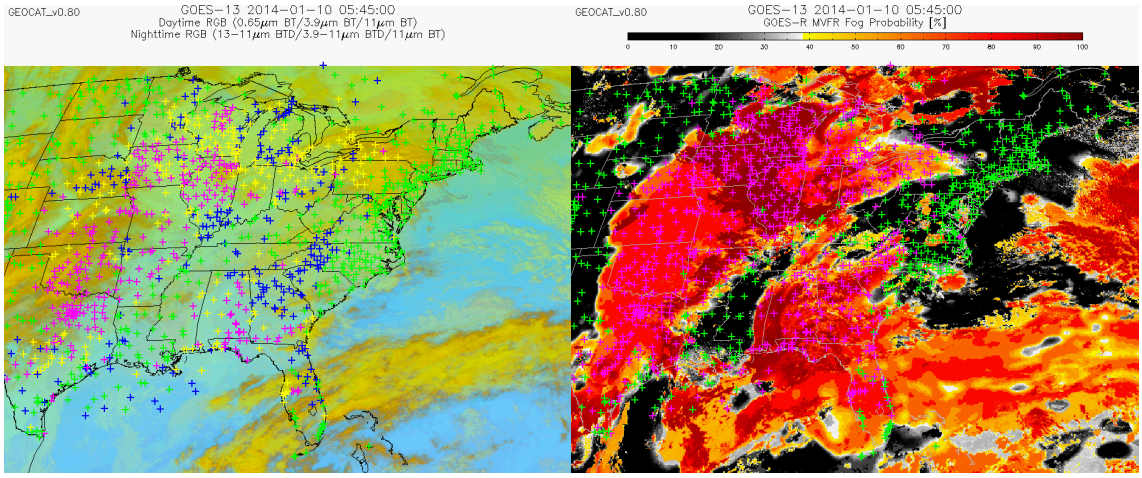

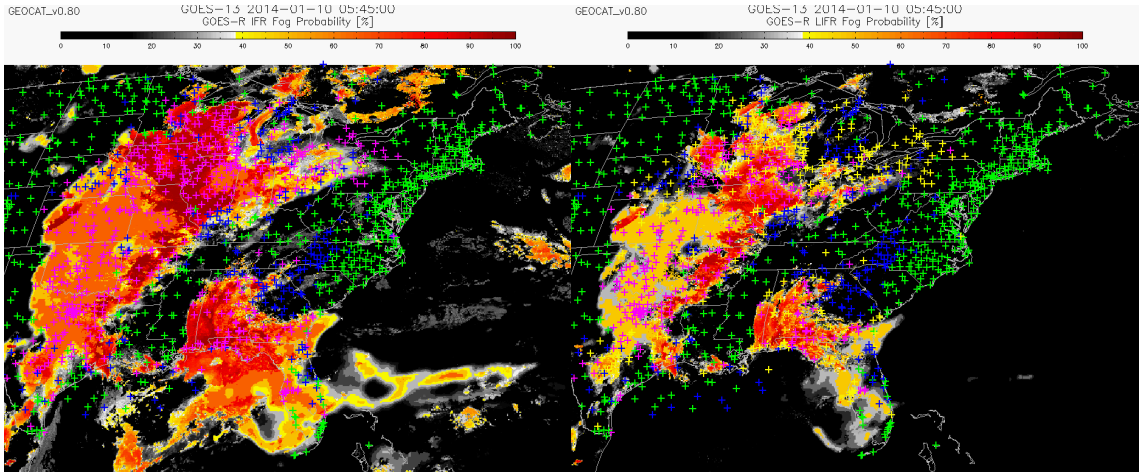

Figure 17 - GOES-13 false color image (top left) using the 13-11 μm BTD, 3.9-11 μm BTD and 11 μm channels with accompanying nighttime MVFR FLS probabilities (top right), IFR FLS probabilities (bottom left) and LIFR FLS probabilities (bottom right) over CONUS on January 10, 2014 at 05:45 UTC. In the false color image, 'crosses' are colored-coded to the following aviation flight rule categories representing surface observations: VFR (green), MVFR (blue), IFR (yellow), LIFR (magenta). For the 3 probability images the surface observations colored magenta represent stations that report the category being detected, or lower.

Figure 15 and Figure 17 show that although the enterprise probability products do not perfectly match the surface reports the higher probabilities for each category do correspond well to areas where surface reports indicate those conditions are present and the lower probabilities correspond well to areas where reports to not meet the given flight rule criteria. When ice or multilayered clouds are present the satellite metrics are not used in the Bayesian calculation so only the modeled RH parameter is used to calculate the probability. If the modeled RH data do not properly pick up on a low cloud layer the probabilities may result in unexpectedly low values since there is no satellite data that may otherwise help boost probabilities. This type of issue is seen mostly in the LIFR probabilities where only the lowest 500 ft AGL layer is queried for the maximum RH. This layer is very thin compared to the vertical resolution of the NWP profiles and therefore the accurate representation of the RH can sometimes be difficult, especially with varying terrain, to obtain. This issue can be seen along the east coast in the LIFR probabilities from Figure 15. Ice clouds are present over the Appalachian mountain chain from Georgia north to New York. The cloud type algorithm in Figure 7 verifies the presence of ice clouds. In this case the low level RH is not accurately accounted for leading to erroneously low LIFR probabilities. When ice and multilayered clouds are not present the satellite metrics can be used and usually result in more accurate probabilities.

It should be noted that detecting FLS near the terminator (solar zenith angles between 70°-90°, called the 'terminator region' herein) is difficult due to high solar zenith angles. For instance, the daytime cloud mask sometimes has trouble identifying low water clouds in the terminator region. Another reason is the daytime radiometric parameters are not

accurately available when solar zenith angles are between 85°-90°, which prohibits the determination of the probability that FLS is present. For these reasons, temporal information is used to make the transition through the terminator region more consistent. The enterprise FLS algorithm uses previous data up to one hour old to assist in the calculation of FLS probability in the terminator region. Large-scale areas of FLS generally do not change (dissipate or grow) drastically in the span of an hour, so using temporal data to assist is a logical solution until the full day/night enterprise FLS algorithm can once again produce probabilities with better accuracy.

Temporal data is used differently depending on solar zenith angle of a given pixel inside the terminator region. For the enterprise FLS algorithm the terminator region is split into three zones defined by solar zenith angle. The first zone contains all pixels with solar zenith angles between 70°-80°. As previously mentioned, due to the high sun angle the detection of low water clouds by the cloud mask is occasionally problematic. The daytime portion of the FLS algorithm relies on the cloud mask for cloud detection at solar zenith angles less than 80° so if clouds are not detected the FLS probabilities will not be calculated for those pixels. To ensure a probability is calculated for all daytime cloudy pixels temporal cloud type (contains cloud mask information) and IFR probability data area used. For a given pixel, if the cloud type from the last valid time step was an ice cloud the current cloud type remains ice. If the previous IFR probability was greater than 30% and the current cloud type is 'clear', the current cloud type is changed to a water cloud. If the previous IFR probability was less than 30% no change is made to the cloud type product. These checks are performed to maintain consistency of the FLS products through the terminator region. Once the cloud type adjustment is made the current refl(3.9μm), stddev(0.65μm), T_{bias} and low-level RH data are used to determine the probability that FLS is present for a given pixel.

The second zone in the terminator region contains all pixels with solar zenith angles between 80°-85°. The cloud mask is no longer used for cloud clearing for solar zenith angles greater than 80°. In this region, temporal IFR probability information is used to determine pixels that current FLS probabilities are calculated for. The enterprise FLS algorithm only determines a current FLS probability for pixels where the previous IFR probability was greater than 30%. The calculations are performed on those pixels using current refl(3.9μm), stddev(0.65μm), T_{bias} and low-level RH data. For pixels that had previous IFR probabilities less than 30% the IFR probability is set to the previous temporal IFR probability to maintain consistency.

The third zone in the terminator region is defined by solar zenith angles between 85°-90°. The enterprise FLS algorithm determines the FLS probability in this zone differently depending on whether the terminator is transitioning from night-to-day or vice versa. When the transition transistions from night-to-day the nighttime probability detection methodology is applied using current T_{bias} and low-level RH data and temporal ems(3.9μm) data from the last valid time step. When the transition is from day-to-night the daytime probability detection methodology is applied using current T_{bias} and low-level RH data and

temporal refl(3.9μm) and stddev(0.65μm) data. The T_{bias} and low-level RH data are independent of solar zenith angle so current data from those parameters are always used.

An example of the FLS probability outputs from the enterprise FLS algorithm for a GOES-13 terminator scene over the eastern CONUS is shown in Figure 18.

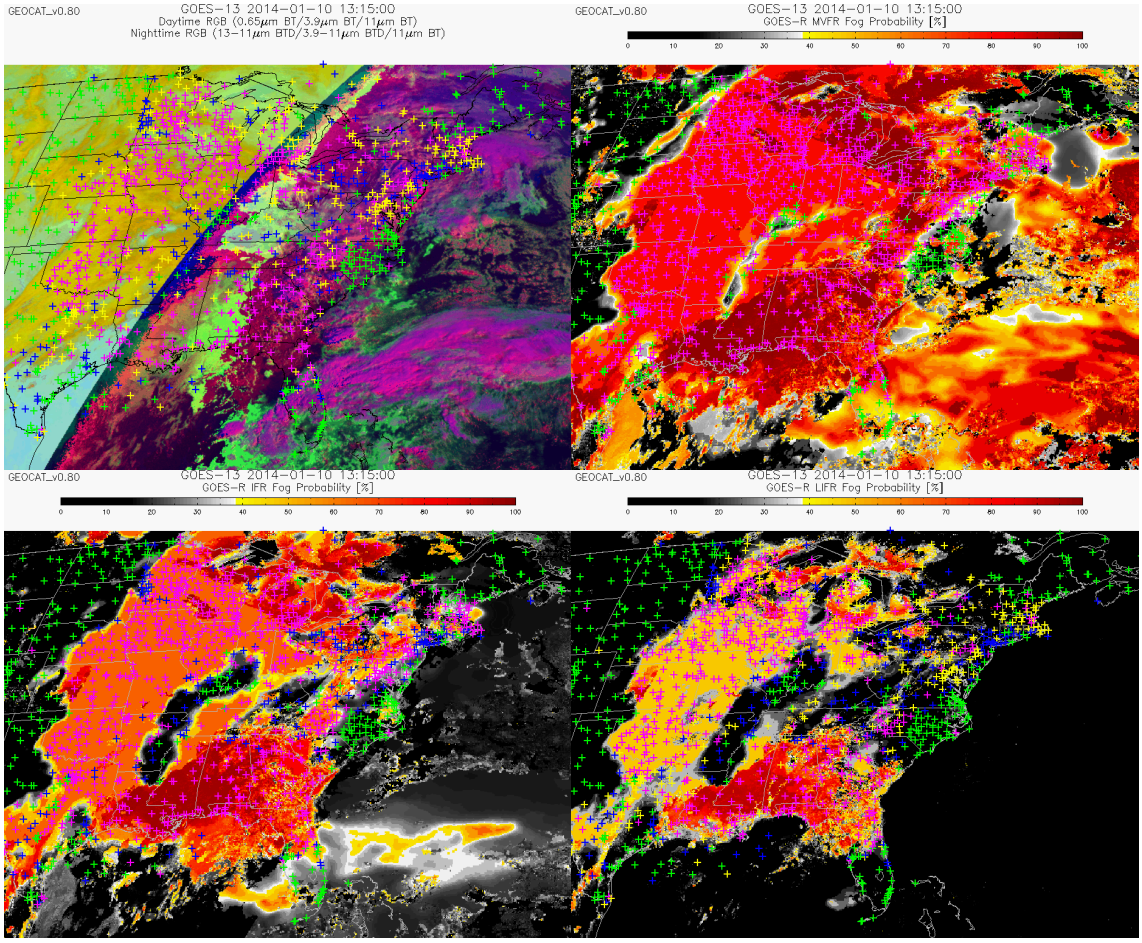

Figure 18 - GOES-13 false color image (top left) (13-11 μm BTD, 3.9-11 μm BTD and 11 μm channels at night and the 0.65 μm, 3.9 μm and 11 μm channels during the day) with accompanying MVFR FLS probabilities (top right), IFR FLS probabilities (bottom left) and LIFR FLS probabilities (bottom right) over CONUS on January 10, 2014 at 13:15 UTC. In the false color image, 'crosses' are colored-coded to the following aviation flight rule categories representing surface observations: VFR (green), MVFR (blue), IFR (yellow), LIFR (magenta). For the 3 probability images the surface observations colored magenta represent stations that report the category being detected, or lower.

3.4.2.3 Determining FLS Depth

The enterprise FLS algorithm uses separate approaches for estimating FLS geometrical thickness during the day and night. The daytime method uses the liquid water path (LWP) calculated from the daytime microphysical properties algorithm while the nighttime method is based on the work of Ellrod (1995). Both are explained in the following sections. Once the FLS depth is calculated for both day and night it is run through a median filter to reduce noise. The median filter simply replaces the value at each pixel with the median value of a 3 x 3 pixel array centered on that pixel. The generic median filter procedure is described in the AIADD Document.

3.4.2.3.1 *Daytime FLS Depth*

The daytime fog/low stratus thickness product utilizes the calculated LWP from the daytime cloud microphysical properties algorithm and an assumed value for the liquid water content (LWC). Using the optical properties of aerosols and clouds and the FLS size distribution model from Tampieri and Tomasi (1976), Hess et al. (1998) determined that a typical LWC of FLS is 0.06 g/m^3. Hess et al. (1998) also found that the LWC of marine and continental stratus clouds was around 0.3 g/m^3. The majority of the pixels that are flagged by the FLS detection algorithm are stratus clouds, so for simplicity, a LWC of 0.3 g/m^3 is currently used for all daytime pixels. The cloud geometrical thickness (m) if computed by dividing the LWP (g/m^2) by the LWC (g/m^3). Figure 19 shows an example daytime GOES-13 scene with the corresponding fog/low cloud thickness result.

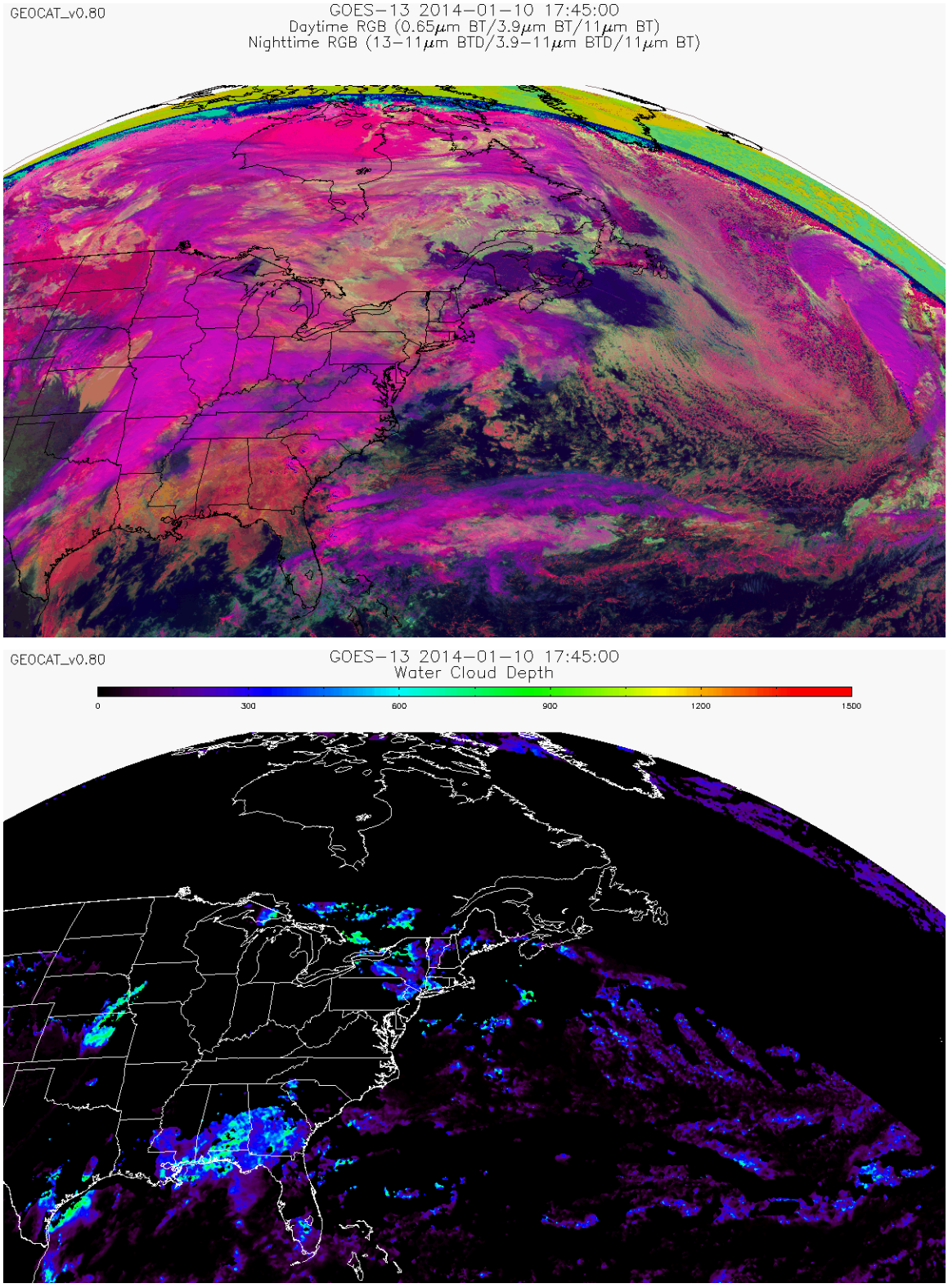

Figure 19 - False color image (top) using the 0.65, 3.9 and 11 μm channels for GOES-13 over CONUS on January 10, 2014 at 17:45 UTC along with the fog/low stratus thickness output (bottom) from the enterprise FLS algorithm.

The cloud thickness is not calculated for pixels identified as ice or multilayered cloud by the cloud type algorithm. FLS can be, and often is, present when ice or multilayered clouds are above, however, the satellite only returns information from the top of the highest cloud layer. For cases where ice or multilayered clouds are detected the satellite is not directly seeing underlying FLS clouds and therefore an accurate estimation of the thickness is not possible. Also, the daytime optical properties are only available for pixels with solar zenith angles less than 70° so the FLS thickness product is not available in the terminator region. This is the reason for the large strip of missing thicknesses in Figure 19 that covers Canada and northern Atlantic Ocean.

3.4.2.3.2 *Nighttime FLS Depth*

Currently the nighttime retrieval of LWP is not adequate to determine the FLS depth. Previously, Ellrod (1995) determined that there is a correlation between nighttime 11-3.9 μm brightness temperature differences (BTD's) and FLS thickness. Building upon this concept, the ems(3.9μm) is used in lieu of the BTD because it takes into account viewing geometry and atmospheric water vapor absorption. Comparing FLS thickness measured using ground-based instruments from the San Francisco Bay area, a linear relationship was found between the ems(3.9μm) and fog/low cloud thickness (Figure 20). The FLS thickness calculated using the ground-based instruments came from subtracting the cloud base measured from ceilometers from the FLS top height measured by a SOnic Detection And Ranging (SODAR) system (Clark et al., 1997).

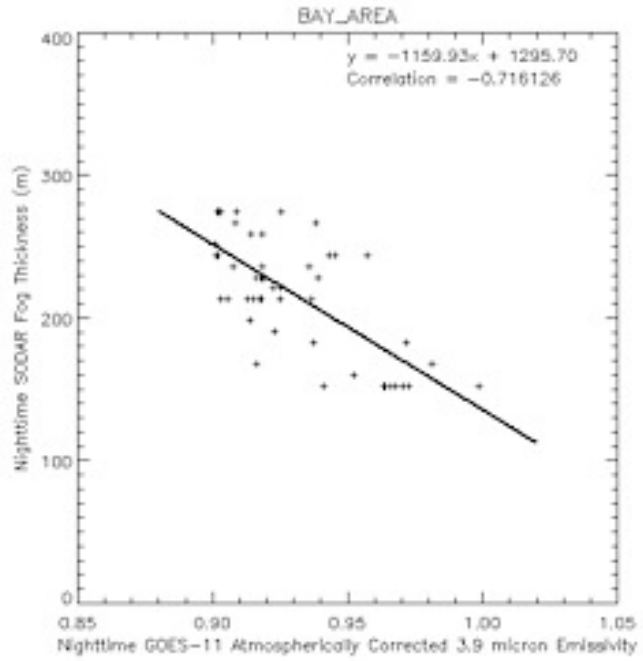

Figure 20 - Scatter plot of FLS thickness measured by ground-based SODAR and ceiling heights vs. collocated 3.9 μm pseudo-emissivity from GOES-11.

By performing a linear regression to the data in Figure 20 a linear equation was found that fits the trend of the data with a correlation coefficient of ~0.72. This equation (see Eq. 9 in section 3.5) is used to calculate the FLS thickness for all nighttime pixels not flagged as ice cloud or multi-layered cloud by the cloud type algorithm. As explained in the daytime FLS depth description, accurate estimation of the FLS depth is not available when ice or multilayered clouds are above the lower cloud layer. Figure 21 shows an example nighttime scene with the FLS thickness regression equation applied to the 3.9 μm pseudo-emissivity channel from GOES-13.

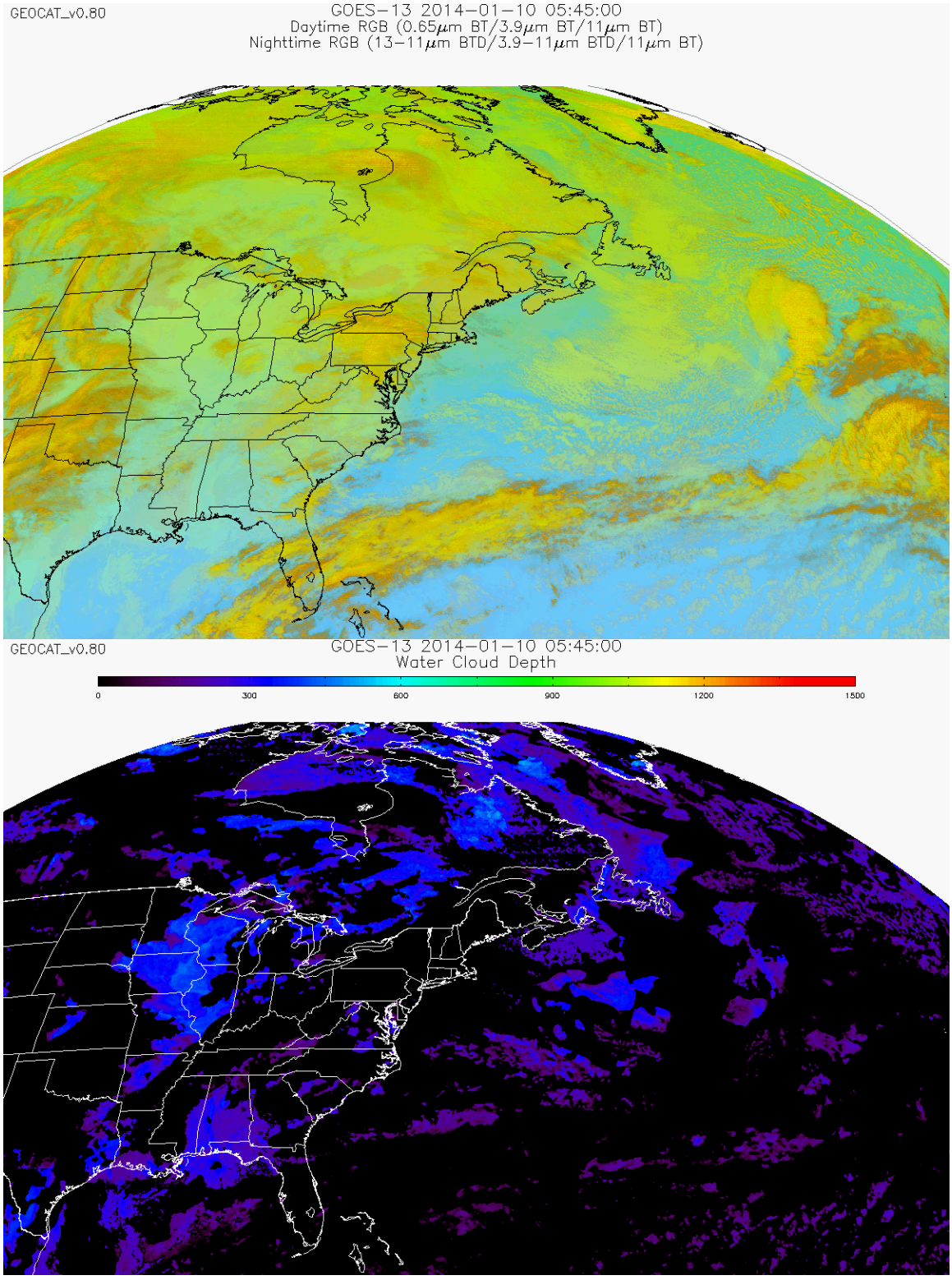

Figure 21 - False color image (top) using the 13-11 μm BTD, 3.9-11 μm BTD and 11 μm channels for GOES-13 over CONUS on January 10, 2014 at 05:45 UTC along with the fog/low stratus thickness output (bottom) from the enterprise FLS algorithm.

3.5 Mathematical Description

The enterprise FLS algorithm data and methodology were described in the previous section. The current logic to derive the final FLS probabilities and cloud thickness is shown in Figure 22.

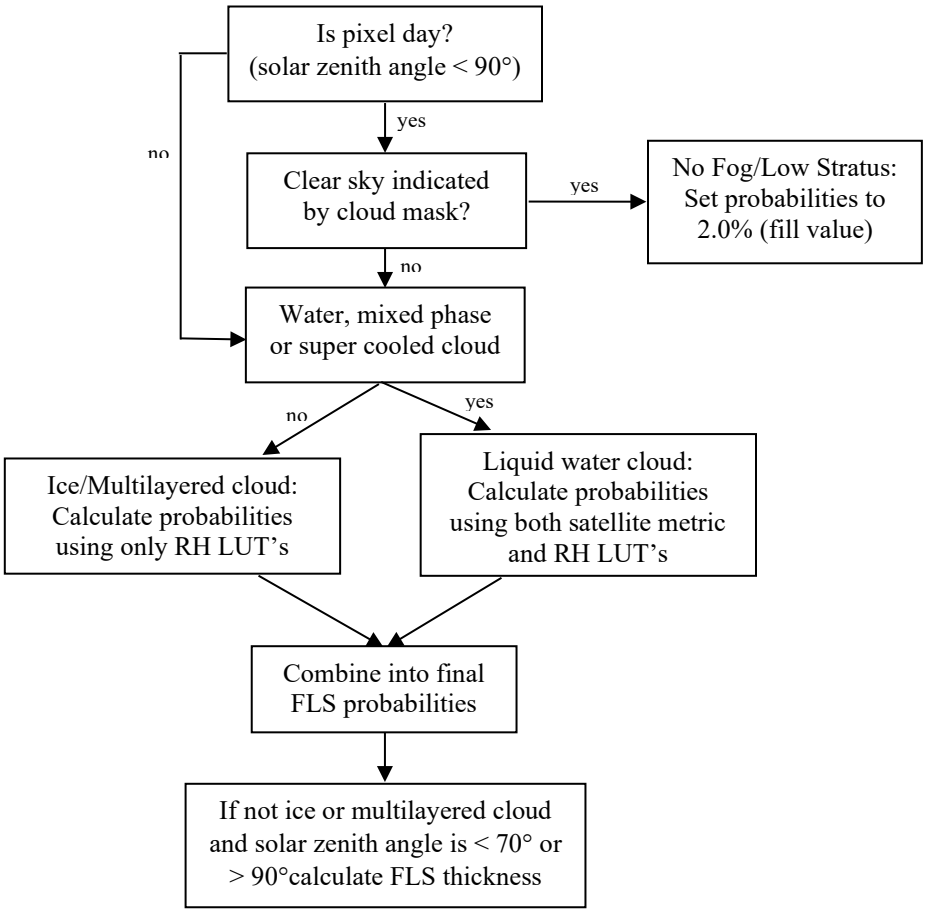

Figure 22 - Schematic illustration of the logic employed to derive the enterprise fog/low stratus probabilities and thickness.

The methods used to estimate the FLS thickness were described in section 3.4.2.3. For the daytime calculation of fog/low stratus thickness when the solar zenith angle is less than 70°, the following equation was used:

$$\Delta Z = LWP/LWC \qquad \text{Eq. 8}$$

where ΔZ is the thickness, LWP is the liquid water path and LWC is the liquid water content. Currently, calculating fog/low status thickness in the terminator region (70° < solar zenith angle < 90°) is not possible.

The nighttime calculation of fog/low stratus thickness is performed using the following linear regression-based relationship between the 3.9 μm pseudo-emissivity and FLS depth determined by ground-based instruments:

$$\Delta Z = A[\text{ems}(3.9\ \mu m)] + B \qquad \text{Eq. 9}$$

where ΔZ is the thickness, ems(3.9 μm) is the 3.9 μm pseudo-emissivity and A and B are regression constants calculated to be -1159.93 and 1295.70 respectively (see Figure 20). This method is analogous to the commonly known relationship used by Ellrod (1995) with the substitution of the 3.9 μm pseudo-emissivity for the 3.9 – 11 μm brightness temperature difference.

3.5.1 Algorithm Output

The final output of the FLS algorithm and description of their meaning is given in Table 8.

Table 8 - Table describing the output from the enterprise FLS algorithm.

Fog/Low Stratus Output	Description
Probability of MVFR	Probability that MVFR conditions are present in %
Probability of IFR	Probability that IFR conditions are present in %
Probability of LIFR	Probability that LIFR conditions are present in %
FLS Thickness	Thickness of fog/low cloud layer in meters
Quality Flags	See Table 9
Product Quality	See Table 10
Metadata	See Table 11

3.5.1.1 Quality Flags (QF)

A complete and self-contained description of the enterprise fog/low cloud quality flag output is listed in Table 9.

Table 9 – A complete description of the fog/low cloud quality flag output is shown.

Bit(s)	QF Description	Bit Interpretation
1	**Fog/low cloud probability quality flag –** the product quality will be dependent on the	0 = 75% - 100% (high) 1 = 50% - 75%

	FLS probability assigned to each pixel. Four levels of quality, with 0 being the highest and 3 being the lowest will be designated.	2 = 25% - 50% 3 = 0% - 25% (low)
2	**Multi-layered cloud quality flag** – this will be set to "low quality" if multi-layered clouds are detected by the GOES-NOP cloud phase algorithm as FLS may be present but may not be detected	0 = multi-layered clouds not detected 1 = multi-layered clouds are detected
3	**Cloud phase quality flag** – this will bet set to "low quality" if ice clouds are detected by the GOES-NOP cloud phase algorithm because the fog/low cloud algorithm will not be run	0 = ice clouds not detected 1 = ice clouds are detected
4	**Freezing FLS flag** – this flag will represent whether each pixel containing fog/low cloud has a temperature below freezing (0 K) indicating the possibility of freezing fog	0 = temperature of fog/low cloud pixel is at or below 0 K 1 = temperature of fog/low cloud pixel is above 0 K
5	**FLS Depth quality flag** – this flag will indicate which pixels have solar zenith angles between 70° – 90°, where FLS depth is not possible due to the lack of lwp or ems(3.9 μm) information	0 = pixel has solar zenith angle either < 70° or > 90° (FLS depth available) 1 = pixel has solar zenith angle between 70° - 90° (FLS depth NOT available)

3.5.1.2 Product Quality Information (PQI)

A complete and self-contained description of the enterprise fog/low cloud Product Quality Information (PQI) output is listed in Table 10.

Table 10 – A complete description of the fog/low cloud Product Quality Information (PQI) output is shown.

Bit(s)	PQI Description	Bit Interpretation
1	Pixel is geolocated and has valid spectral data	0 = FALSE 1 = TRUE
2	Pixel is considered a daylight pixel (solar zenith angle > 90°)	0 = FALSE 1 = TRUE
3	Pixel is located over land	0 = FALSE 1 = TRUE

3.5.1.3 Product Metadata

A complete and self-contained description of the enterprise fog/low cloud metadata output is listed in Table 11.

Table 11 – A complete description of the fog/low cloud metadata output is shown.

Metadata Description
Number of FLS eligible pixels (i.e., number of pixels given a valid FLS probability)
Fraction of pixels in scene detected as fog/low cloud
Mean FLS depth from pixels detected as containing fog/low cloud
Standard deviation of FLS depth from pixels detected as containing fog/low cloud

4 TEST DATA SETS AND OUTPUTS

4.1 Simulated/Proxy Input Data Sets

The data used to test the enterprise fog/low stratus cloud algorithm consists of GOES-12, GOES-13 and GOES-16 observations. The fog/low cloud algorithm is validated using surface observations for detection and surface observations and SODAR data for thickness. All of these data sets are described below.

4.1.1 GOES-NOP Data

The GOES-NOP imager provides five spectral channels with a spatial resolution of 4 km and provides spatial coverage of the full disk with a temporal resolution of 3 hours. Smaller CONUS and Northern Hemisphere domains are available every 15 minutes. GOES-12/13 provides a good source of data for testing and developing the fog/low cloud algorithm due to the abundance of data that can be used to train the algorithm. Figure 23 is a full-disk GOES-13 image from 17:45 UTC on January 10, 2014. GOES-12/13 data are readily available from the University of Wisconsin Space Science and Engineering Center (SSEC) Data Center.

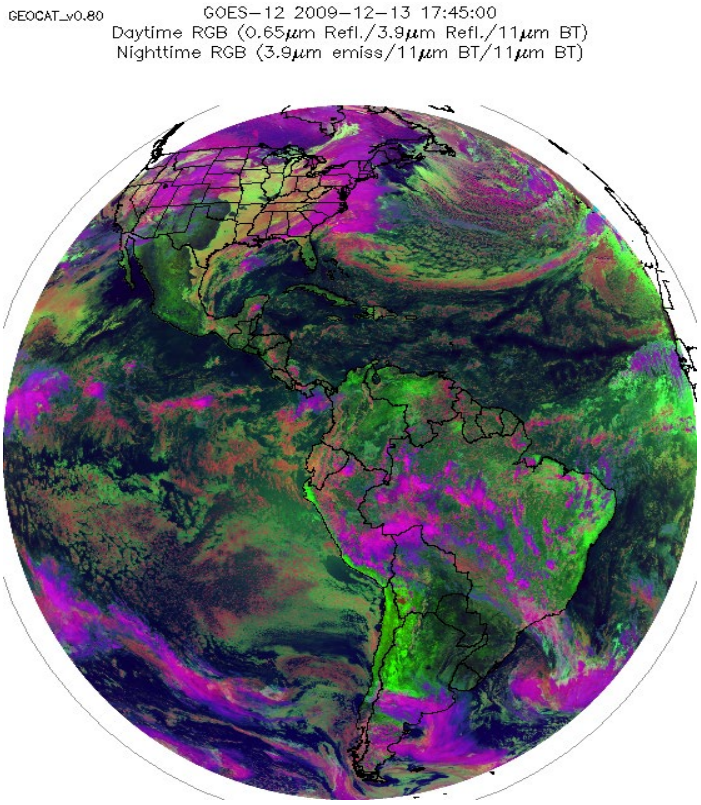

Figure 23 – GOES-13 false color image using the 0.65, 3.9 and 11 μm channels from 17:45 UTC on January 10, 2014.

4.1.2 GOES-16/17 Data

The ABI on the GOES-R series (GOES-16 and GOES-17) geostationary satellites provides 16 spectral channels with a spatial resolution of 2 km and provides spatial coverage of the full disk with a temporal resolution of 10 min. A smaller CONUS domain is also available every 5 minutes. These satellites provide good sources of data for testing and developing the fog/low cloud algorithm due to the abundance of data that can be used for training. Figure 24 shows examples of full-disk GOES-16 and. GOES-17 images. Data from these satellites are readily available from the National Centers for Environmental Information (NCEI).

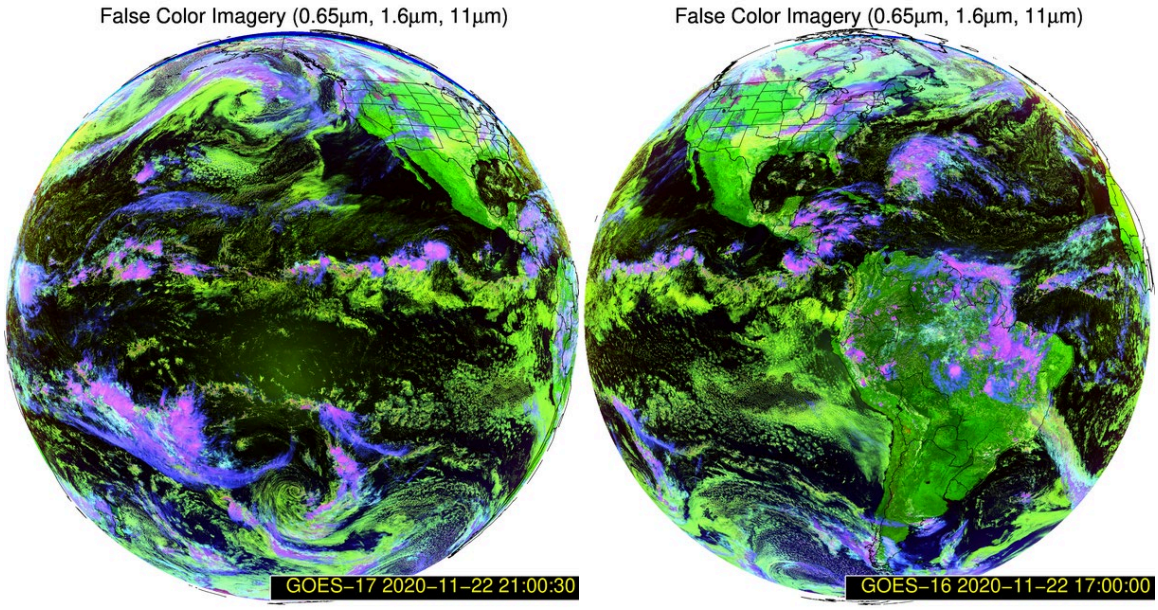

Figure 24 – Example full disk GOES-17 (left) and GOES-16 (right) false color images using the 0.65, 1.6 and 11 μm channels.

4.1.3 Surface Observations

Surface observations are received from both manned and automated ground stations all over the world. They provide accurate ground-based measurements of weather parameters such as temperature, pressure, weather conditions, etc., with relatively high temporal coverage (usually every hour, but varies by station). A useful surface observation parameter for validating fog/low cloud is the observed cloud ceiling. The most densely concentrated number of surface observations comes from the United States and Europe. Due to their positioning, GOES-12/13/16 do not provide information over Europe. For validation purposes surface observations over CONUS provide the greatest amount of data.

The surface observations over CONUS come from Automated Surface Observing System (ASOS) sites across the country. The ASOS program was created and is maintained by a joint effort between the National Weather Service (NWS), the Federal Aviation Administration (FAA) and Department of Defense (DOD). The cloud ceiling observations used to create the FLS probability LUT's (see sections 3.4.2.2.2.1 and 3.4.2.2.3.1) and to validate the enterprise fog/low cloud product are measured using a laser ceilometer. The valid range of the laser ceilometer at the ASOS stations is 100-12,000 ft with an accuracy of ±100 ft or 5% (whichever is greater). The product range and accuracy information was obtained from the ASOS User's Guide and ASOS User's Guide Appendices, which can be found at the NWS ASOS website (www.nws.noaa.gov/asos).

4.1.4 SODAR Data

The acoustic SODAR is an upwardly pointing parabolic antenna that emits an audible pulse whose return signal is proportional to the vertical gradient of air density. This gives it the capability of detecting the base of the atmospheric inversion, which defines the top of the stratus deck. Combining this data with the measured cloud ceiling from a ceilometer allows for the calculation of the geometric boundaries of low clouds.

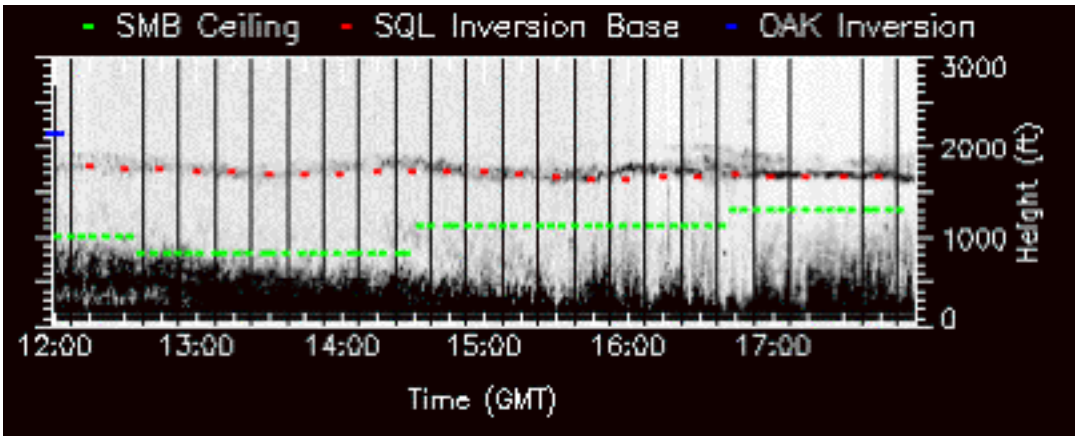

Figure 25 – An example of SODAR data combined with cloud ceiling. The red dashed line represents the base of the atmospheric inversion (i.e., stratus top) and the green dashed line represents the measured cloud ceiling. The difference between the two lines is the stratus deck thickness.

Unfortunately, SODAR data is only available at a small number of locations and not at every surface observation site. For the enterprise fog/low cloud validation the SODAR data came from two sites around the San Francisco Bay Area courtesy of the NWS San Francisco Bay Area Forecast Office (Clark et al., 1997).

4.2 Output from Simulated/Proxy Inputs Data Sets

The enterprise fog/low cloud algorithm was tested using GOES-13, GOES-16 and GOES-17 satellite data. As an example, results produced using GOES-13 data are shown in Figure 26 and Figure 27. A more detailed zoomed-in region over CONUS is also shown in Figure 28 and Figure 29. Manual analysis of the results compared to false color images show that areas of fog/low cloud are detected well and are verified by surface observations shown in Figure 15 and Figure 17. Example FLS products using GOES-16/GOES-17 data are shown over CONUS in Figure 30/Figure 31 and Figure 32/Figure 33, respectively. A more quantitative validation is shown in the next section.

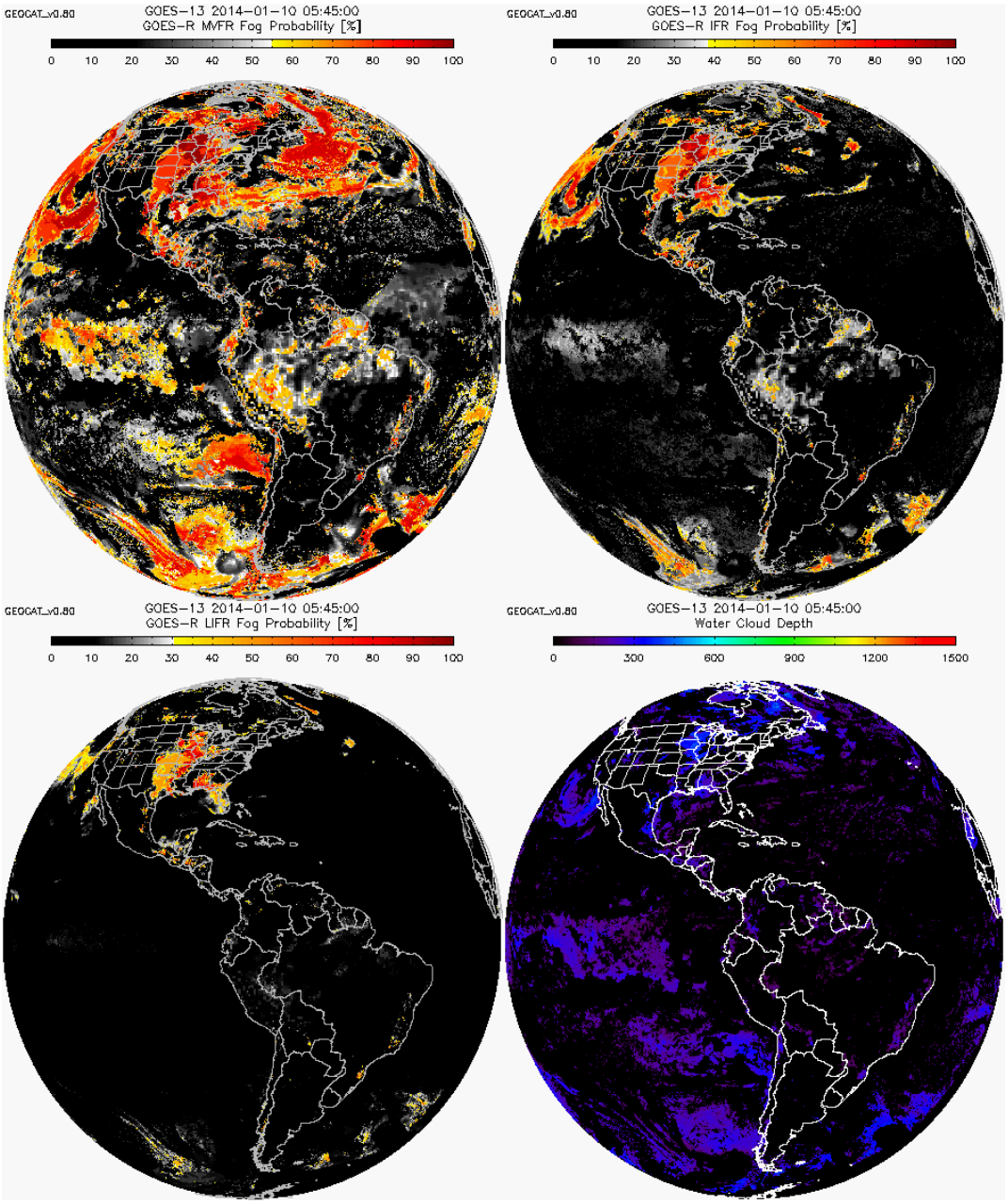

Figure 26 - Example nighttime results (using GOES-13) from the enterprise FLS algorithm for January 10, 2014 at 5:45 UTC. The top left panel is MVFR

probabilities, the top right panel is the IFR probabilities, the bottom left panel is the LIFR probabilities and the bottom right panel is the cloud thickness results.

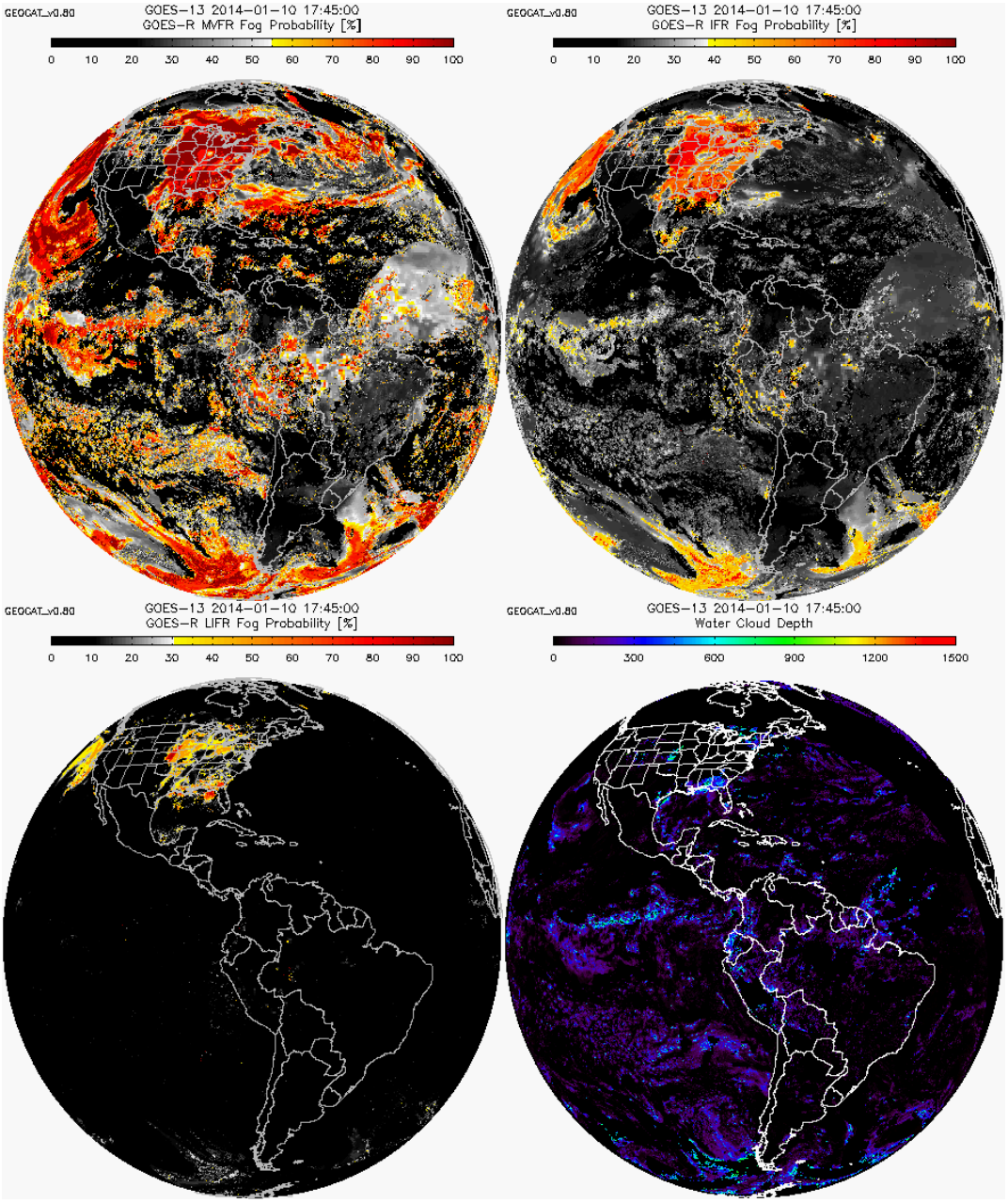

Figure 27 – Example daytime results (using GOES-13) from the enterprise FLS algorithm for January 10, 2014 at 17:45 UTC. The top left panel is MVFR probabilities, the top right panel is the IFR probabilities, the bottom left panel is the LIFR probabilities and the bottom right panel is the cloud thickness results.

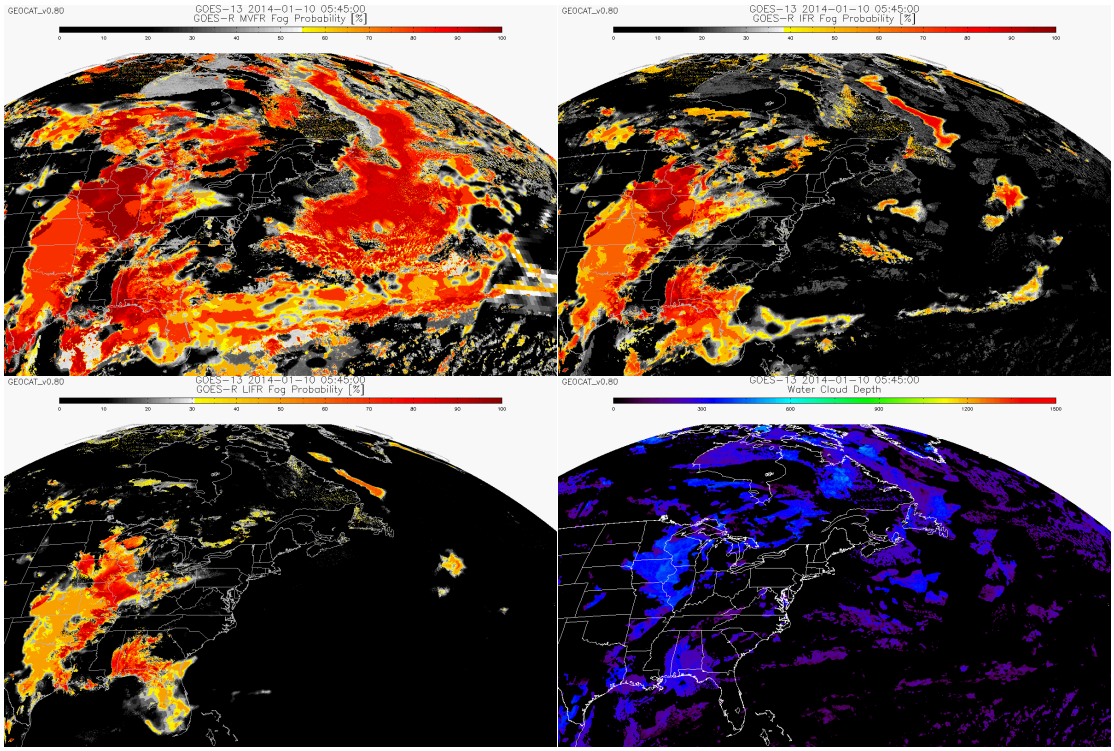

Figure 28 - A zoomed-in look at the nighttime fog/low cloud detection and thickness results shown in Figure 26 over the eastern CONUS and Atlantic Ocean. The top left panel is MVFR probabilities, the top right panel is the IFR probabilities, the bottom left panel is the LIFR probabilities and the bottom right panel is the cloud thickness results.

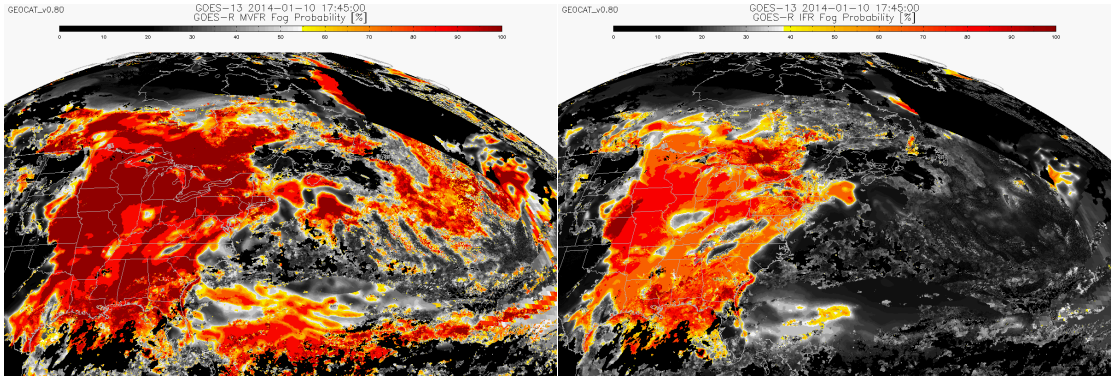

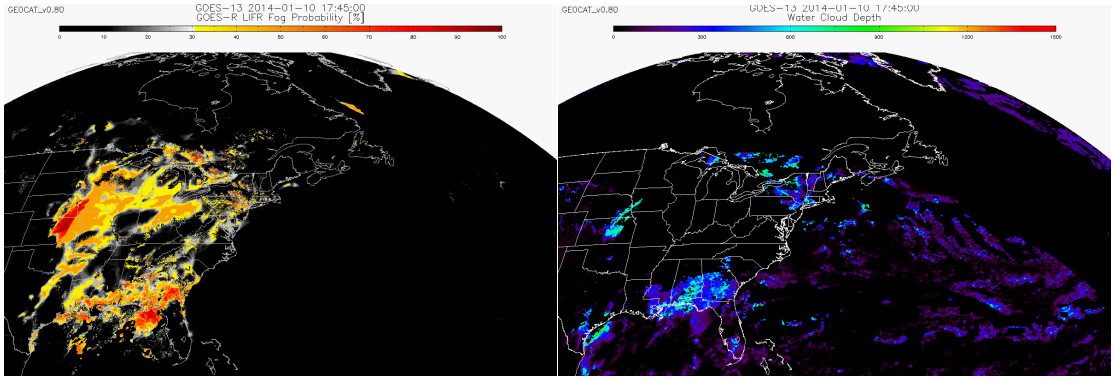

Figure 29 – A zoomed-in look at the daytime fog/low cloud detection and thickness results shown in Figure 27 over CONUS. The top left panel is MVFR probabilities, the top right panel is the IFR probabilities, the bottom left panel is the LIFR probabilities and the bottom right panel is the cloud thickness results.

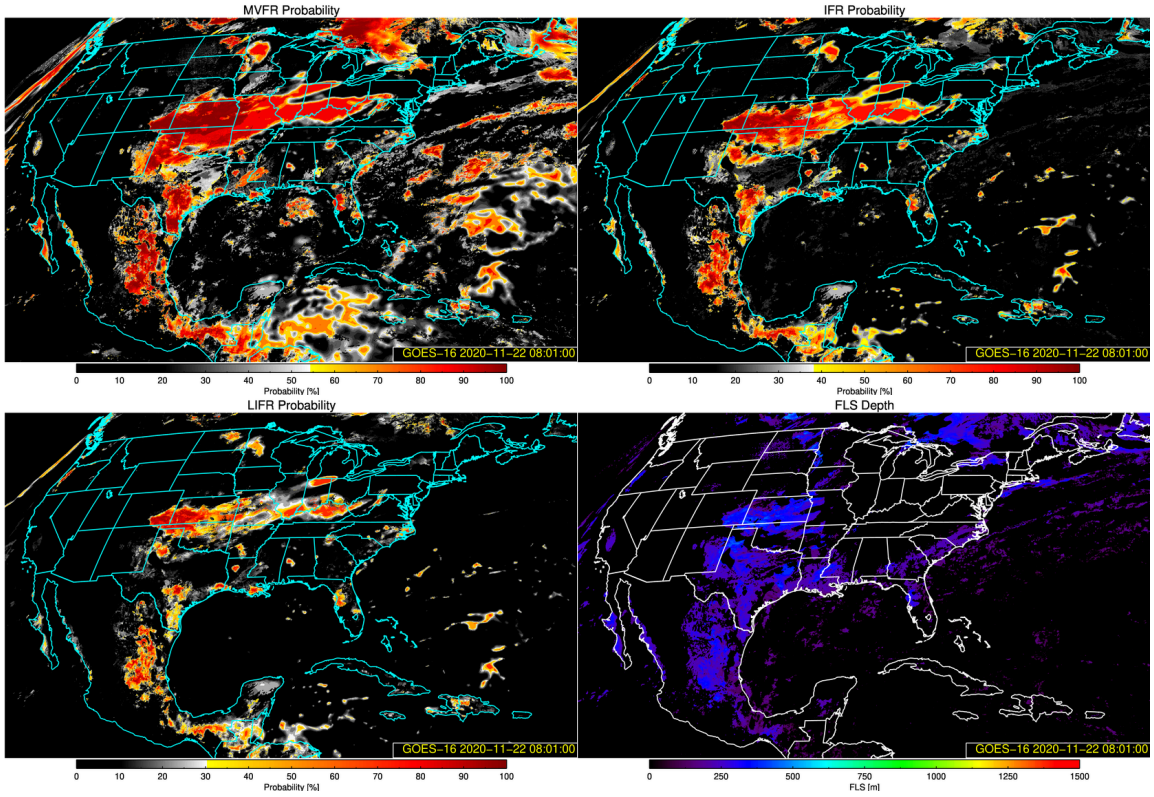

Figure 30 - Example nighttime results (using GOES-16) from the enterprise FLS algorithm from November 22, 2020 at 8:01 UTC. The top left panel is MVFR probabilities, the top right panel is the IFR probabilities, the bottom left panel is the LIFR probabilities and the bottom right panel is the cloud thickness results.

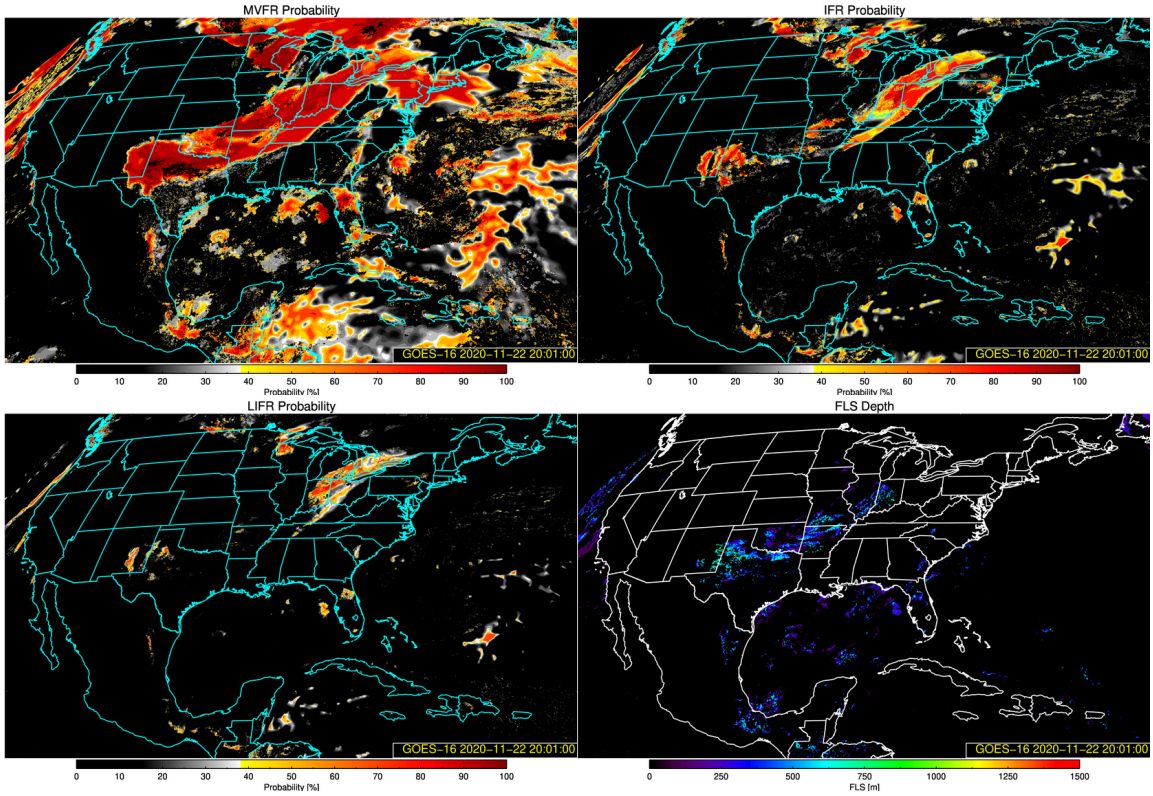

Figure 31 - Example daytime results (using GOES-16) from the enterprise FLS algorithm for November 22, 2020 at 20:01 UTC. The top left panel is MVFR probabilities, the top right panel is the IFR probabilities, the bottom left panel is the LIFR probabilities and the bottom right panel is the cloud thickness results.

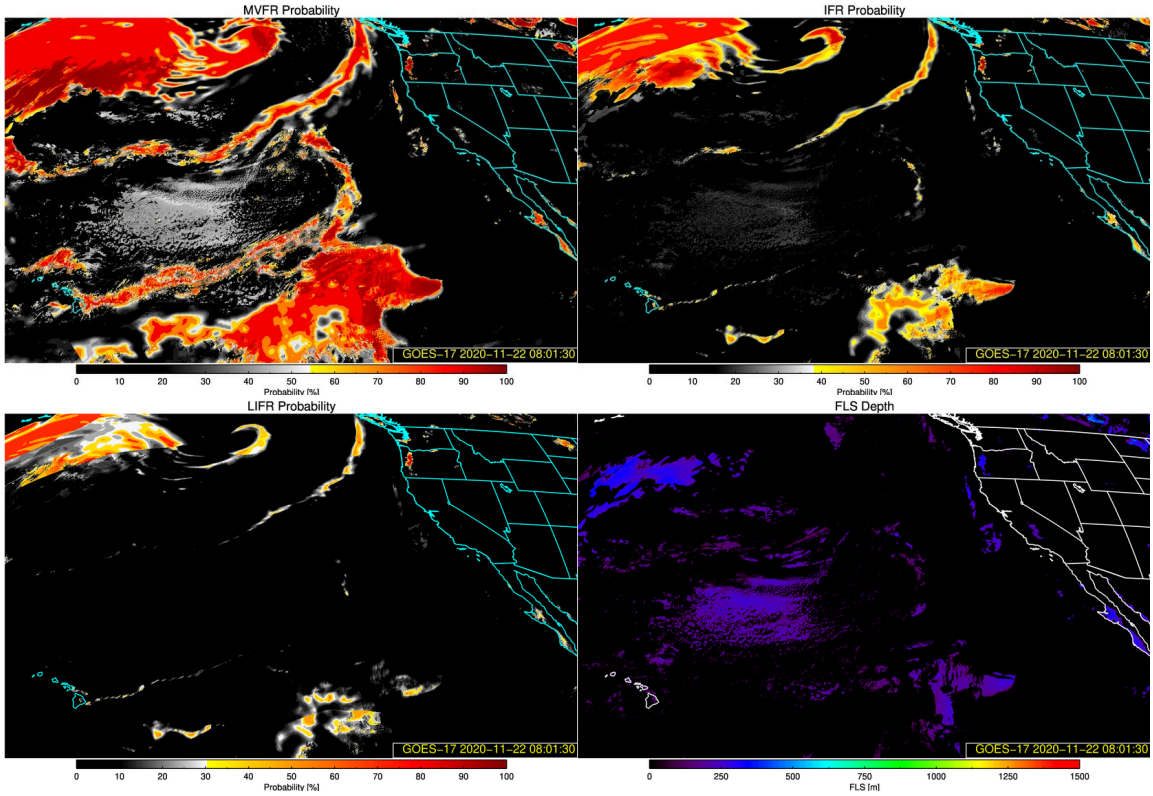

Figure 32 - Example nighttime results (using GOES-17) from the enterprise FLS algorithm for November 22, 2020 at 8:01 UTC. The top left panel is MVFR probabilities, the top right panel is the IFR probabilities, the bottom left panel is the LIFR probabilities and the bottom right panel is the cloud thickness results.

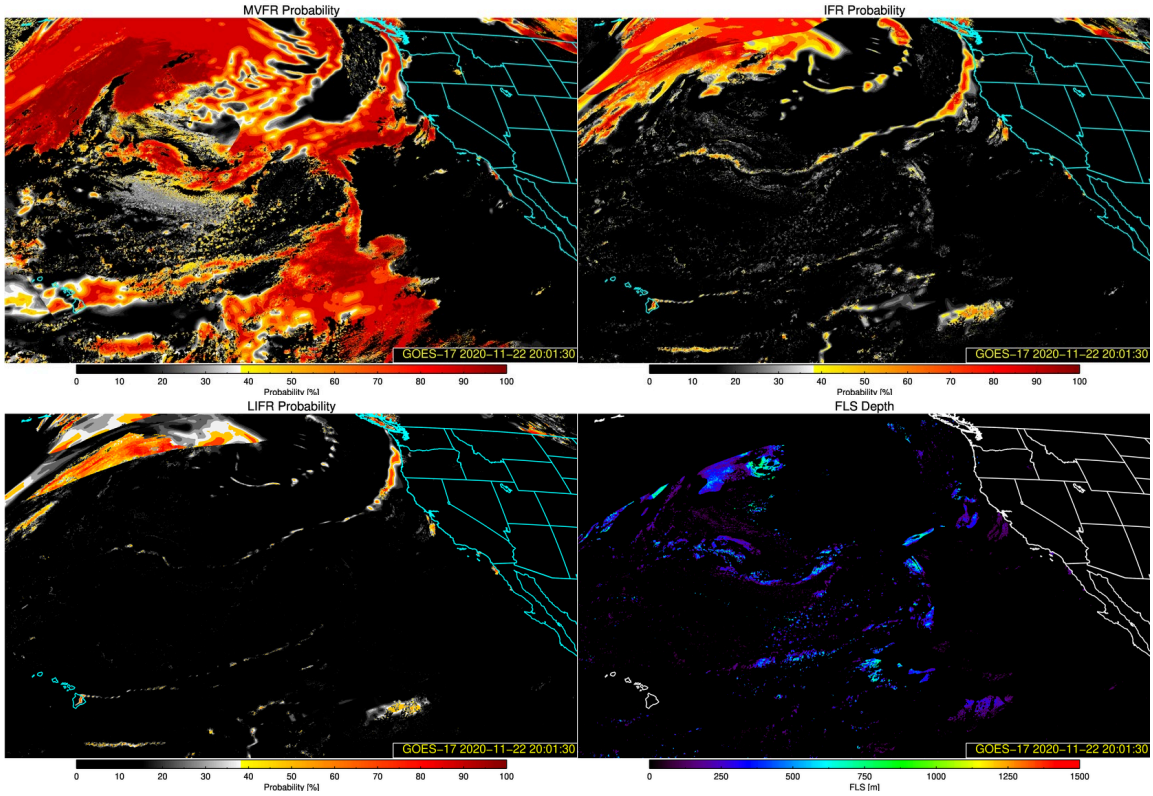

Figure 33 - Example daytime results (using GOES-17) from the enterprise FLS algorithm for November 22, 2020 at 20:01 UTC. The top left panel is MVFR probabilities, the top right panel is the IFR probabilities, the bottom left panel is the LIFR probabilities and the bottom right panel is the cloud thickness results.

4.2.1 Precisions and Accuracy Estimates

To estimate the precision and accuracy of the enterprise fog/low cloud detection algorithm, measurements of cloud ceiling from surface observations were used. As previously mentioned, the enterprise fog/low cloud detection product is designed to quantitatively identify clouds that produce at least MVFR, IFR and LIFR conditions. Surface observations of cloud ceiling depict areas that meet those conditions and can be collocated with the satellite pixels in order to validate the fog/low cloud product. Future validation efforts will focus on using surface observations.

To estimate the precision and accuracy of the enterprise fog/low cloud thickness algorithm, comparisons to measured FLS thicknesses using ground-based SODAR and ceilometer data were performed. The acoustic SODAR system allows the bottom of the atmospheric inversion to be detected, which corresponds to the top of the stratus layer overhead. The ceilometer data is used to find the base of the stratus layer. The thickness of the cloud layer is the height difference between the inversion level and the cloud ceiling and is used to validate the fog/low cloud thickness algorithm.

4.2.2 Error Budget

The enterprise FLS detection algorithm was applied to 12 days (1 day from each month) of GOES-13 data from 2013, GOES-16 data from 2017 and GOES-17 data from 2020. Each data set was validated using surface observations of cloud ceiling and surface visibility as discussed in the previous section. The enterprise FLS thickness algorithm was also applied to GOES-11 and validated using a combination of ground-based SODAR data and cloud ceiling. SODAR data was not available to validate the GOES-16/17 thickness product, however, comparisons were made with the GOES-13/16 thicknesses to infer errors.

4.2.2.1 Fog/Low Cloud Detection Error Budget

The enterprise FLS algorithm was validated using a calculation of the accuracy. The F&PS requirement for the enterprise FLS algorithm is to achieve an accuracy of 70% or greater. There are four possible outcomes from the FLS detection algorithm (hit, miss, false alarm or non-event) that are used to assess the accuracy that are shown in Table 12.

Table 12 – Possible outcomes from the enterprise FLS algorithm.

fog/low stratus cloud detected	*fog/low stratus cloud observed*	
	YES	**NO**
YES	h (hit)	f (false alarm)
NO	m (miss)	z (non-event)

The accuracy of the FLS detection algorithm is calculated by dividing the total number of correctly identified FLS (hits) and non-FLS (non-event) pixels by the total number pixels used for the validation. This can be written as the following equation:

$$Accuracy = \frac{h+z}{h+m+f+z} \qquad \text{Eq. 10}$$

The accuracy ranges from 0.0-1.0, with 1.0 meaning that all pixels were correctly classified as FLS/non-FLS and 0.0 meaning that no pixels were correctly classified as FLS/non FLS.

Surface observations were used to validate the accuracy of the enterprise FLS algorithm. Analyses of the accuracy of the enterprise FLS detection algorithm applied to GOES-13, GOES-16 and GOES-17 as a function of FLS probability using surface observations are shown in Figure 34, Figure 35 and Figure 36, respectively.

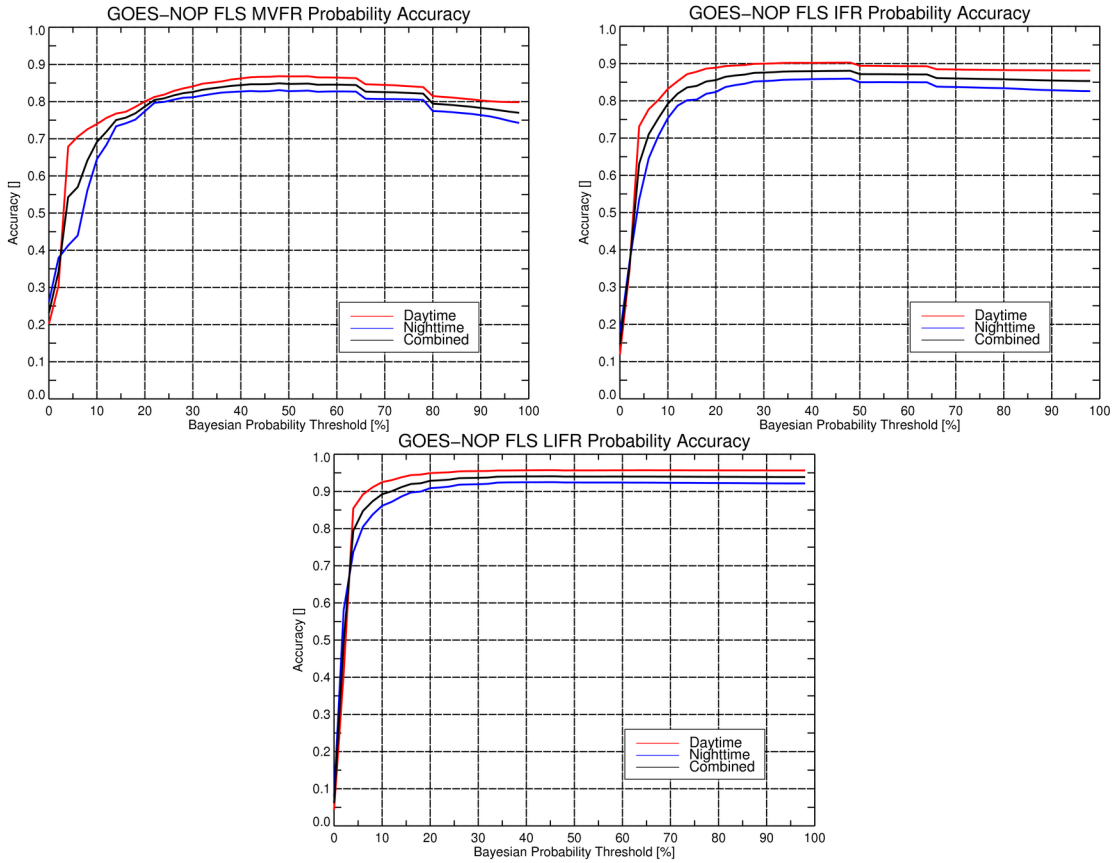

Figure 34 – FLS accuracy shown as a function of MVFR probability (top left), IFR probability (top right) and LIFR probability (bottom), calculated using GOES-13 data over CONUS. Surface observations of cloud ceiling and surface visibility were used to determine MVFR/IFR/LIFR conditions. 12 days of data from 2013 were used for this analysis.

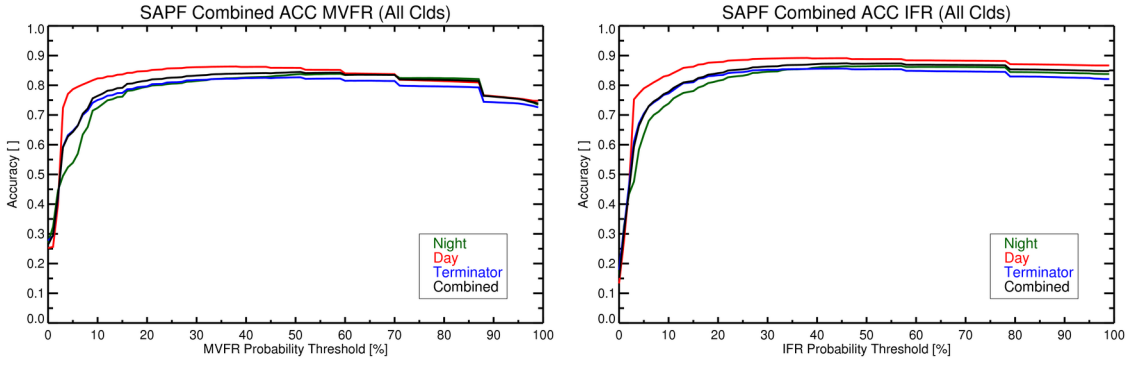

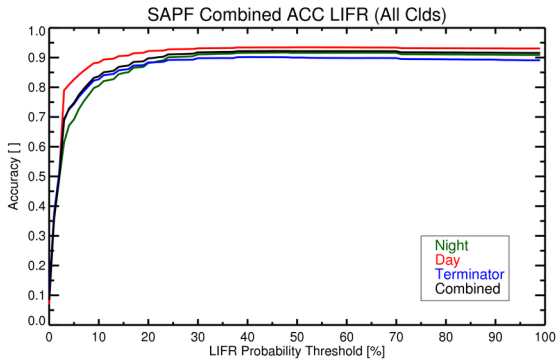

Figure 35 - FLS accuracy shown as a function of MVFR probability (top left), IFR probability (top right) and LIFR probability (bottom), calculated using GOES-16 data over CONUS. Surface observations of cloud ceiling and surface visibility were used to determine MVFR/IFR/LIFR conditions. 12 days of data from 2017 were used for this analysis.

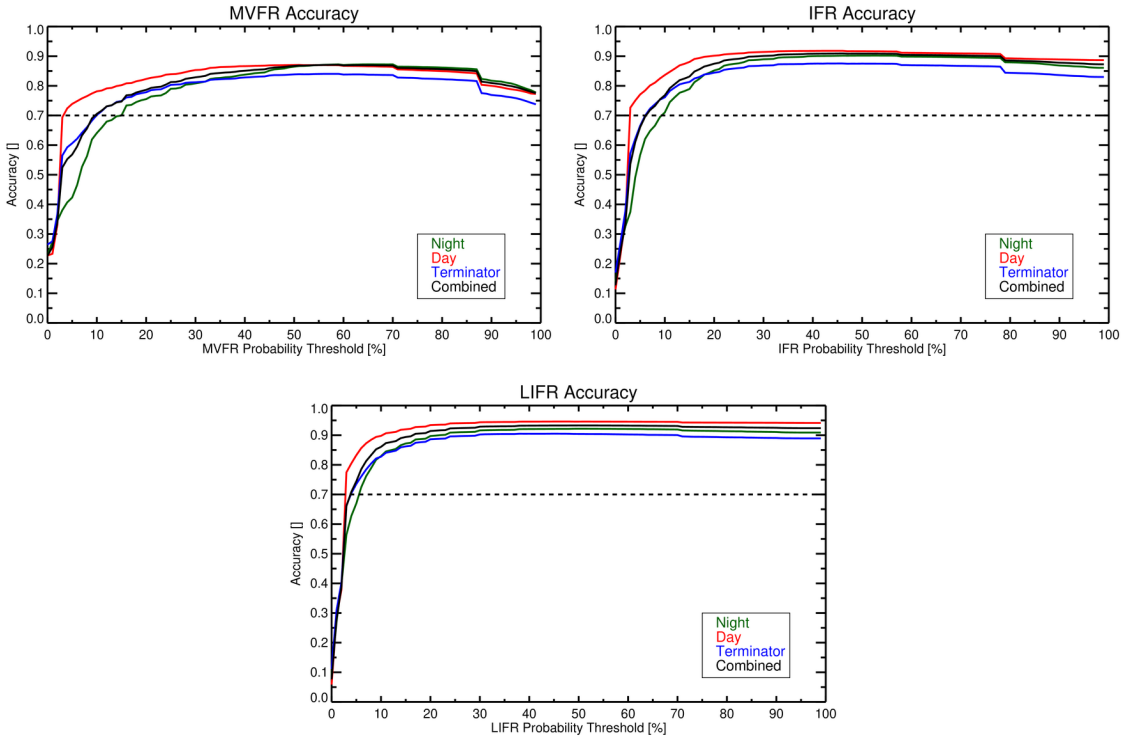

Figure 36 - FLS accuracy shown as a function of MVFR probability (top left), IFR probability (top right) and LIFR probability (bottom), calculated using GOES-17 data over CONUS. Surface observations of cloud ceiling and surface visibility were used to determine MVFR/IFR/LIFR conditions. The dashed line represents the accuracy requirement. 12 days of data from 2020 were used for this analysis.

The maximum accuracy obtained for the combined day/night pixels exceeded 80% for all flight rule categories for all three satellites. In general, the maximum accuracy was found to be slightly higher for daytime pixels than for nighttime pixels, however, the accuracy for nighttime pixels still exceeds the enterprise FLS accuracy requirement. These results show that the enterprise FLS algorithm meets the F&PS detection accuracy requirement of 0.70 when using surface observations to validate the algorithm.

While the enterprise FLS algorithm was validated using a calculation of the overall accuracy, the critical success index (CSI), also known as the threat score, was also used to help evaluate the performance of the enterprise FLS algorithm. This method can also be described as the algorithm accuracy when correct non-detected events are removed. Values for the CSI range from 0 to 1, where 0 represents no skill and 1 represents perfect detection. This method is frequently used because it takes into account both false alarms and missed events, making it a more balanced score. However, the CSI can be sensitive to the climatology of the event and tends to produce lower scores for rare events. The four possible outcomes from the enterprise FLS algorithm shown in Table 12 are again used to calculate the CSI.

The CSI is defined as the number of FLS pixels properly detected divided by the total number of pixels falsely detected as FLS and observed as FLS by surface observations, or from Table 12 above:

$$CSI = \frac{h}{h+m+f} \qquad \text{Eq. 11}$$

The CSI allows further evaluation of the performance of the algorithm and can be used to show improvements to the performance of the enterprise FLS algorithm. One example of how the CSI was used to show improvement to the algorithm was an analysis of the nighttime CSI for the heritage BTD method, as a function of BTD threshold, and the enterprise Bayesian method using the 3.9 μm pseudo-emissivity, radiometric surface temperature bias and the modeled RH information, as a function of MVFR/IFR/LIFR FLS probability threshold. Only nighttime data was analyzed since the heritage BTD method is generally not used during the day. The results of this analysis are shown in Figure 37.

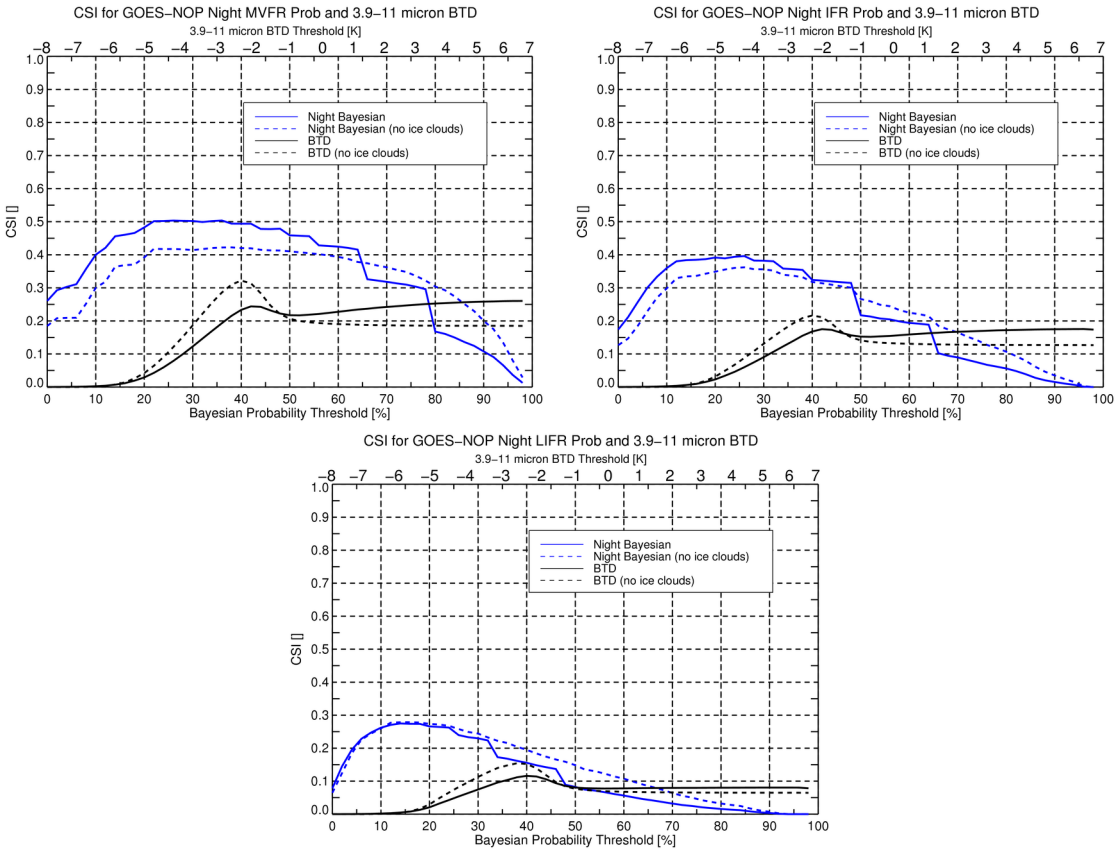

Figure 37 – Nighttime CSI analysis for the heritage BTD FLS method (black) and the enterprise FLS Bayesian algorithm (Blue) using pixels containing all types of clouds (solid lines) and pixels not containing ice or multilayered clouds (dashed lines). GOES-13 data were used for this analysis.

Figure 37 illustrates that the enterprise FLS algorithm produces higher maximum skill scores than the heritage BTD method for each flight rule category. When ice and multilayered clouds are included in the analysis the maximum CSI from the enterprise FLS probabilities is nearly double that of the heritage BTD methodology. Even when excluding ice and multilayered clouds (where the 3.9-11 micron BTD is known to do poorly) the enterprise Bayesian FLS probabilities are still more skillful. This analysis confirms the Bayesian method using the 3.9 μm pseudo-emissivity, radiometric surface temperature bias and modeled RH information out-performs than the heritage BTD methodology and justifies why it was chosen for the enterprise FLS algorithm.

The CSI scores were calculated for the final enterprise FLS algorithm validation datasets using surface observations of cloud ceiling and surface visibility to identify pixels that meet MVFR/IFR/LIFR criteria. The results using GOES-13, GOES-16 and GOES-17 data are shown in Figure 38, Figure 39 and Figure 40, respectively.

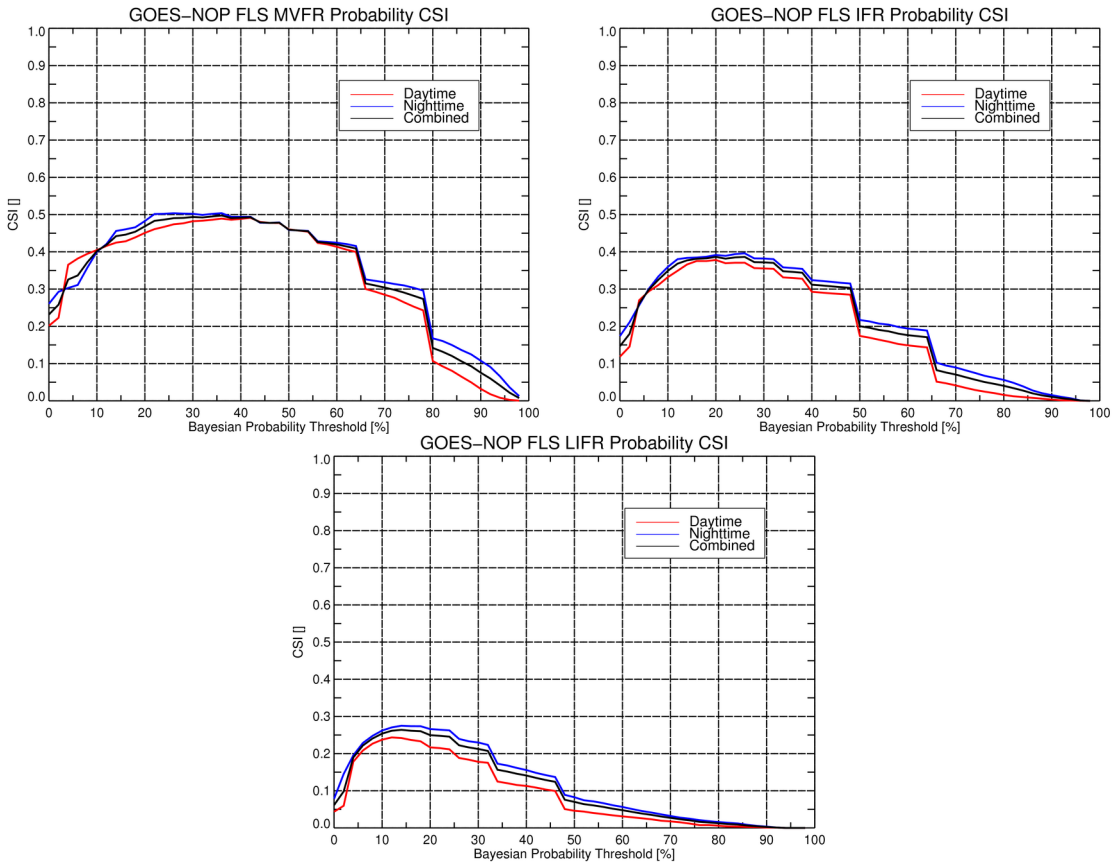

Figure 38 – Critical success index (CSI) analysis for the enterprise FLS algorithm applied to GOES-13 as a function of MVFR probability (top left), IFR probability (top right) and LIFR probability (bottom) using surface observations of cloud ceiling and surface visibility to identify pixels that meet MVFR/IFR/LIFR criteria. 12 days of data from 2013 were used for this analysis.

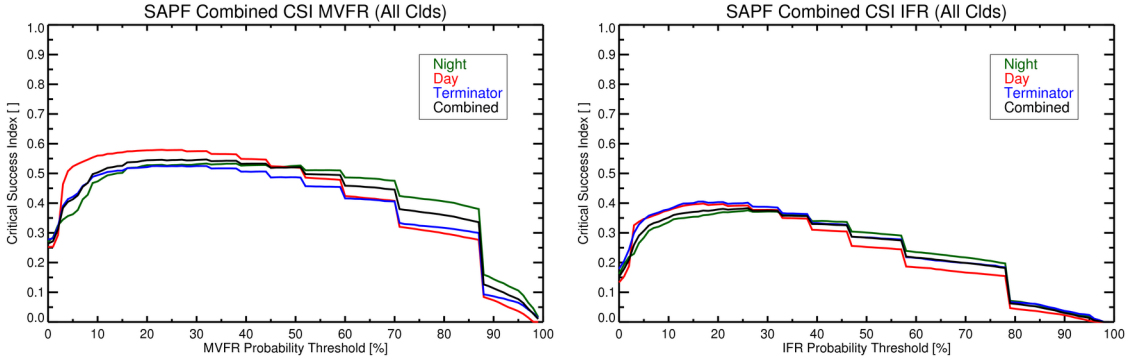

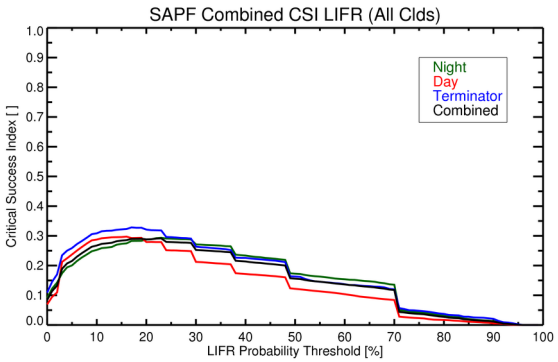

Figure 39 - Critical success index (CSI) analysis for the enterprise FLS algorithm applied to GOES-16 as a function of MVFR probability (top left), IFR probability (top right) and LIFR probability (bottom) using surface observations of cloud ceiling and surface visibility to identify pixels that meet MVFR/IFR/LIFR criteria. 12 days of data from 2017 were used for this analysis.

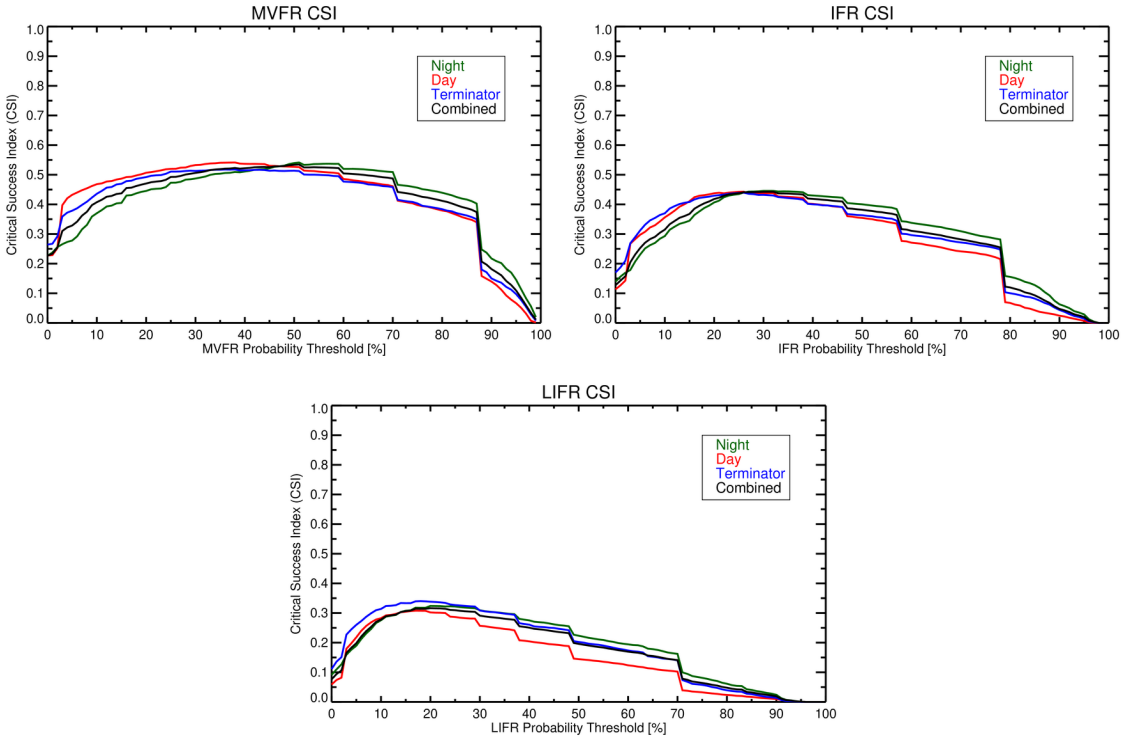

Figure 40 - Critical success index (CSI) analysis for the enterprise FLS algorithm applied to GOES-17 as a function of MVFR probability (top left), IFR probability (top right) and LIFR probability (bottom) using surface observations of cloud ceiling and surface visibility to identify pixels that meet MVFR/IFR/LIFR criteria. 12 days of data from 2020 were used for this analysis.

The CSI analysis is used to determine the probability threshold for each flight rule category that yields the highest skill. If a yes/no determination of FLS were required, these

probabilities would represent the thresholds that maximize algorithm performance. The maximum skill for MVFR/IFR/LIFR was found using probability thresholds of 36%/20%/14% for GOES-13, 38%/26%/21% for GOES-16, and 51%/33%/20% for GOES-17. Although these thresholds do not reflect the FLS probabilities that yielded the maximum accuracy (Figure 34, Figure 35 and Figure 36), the accuracies associated with them are still comfortably above the requirement of 0.70 and are shown in Table 13.

Table 13 – The enterprise FLS probability accuracy score using GOES-13, GOES-16 and GOES-17 data calculated at the probability threshold (in parentheses) that yielded the highest CSI.

Flight Rule Category	GOES-13 Accuracy (prob threshold from max CSI)	GOES-16 Accuracy (prob threshold from max CSI)	GOES-17 Accuracy (prob threshold from max CSI)
MVFR	0.84 (36%)	0.87 (38%)	0.87 (51%)
IFR	0.86 (20%)	0.90 (26%)	0.90 (33%)
LIFR	0.91 (14%)	0.92 (21%)	0.91 (20%)

The results in Table 13 indicate the accuracy of the enterprise FLS probability products still surpass the F&PS requirement of 0.70 when the probability threshold that produced the highest CSI values was used. It also should be noted that the accuracies produced using GOES-16/17 data are higher than those calculated using GOES-13 meaning the GOES-16/17 FLS products are slightly more accurate.

Although the previous accuracy and CSI analyses show the enterprise FLS products meet the specified performance requirements we also produced attribute diagrams for each probability product. The attributes diagram, also called a reliability diagram, is a useful verification tool that shows how accurate a probabilistic forecast correlates to the actual probability of an observed event. The dashed line running at a 45° angle from the lower left corner to the upper right corner represents perfect reliability. The shaded region is determined by the climatology of the event. Points that lie within the shaded region indicate increased model skill and points that lie outside the shaded region indicate decreased model skill with respect to climatological probability (Wilks 2006). Diagrams were produced for all three flight rule categories using GOES-13 and are shown in Figure 41 (daytime pixels) and Figure 42 (nighttime pixels).

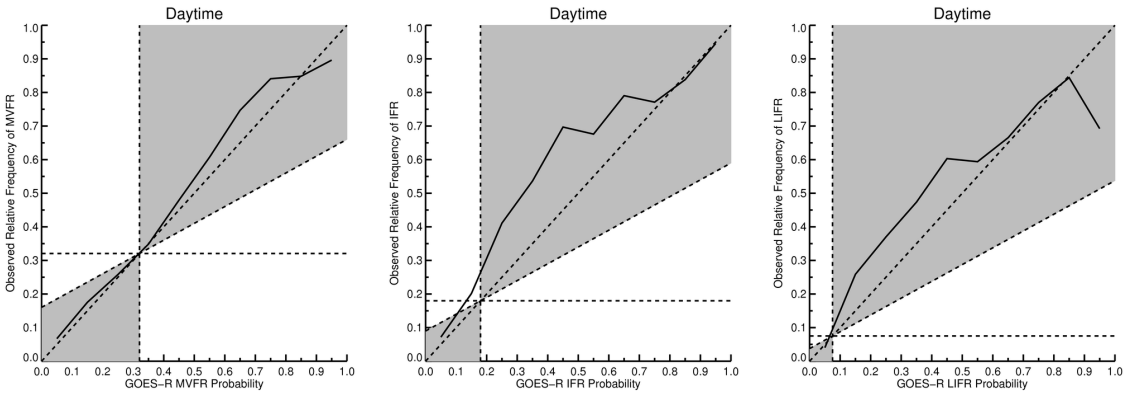

Figure 41 - The attributes diagrams for the GOES-13 MVFR (left), IFR (middle) and LIFR (right) FLS probability products for all daytime pixels. Points that lie within the shaded region indicate increased model skill.

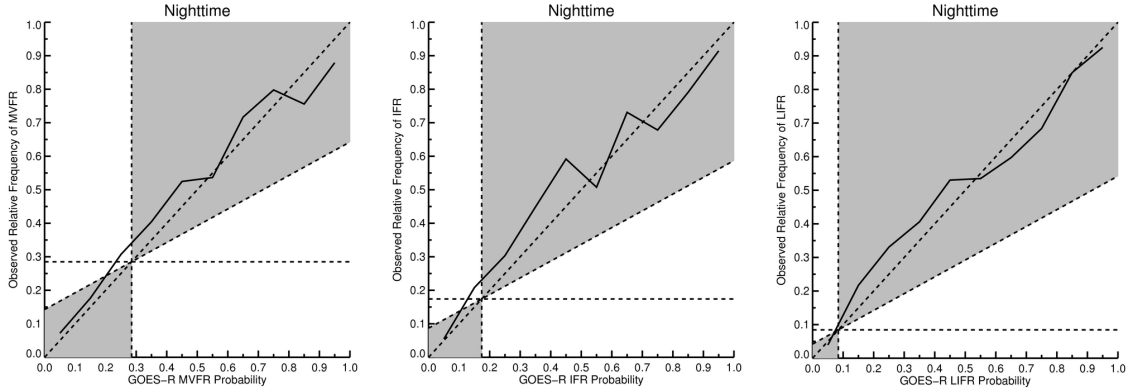

Figure 42 - The attributes diagrams for the GOES-13 MVFR (left), IFR (middle) and LIFR (right) FLS probability products for all nighttime pixels. Points that lie within the shaded region indicate increased model skill.

The attributes diagrams show that overall the enterprise FLS probability products are reliable detection models as the majority of the points lay within the shaded area relatively close to the perfect reliability line. The same diagrams were produced using GOES-16 data and are shown in Figure 43 (daytime) and Figure 44 (nighttime).

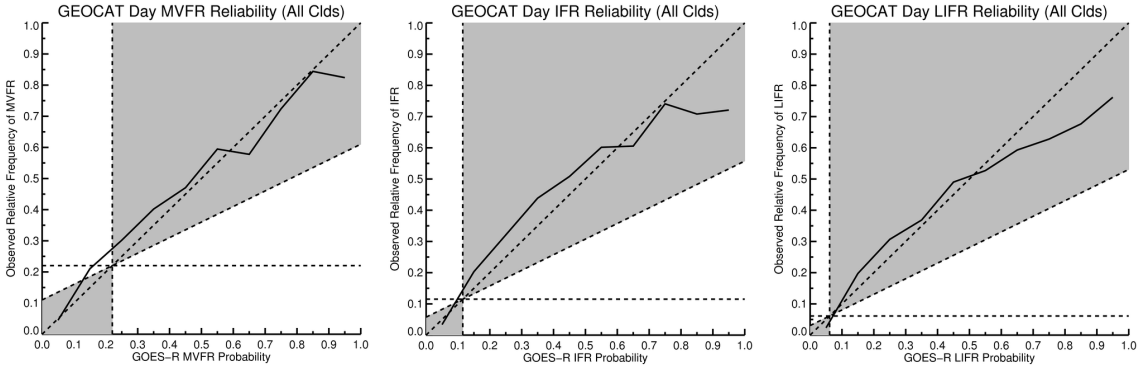

Figure 43 - The attributes diagrams for the GOES-16 MVFR (left), IFR (middle) and LIFR (right) FLS probability products for all daytime pixels. Points that lie within the shaded region indicate increased model skill.

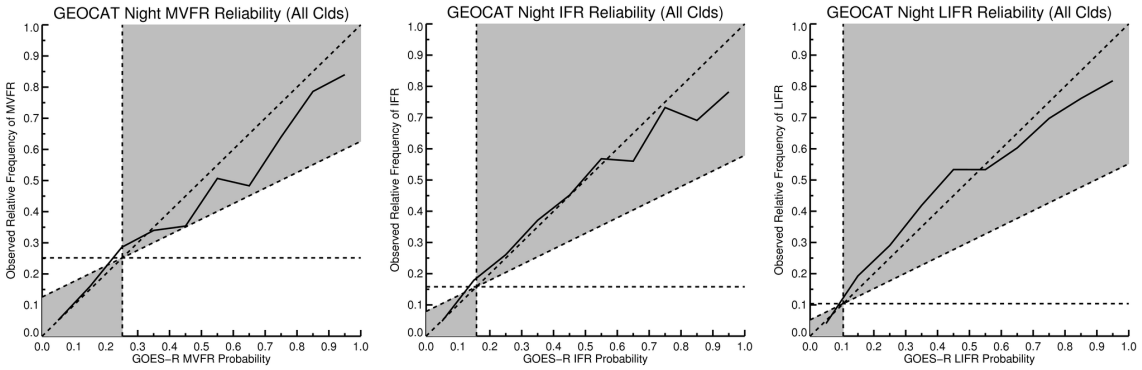

Figure 44 - The attributes diagrams for the GOES-16 MVFR (left), IFR (middle) and LIFR (right) FLS probability products for all nighttime pixels. Points that lie within the shaded region indicate increased model skill.

The attributes diagrams again show that overall the enterprise FLS probability products are reliable. The GOES-16 products also appear to be better calibrated.

The attributes diagrams produced using GOES-17 data are shown in Figure 45 (daytime) and Figure 46 (nighttime).

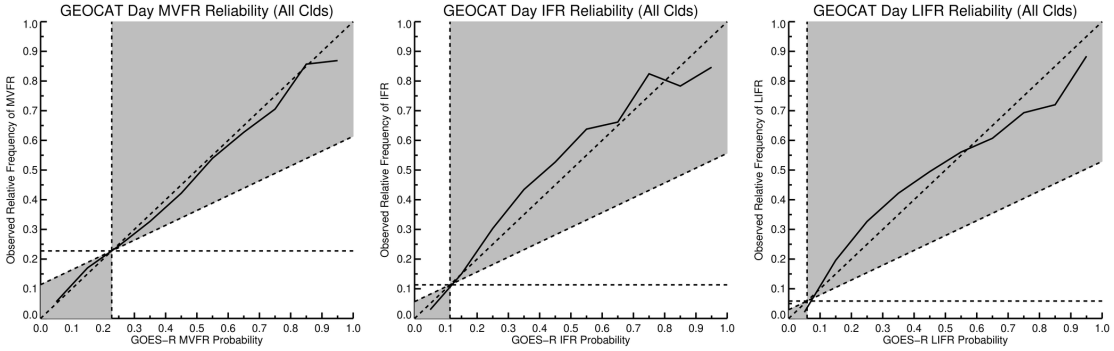

Figure 45 - The attributes diagrams for the GOES-17 MVFR (left), IFR (middle) and LIFR (right) FLS probability products for all daytime pixels. Points that lie within the shaded region indicate increased model skill.

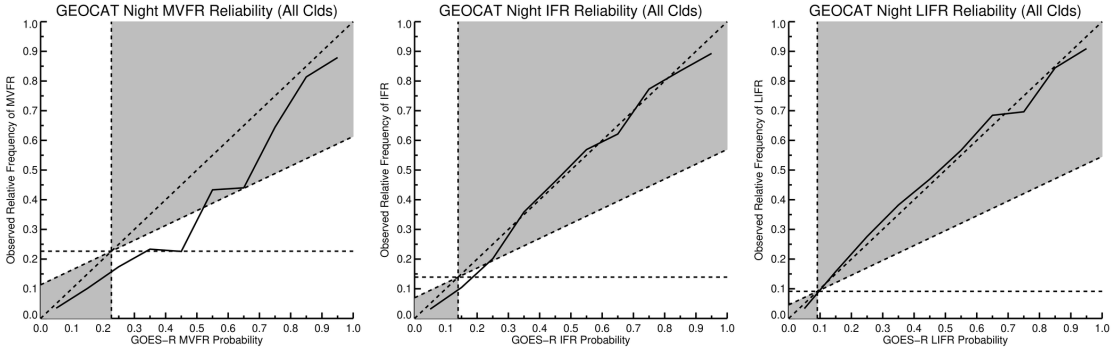

Figure 46 - The attributes diagrams for the GOES-17 MVFR (left), IFR (middle) and LIFR (right) FLS probability products for all nighttime pixels. Points that lie within the shaded region indicate increased model skill.

Once again these diagrams show the GOES-17 FLS probability products are reliable and generally well-calibrated. However, the nighttime GOES-17 MVFR probability product appears to slightly overestimate for mid-range probabilities. This may be the result of a sampling issue with data used for the analysis or the fact that the LUTs used to generate the GOES-17 FLS probabilities were trained using GOES-16 data. The same ABI is utilized by both GOES-16 and GOES-17 which rationalizes using the same LUTs. However, any differences in instrument calibration or cloud climatology in the geographic viewing area would support the need for updated LUTs optimized for GOES-17. This would involve a future maintenance update if required. It should also be noted that of the 3 flight rule categories, IFR and LIFR are by far a greater concern to the aviation community than MVFR.

It should also be noted that the 12 day validation data set for GOES-17 includes varying levels of impact due to the loop heat pipe (LHP) anomaly that impacts instrument cooling. During optimal periods of operation the GOES-17 focal plane temperature (FPT) stays below 82 K. During high impact periods the FPT can increase to well over 100 K resulting in increased noise and possible saturation of the IR channels, severely impacting the quality of the data. The 12-day GOES-17 validation data set is composed of four days when the FPT for each day remained below 85 K (minimal impact), four days when the FPT peaked ~90 K (moderate impact) and four days when the FPT peaked over 100 K (high impact). The validation results discussed above show that the enterprise FLS products applied to GOES-17, including data negatively impacted by the LHP anomaly, comfortably meet the required 70% accuracy requirement. When the FPT warms above 82 K, striping and noise may increase in the probability products, however, the main features of interest remain discernable so at no point will the products become unusable. Due to the fused nature of the enterprise FLS algorithm, impacts due to the LHP anomaly are significantly reduced compared to those associated with algorithms that rely solely on satellite data, especially those that use only IR channels.

4.2.2.2 Fog/Low Cloud Thickness Error Budget

Cloud thickness is a difficult parameter to accurately validate as there are extremely limited truth data sets available. SODAR data was originally used to develop the algorithm and validate the GOES-NOP version, however, limited geographic coverage and declining instrument health has made SODAR data an unreliable validation source for GOES-16/17. The following sections describe the processes used to validate the cloud thickness product for each sensor.

4.2.2.2.1 *GOES-NOP Fog/Low Cloud Thickness Error Budget*

Data from two stations in the San Francisco Bay Area were used to validate the enterprise fog/low cloud algorithm applied to GOES-11. FLS thicknesses were calculated manually from several single-layer low cloud events like the one shown in Figure 25. Due to the lack of SODAR stations and the difficulty in manually finding single-layered FLS events over such a small area, a large validation data set was not available. With the limited number of validation points that were obtained, an estimation of the accuracy of the fog/low cloud thickness algorithm was calculated. The F&PS requires the fog/low cloud thickness be detected within 500 m. Results gathered using SODAR data from several scenes are shown in Figure 47.

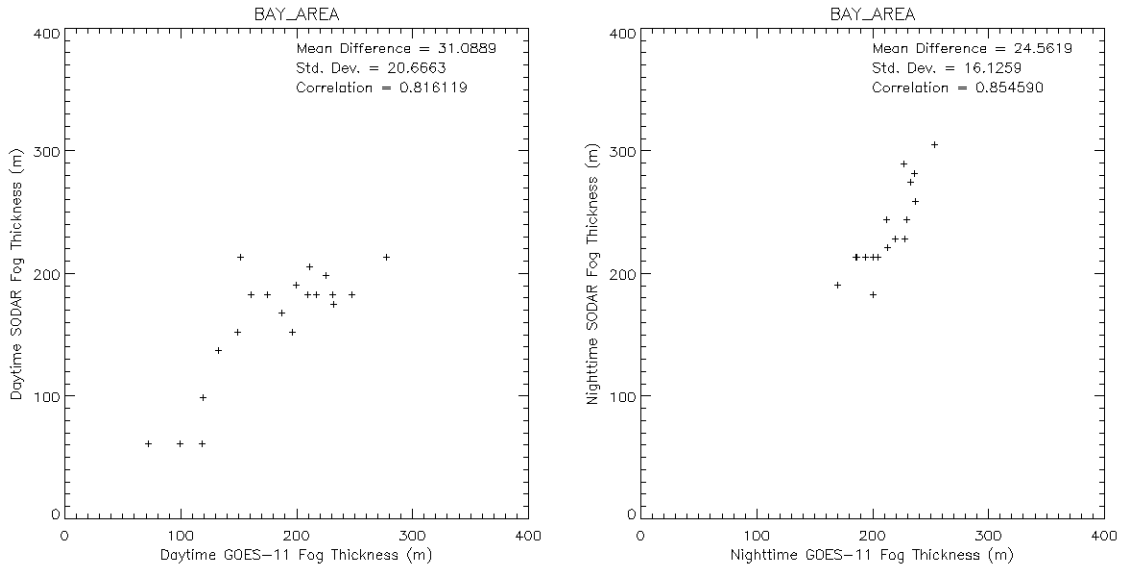

Figure 47 – Scatter plot comparing measured FLS thicknesses using SODAR and ceiling data with thicknesses output from the enterprise fog/low cloud thickness algorithm applied to GOES-11 for both day (left panel) and night (right panel).

The SODAR data analysis above indicates that the accuracy of the enterprise FLS thickness product applied to GOES-11 is well within F&PS requirements with a daytime bias of about 31 m and a nighttime bias of around 25 m. Additionally, the strong correlations indicate that the spatial and temporal patterns are also useful.

4.2.2.2.2 *GOES-16 Fog/Low Cloud Thickness Error Budget*

Unfortunately, SODAR data was not available for validating the FLS thickness product for GOES-16. However, comparisons can be made to the GOES-NOP thicknesses and be used to infer if the GOES-16 thickness product meets the 500 m bias requirement. Images of the enterprise FLS thickness product applied to both GOES-13 and GOES-16 are shown in Figure 48 (nighttime) and Figure 49 (daytime).

FLS Depth

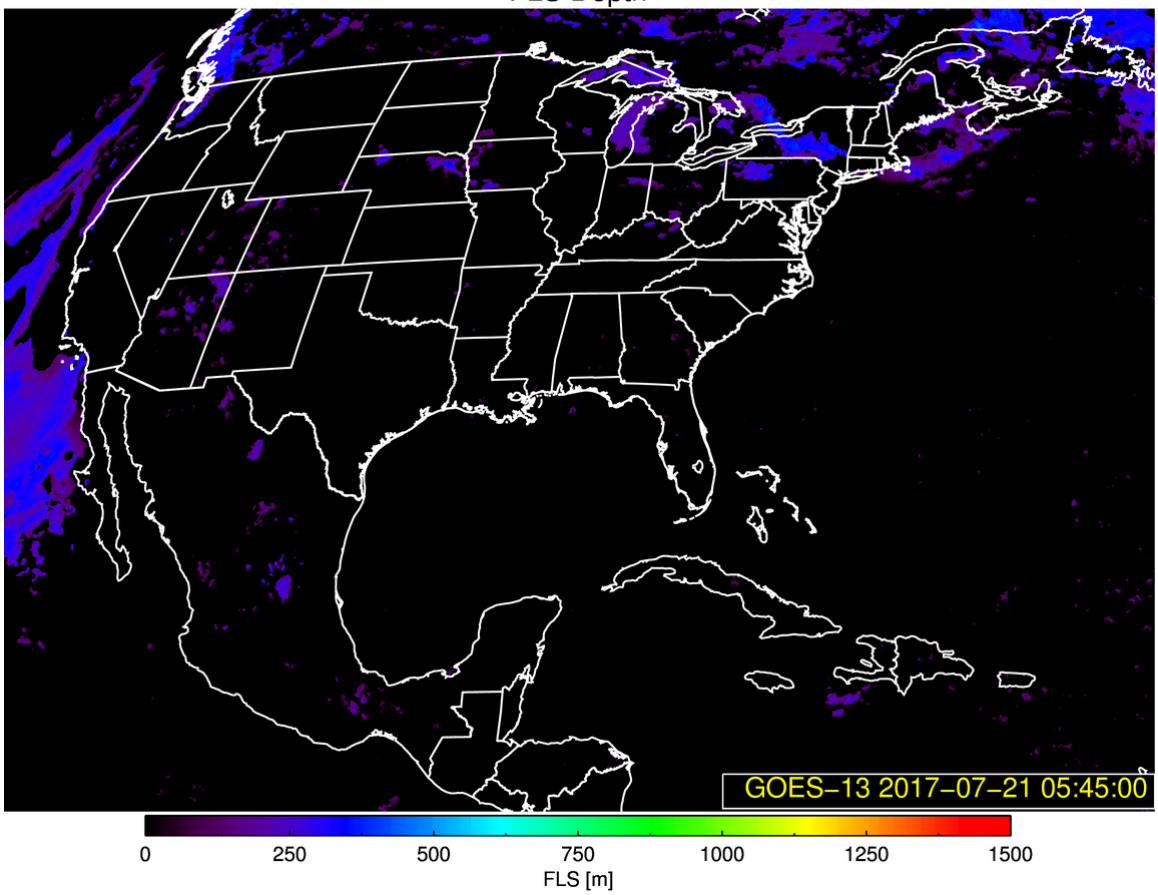

FLS Depth

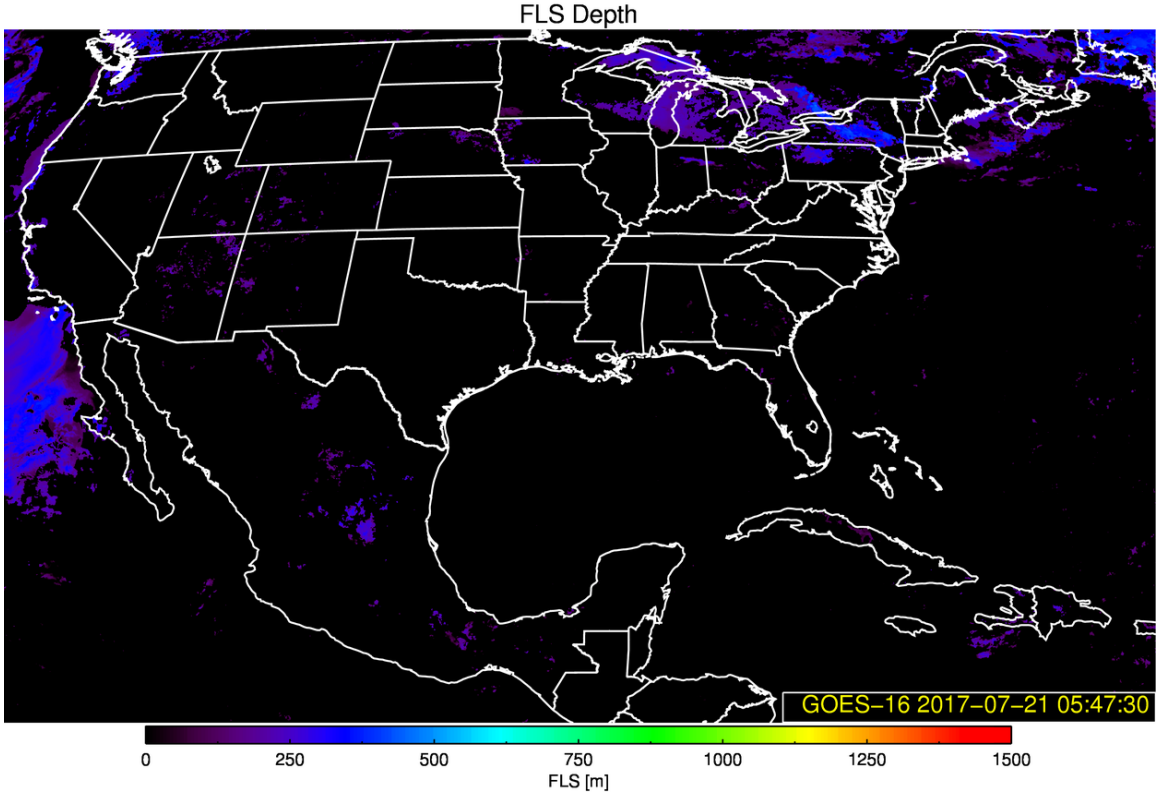

Figure 48 – The enterprise FLS thickness product produced using GOES-13 (top) and GOES-16 (bottom) over CONUS. This is a nighttime scene from July 21, 2017 at 5:45 UTC.

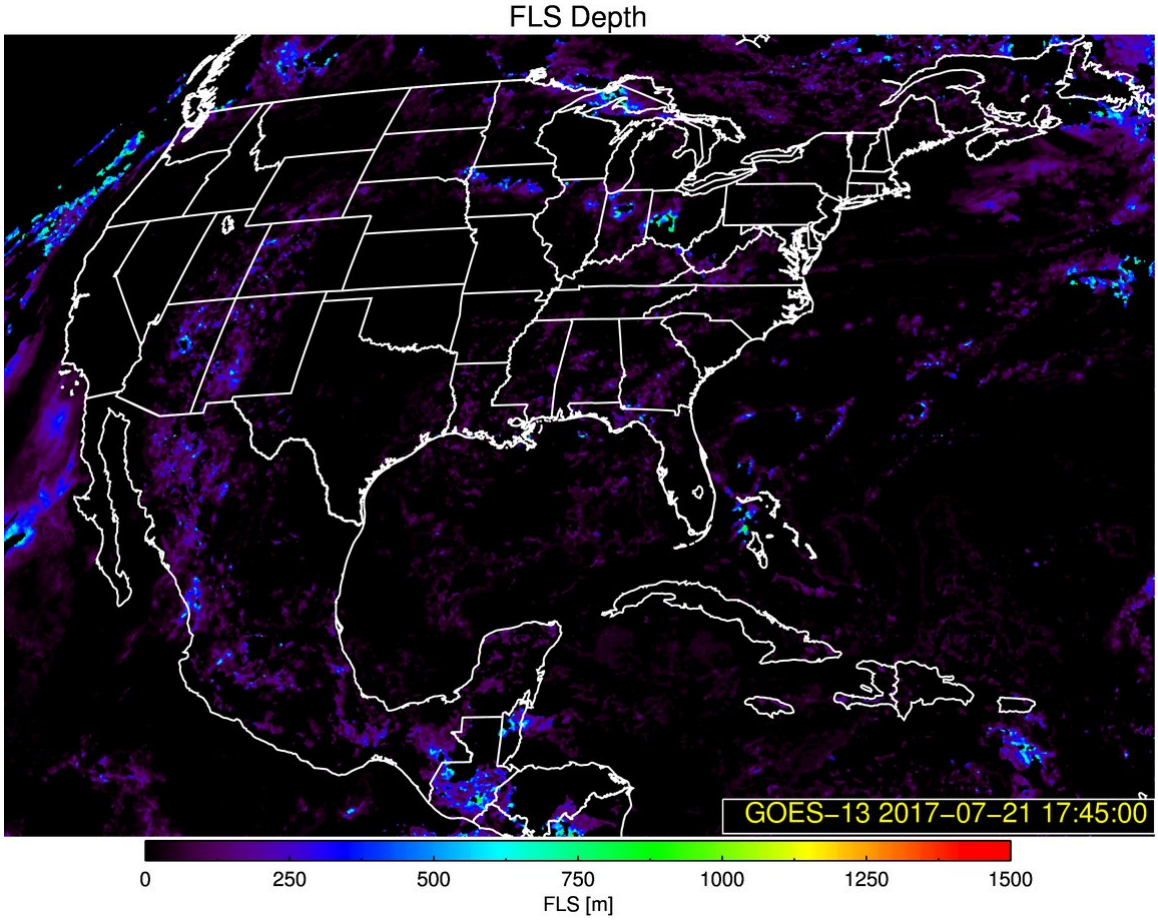

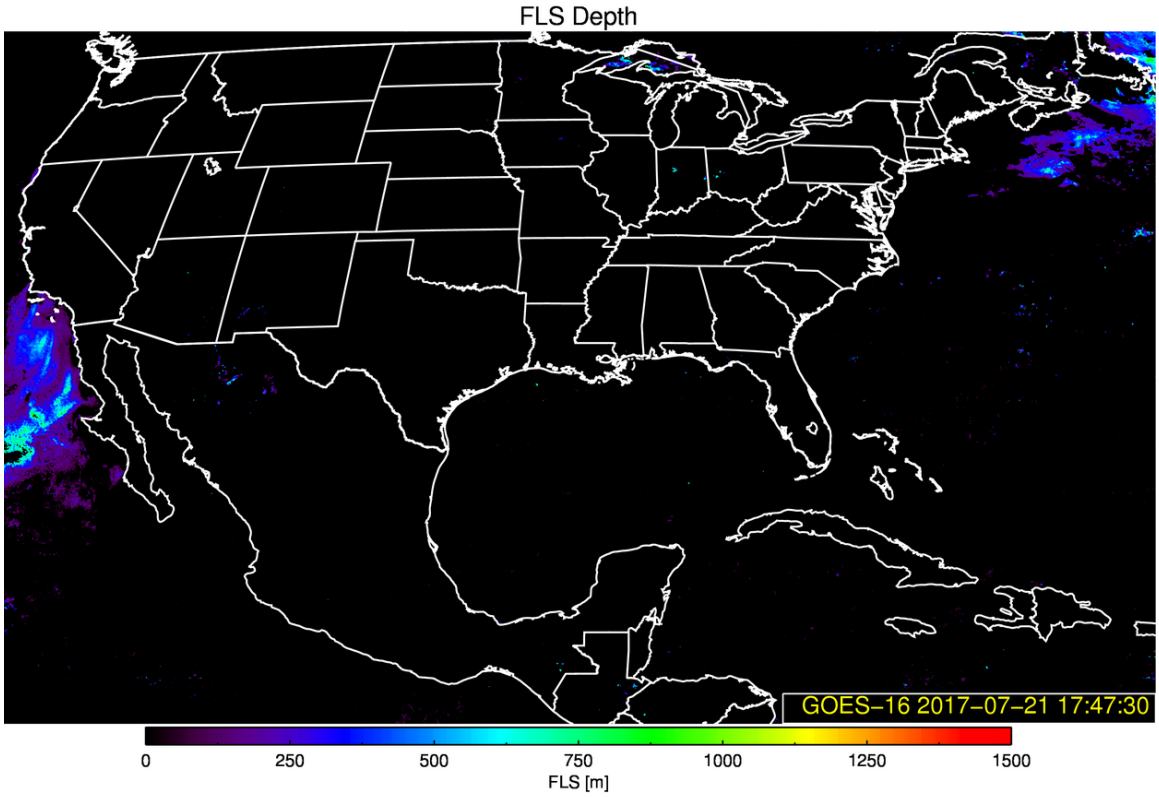

Figure 49 - The enterprise FLS thickness product produced using GOES-13 (top) and GOES-16 (bottom) over CONUS. This is a daytime scene from July 21, 2017 at 17:45 UTC.

The enterprise FLS thickness product applied to GOES-13 can be co-located in space and time with thicknesses produced using GOES-16. For this comparison, only co-located pixels containing valid thicknesses (no missing data) for both GOES-13 and GOES-16 FLS were used. Scatterplots of these co-located pixels from Figure 48 and Figure 49 are shown in Figure 50.

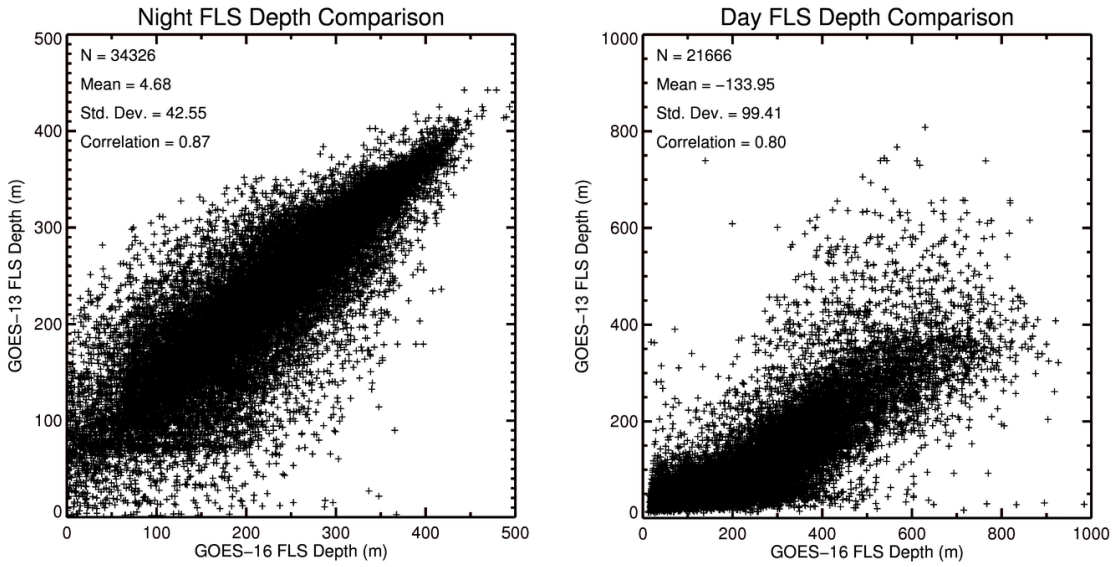

Figure 50 – Scatterplots of valid co-located GOES-13 and GOES-16 FLS thicknesses from July 21, 2017 over CONUS. The left plot contains nighttime pixels from 5:45 UTC (Figure 48). The right plot contains daytime pixels from 17:45 UTC (Figure 49).

The scatterplots from Figure 50 show that the nighttime GOES-13/16 FLS thickness products are well correlated with a correlation coefficient of 0.87. The daytime FLS thicknesses appear slightly less correlated with a correlation coefficient of 0.80. While both GOES-13 and GOES-16 were in a position to view CONUS for this comparison, the difference in spatial resolution and viewing geometry (GOES-13 was positioned at -75W longitude while GOES-16 was positioned at -89.5W longitude) between the 2 imagers will likely account for a large portion of the differences observed between the two FLS thickness products. Another significant source of differences between the daytime pixels is the use of an updated daytime optical properties algorithm for GOES-16. As mentioned above, the enterprise FLS thickness algorithm is based off a calculated daytime optical properties LWP product for daytime pixels. The updated algorithm for GOES-16 has been further developed from the previous GOES-NOP version so larger differences between the GOES-13 and GOES-16 FLS thicknesses are expected.

For further comparison, differences were calculated between the co-located GOES-13 and GOES-16 FLS thicknesses and used to create the histograms shown in Figure 51.

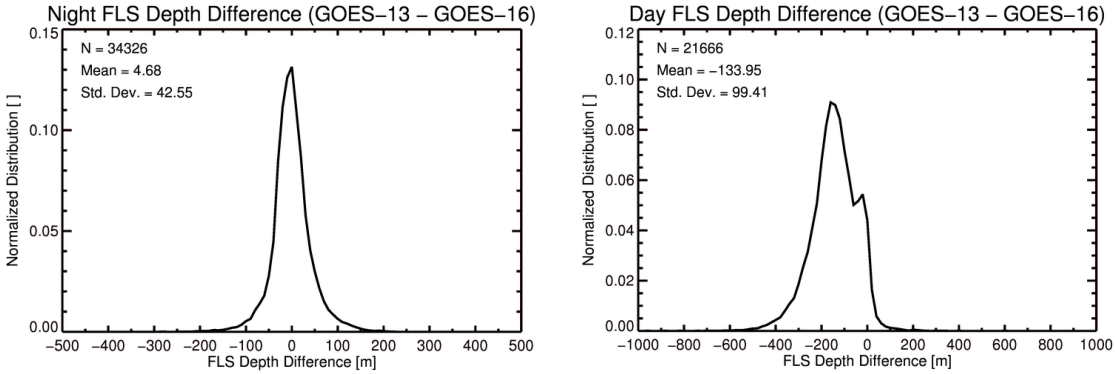

Figure 51 – Histograms of the differences between co-located GOES-13 and GOES-16 FLS thicknesses from July 21, 2017 over CONUS. The left plot contains nighttime pixels from 5:45 UTC (Figure 48). The right plot contains daytime pixels from 17:45 UTC (Figure 49).

The histograms in Figure 51 show the distribution of the differences observed between the co-located GOES-13 and GOES-16 FLS thickness products. The distribution for night pixels produced a bias of 5 m with a standard deviation of 43 m. The distribution for daytime pixels showed a bias of -134 m with a standard deviation of 99 m. The differences were calculated by subtracting the co-located GOES-16 FLS thicknesses from the GOES-13 FLS thicknesses so positive bias values correspond to the GOES-16 FLS thicknesses being low-biased compared to the GOES-13 thicknesses and negative values correspond to the GOES-16 thicknesses being biased higher. Considering the validation of the GOES-NOP FLS thickness product using SODAR data produced biases of 25 m (night) and 31 m (day) and the biases seen between the GOES-13 and GOES-16 FLS thickness products, the GOES-16 FLS thickness product still comfortably meets the F&PS bias requirement of 500 m.

4.2.2.2.3 *GOES-17 Fog/Low Cloud Thickness Error Budget*

Like GOES-16, SODAR data was not available for validating the GOES-17 FLS thickness product. However, comparisons were made to co-located GOES-16 thicknesses to determine if the 500 m bias requirement is achievable. Due to an overlap in the geographic viewing area of GOES-16 and GOES-17, the cloud thickness produced by each sensor can be co-located in both space and time for comparison. The overlap region consists of the far western GOES-16 and far eastern GOES-17 full disk domains. The region was also constricted to viewing angles of < 70º to reduce the impact of edge pixels. Images of the enterprise FLS thickness product applied to both GOES-16 and GOES-17 in this overlap region are shown in Figure 52 (nighttime) and Figure 53 (daytime).

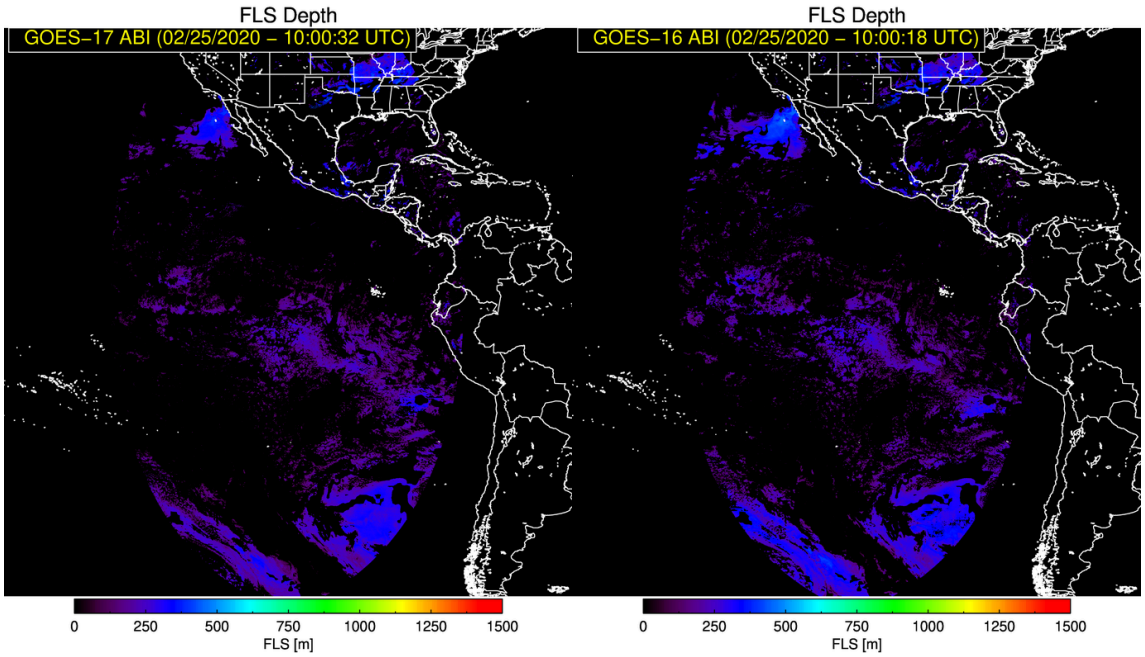

Figure 52 – Enterprise FLS cloud thickness product comparison between GOES-17 (left) and GOES-16 (right) in a region where both full disk domains overlap on January 25, 2020 at 10:00 UTC.

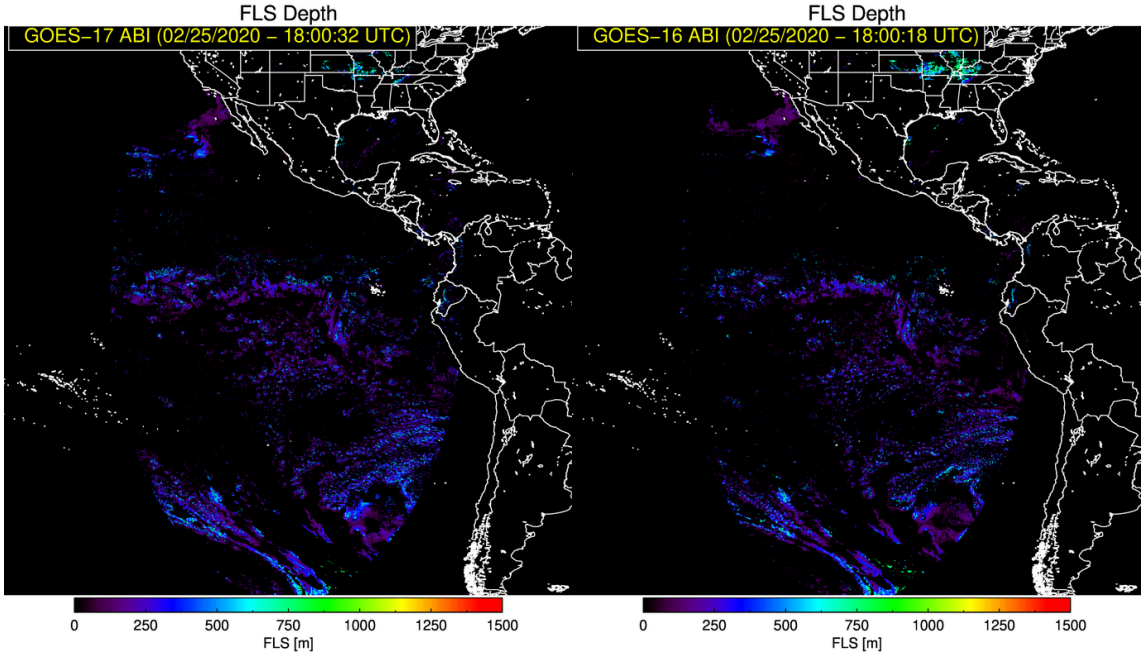

Figure 53 - Enterprise FLS cloud thickness product comparison between GOES-17 (left) and GOES-16 (right) in a region where both full disk domains overlap on January 25, 2020 at 18:00 UTC.

Co-located pixels were compared where both the GOES-16 and GOES-17 products produced valid cloud thicknesses (neither contain missing values). The resulting nighttime/daytime density, scatter and histogram plots are shown in Figure 54 and Figure 55 respectively.

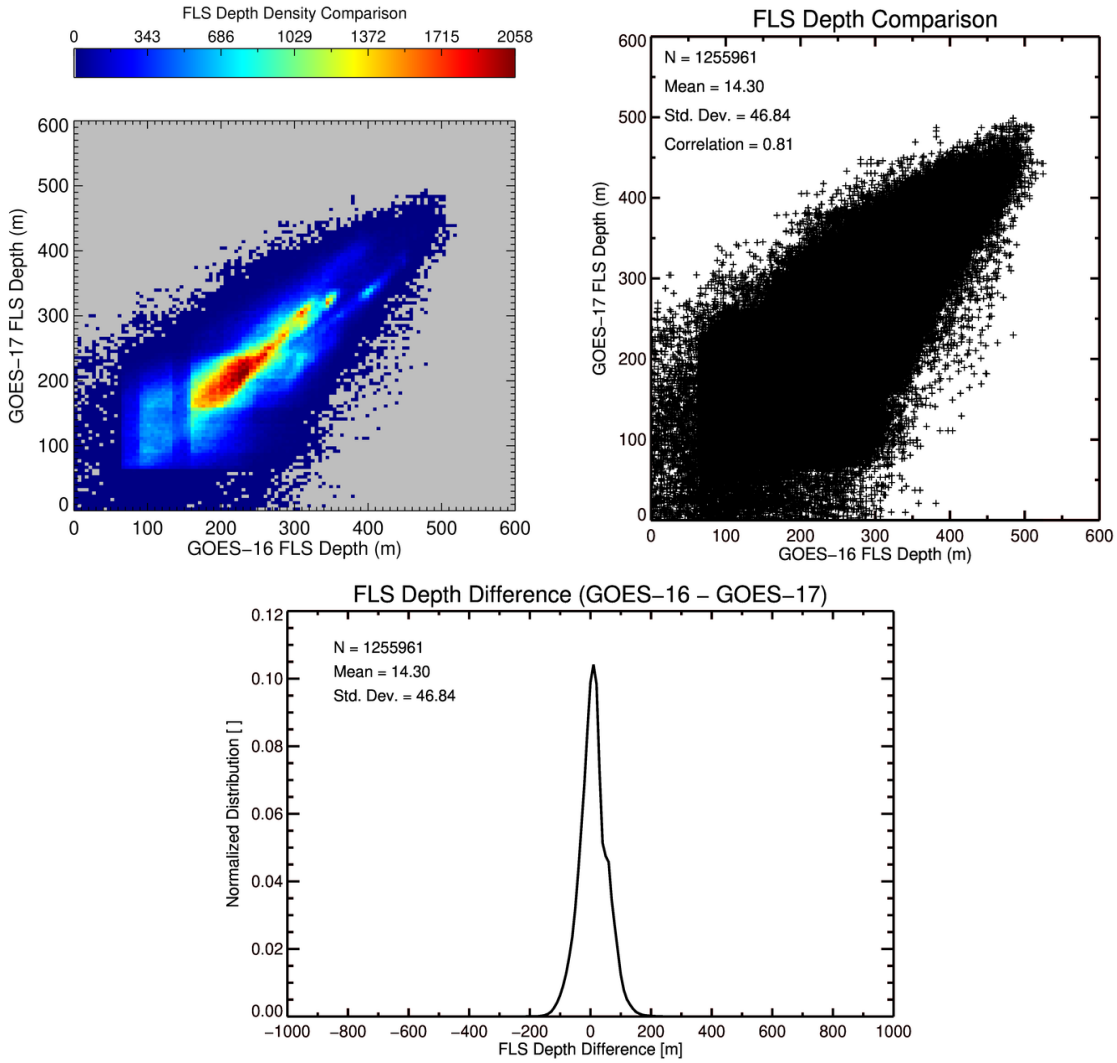

Figure 54 – Density plot (upper left), scatter plot (upper right) and difference histogram (bottom) showing the comparison of the nighttime GOES-16/17 FLS depth products from January 25, 2020 at 10:00 UTC.

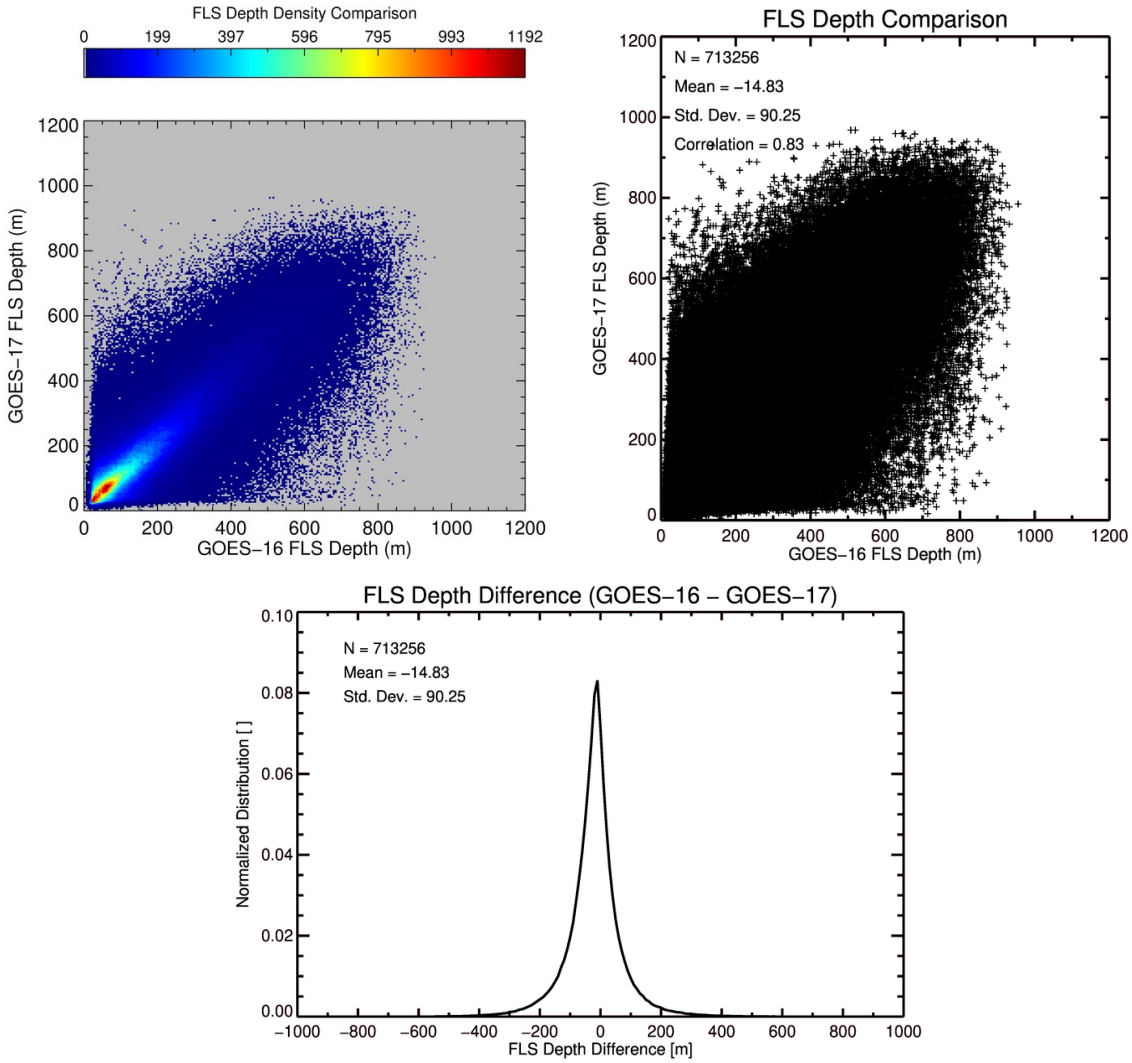

Figure 55 - Density plot (upper left), scatter plot (upper right) and difference histogram (bottom) showing the comparison of the nighttime GOES-16/17 FLS depth products from January 25, 2020 at 18:00 UTC.

Although the co-located GOES-16/17 cloud thicknesses do not appear highly correlated (correlation coefficients were 0.81 (night) and 0.83 (day)) it is important to note that parallax was not taken into account. GOES-16 is located at -75.2 W longitude while GOES-17 is located at -137.2 W. This difference in viewing angle between the 2 sensors will likely account for a large portion of the differences observed between the two FLS thickness products, especially for elevated clouds. The density plots show that the highest concentrations of pixel matchups do appear to be better-correlated.

The histograms show the distribution of the differences observed between the co-located GOES-16 and GOES-17 FLS thickness products. The distribution for night pixels produced a bias of 14 m with a standard deviation of 47 m. The distribution for daytime pixels showed a bias of -15 m with a standard deviation of 90 m. The differences were calculated by subtracting the co-located GOES-17 FLS thicknesses from the GOES-16 FLS

thicknesses so positive bias values correspond to the GOES-17 FLS thicknesses being low-biased compared to the GOES-16 thicknesses and negative values correspond to the GOES-17 thicknesses being biased higher. Considering the results of the GOES-NOP and GOES-16 FLS cloud thickness validation in sections 4.2.2.2.1 and 4.2.2.2.2, the GOES-17 FLS thickness product still comfortably meets the F&PS bias requirement of 500 m.

While the usefulness of the cloud thickness product will depend on individual needs, the more user-centric value in the cloud thickness product is how it can be used to infer dissipation time for specific fog events. Although dissipation time is not a direct output from the Enterprise FLS product suite, additional information (examples and training) on using the cloud thickness to estimate the clearing time of radiation fog can be found here: https://fusedfog.ssec.wisc.edu/training/

4.2.3 Validation Summary

The following points summarize the results of the enterprise FLS detection and depth algorithm validation analysis.

- According to the F&PS, the FLS detection must have an accuracy of 0.70 or greater and the FLS thickness must have an accuracy (bias) of 500 m or less.

- Surface observations of cloud ceiling and surface visibility were used to validate the FLS detection algorithm. Surface observations of cloud ceiling combined with SODAR data were used to validate the FLS depth product.

- Using surface observations as the validation source yielded GOES-13 FLS detection accuracies for MVFR/IFR/LIFR of 0.84/0.86/0.91 for the probability threshold that yielded the highest CSI scores (36%/20%/14%) respectively.

- Using surface observations as the validation source yielded GOES-16 FLS detection accuracies for MVFR/IFR/LIFR of 0.87/0.90/0.92 for the probability threshold that yielded the highest CSI scores (38%/26%/21%) respectively.

- Using surface observations as the validation source yielded GOES-17 FLS detection accuracies for MVFR/IFR/LIFR of 0.87/0.90/0.91 for the probability threshold that yielded the highest CSI scores (51%/33%/20%) respectively.

- Using the SODAR data as the validation source yielded GOES-NOP FLS thickness biases of 31 m (day) and 25 m (night).

- Comparisons between co-located GOES-13 and GOES-16 pixels yielded GOES-16 FLS thickness biases of 134 m (day) and -5 m (night).

- Comparisons between co-located GOES-16 and GOES-17 pixels yielded GOES-17 FLS thickness biases of -15 m (day) and 14 m (night).

- Thus, the enterprise FLS detection and thickness products meet the F&PS accuracy specifications.

5 PRACTICAL CONSIDERATIONS

5.1 Numerical Computation Considerations

The FLS algorithm is implemented sequentially. Because it relies on the results of other cloud algorithms, the cloud mask, cloud phase and daytime optical properties must be run before the FLS algorithm. In addition, the necessary RTM and NWP calculations also need to be processed and fed into the FLS algorithm. The FLS algorithm currently uses 12-hr forecasts from the GFS and 2-and 3-hr forecasts from the RAP. However, if these are not available, up to 24-hr forecasts can be utilized. All tests are applied before the final fog/low stratus mask and thickness are determined.

5.2 Programming and Procedural Considerations

The FLS algorithm is, for the most part, a pixel-by-pixel algorithm. However, a spatial uniformity filter is currently used to reduce noise by taking into account the surrounding pixels.

5.3 Quality Assessment and Diagnostics

The following procedures are recommended for diagnosing the performance of the FLS algorithm.

- Periodically image the FLS probabilities and compare them to true color images and surface observations of cloud ceiling and surface visibility to ensure proper areas are being correctly detected with minimal false detection (exceptionally large probabilities).
- Continue to validate the FLS algorithm using surface observations.

5.4 Exception Handling

The FLS algorithm currently checks the validity of all channels before running. If any channels are unavailable, the algorithm will still run disregarding tests reliant on those channels. The FLS algorithm also expects the main processing framework to flag any pixels with missing geolocation or viewing geometry information.

5.5 Algorithm Validation

Surface observations are used to validate the fog/low cloud detection algorithm. These will continue to serve as the main source of validation data in the future. For FLS thickness, ground-based measurements of cloud thickness using ceiling height and SODAR data are used as the main source of validation.

6 ASSUMPTIONS AND LIMITATIONS

The following sections describe the current limitations and assumptions in the current version of the enterprise fog/low cloud algorithm.

6.1 Performance

The following assumptions have been made in developing and estimating the performance of the fog/low cloud algorithm. The following list contains the current assumptions (numbered) and proposed mitigation strategies (lettered).

1. NWP data of comparable or superior quality to the current 12 hour GFS and 2- and 3- hour RAP forecasts are available.
    a. Use longer-range GFS and RAP forecasts or switch to another NWP source

2. All of the static ancillary data are available at the pixel level.
    a. Reduce the spatial resolution of the available ancillary data

3. The processing system allows for processing of multiple scan lines at once for application of important spatial analysis techniques.
    a. No mitigation is possible

4. A more robust assumption of the LWC is necessary for daytime FLS thickness calculation.
    a. Create a variable assumption for LWC depending on whether the algorithm detects FLS or low stratus.

In addition, the clear sky radiance calculations are prone to large errors, especially near coastlines, in mountainous regions, snow/ice field edges, and atmospheric frontal zones, where the NWP surface temperature and atmospheric profiles are less accurate. Improvements in NWP fields should lead to additional improvements in the enterprise fog/low cloud products.

6.2 Assumed Sensor Performance

We assume the sensor will meet its current specifications. However, the FLS algorithm will be dependent on the following instrumental characteristics.

- The FLS algorithm is dependent on several other cloud algorithms (see section 3.2); therefore any issues that degrade those algorithms may also affect the fog/low cloud algorithm. An example is how the amount of striping in the data may affect spatial uniformity tests in the other cloud algorithms leading to issues absorbed by the FLS algorithm.
- Unknown spectral shifts in some channels will cause biases in the clear-sky RTM calculations that may impact the ability to accurately calculate the surface temperature bias relied upon in the enterprise FLS algorithm

6.3 Pre-Planned Product Improvements

While development of the enterprise fog/low cloud algorithm continues, we expect in the coming years to focus on the following issues.

6.3.1 Additional Capability to Run On SEVIRI

Due to wider 3.9 μm channel window on SEVIRI, the current nighttime LUT's used for GOES-NOP and the ABI are not applicable. In order to accurately use the enterprise FLS algorithm on SEVIRI new LUT's need to be created.

7 REFERENCES

Bendix, J., 2002. A satellite-based climatology of FLS and low stratus in Germany and adjacent areas. *Atmos. Res.,* **64,** 3-18.

Cermak, J. and J Bendix, 2008. A Novel Approach to Fog/Low Stratus Detection Using Meteosat 8 Data. *Atmos. Res.*, **87,** 279-292.

Clark, D. A. and F. W. Wilson, 1997. "The San Francisco Marine Stratus Initiative", 7th Conference on Aviation, Range, and Aerospace Meteorology. Long Beach, CA, pp. 384-389.

Domingos, P and M. Pazzani, 1997. On the Optimality of the Simple Bayesian Classifier Under Zero-One Loss. *Machine Learning,* **29**, 103–130.

Ellrod, G. P., 1995: Advances in the Detection and Analysis of FLS at Night Using GOES Multispectral Infrared Imagery. *Weather and Forecasting*, **10**, 606-619.

Ellrod, G. P., 2003: Estimation of Low Cloud Base Heights at Night Using GOES Infrared and Surface Temperature Data. *National Weather Digest*, **26** (1-2), 39-44.

Eyre, J. R., J. L. Brownscombe, and R. J. Allam, 1984. Detection of FLS At Night Using Advanced Resolution Radiometer (AVHRR) imagery. *Meteor. Mag.*, **113,** 266 271.

Heidinger, A. K. and M. J. Pavolonis, 2009: Gazing at Cirrus Clouds for 25 Years Through A Split Window. Part I: Methodology. *J. of Appl. Met. and Clim.*, **48,** 1100-1116.

Hess, M., P. Koepke and I. Schult, 1998: Optical Properties of Aerosols and Clouds. *Bull. Amer. Meteor. Soc.*, **79**, 831-44.

Kossin, J.P. and M. Sitkowski, 2008: An Objective Model for Identifying Secondary Eyewall Formation in Hurricanes. *Mon. Wea. Rev.,* **137,** 876-892.

Lee, T. F., F. J. Turk and K. Richardson, 1997. Stratus and FLS Products Using GOES-8-9 3.9 μm Data. *Weather Forecast,* **12,** 664-677.

Pavolonis, M. J. and Heidinger, A. K., 2004: Advances in identifying cirrus and multilayered cloud systems from operational satellite imagers at night. Applications with Weather Satellites II, Honolulu, Hawaii, 9-11 November 2004. Proceedings. SPIE-International Society for Optical Engineering, Bellingham, WA, 2005, pp. 225-234.

Pavolonis, M. J., 2011b: Advances in extracting cloud composition information from spaceborne infrared radiances: A robust alternative to brightness temperatures. Part II: Proof of concept. To be submitted to *J. Applied Meteorology and Climatology.*

Pruppacher, H. R. and J. D. Klett, 1997: Microphysics of clouds and precipitation. Second Edition. Kluwer Academic Publishers. 954 pp.

Rogers, R. R. and M. K. Yau, 1989: A short course in cloud physics. Third Edition. Butterworth-Heinemann. 290 pp.

Seemann, S., E. Borbas, R. Knuteson, G. Stephenson and H Huang, 2008: Development of a Global Infrared Land Surface Emissivity Database for Application to Clear Sky Sounding Retrievals from Multispectral Satellite Radiance Measurements. *J. of Appl. Met. and Clim.*, **47,** 108-123.

Tampieri F., and C. Tomasi, 1976: Size Distribution Models of FLS and cloud droplets in terms of the modified gamma function. *Tellus*, **28,** 333-347.

Turner, J., R. J. Allam and D. R. Maine, 1986. A Case Study of the Detection of FLS At Night Using Channel 3 and 4 on the Advanced Very High Resolution Radiometer (AVHRR). *Meteor. Mag.*, **115,** 285-290.

Wielicki, B. A. and R. M. Welch, 1986: Cumulus cloud properties derived using Landsat Satellite Data. *J. Climate and Meteorology*, **25(3)**, 261-276.

Wilks, D. S., 2006. Statistical Methods in the Atmospheric Sciences. 2nd ed. International Geophysics Series, Vol. 91, Academic Press, 627

Zhang, H, 2006. On the Optimality of naïve Bayes with dependent binary features. *Pattern Recog. Lett.,* **27,** 830-837.